

2017

# Autonomous Locomotion Mode Transition of Ground Hybrid Robots

Wang, Jie

---

Wang, J. (2017). Autonomous Locomotion Mode Transition of Ground Hybrid Robots (Doctoral thesis, University of Calgary, Calgary, Canada). Retrieved from <https://prism.ucalgary.ca>. doi:10.11575/PRISM/25085 <http://hdl.handle.net/11023/3606>

*Downloaded from PRISM Repository, University of Calgary*

UNIVERSITY OF CALGARY

Autonomous Locomotion Mode Transition of Ground Hybrid Robots

by

Jie Wang

A THESIS

SUBMITTED TO THE FACULTY OF GRADUATE STUDIES  
IN PARTIAL FULFILMENT OF THE REQUIREMENTS FOR THE  
DEGREE OF DOCTOR OF PHILOSOPHY

GRADUATE PROGRAM IN MECHANICAL AND MANUFACTURING ENGINEERING

CALGARY, ALBERTA

JANUARY, 2017

© Jie Wang 2017

## ABSTRACT

Multi-modal locomotion (e.g. terrestrial, aerial, and aquatic) is gaining increasing interest in robotics research as it improves the robots' environmental adaptability, locomotion versatility, and operational flexibility. Within the terrestrial multiple locomotion robots, the main advantage of hybrid robots stems from their multiple (two or more) locomotion modes, among which robots can select from depending on the encountering terrain conditions. The majority of the ground hybrid robots proposed in the past two decades are wheel/track-legged systems due to their excellence in both locomotive efficiency and rough terrain negotiation abilities. However, there are many challenges in improving the autonomy of the locomotion mode transition between their multiple locomotion modes.

The main goal of this research is to develop a method to enable an autonomous locomotion mode transition for ground hybrid robots. To achieve this goal, simplified dynamic modeling methods for the rolling and walking locomotion modes of wheel/track-legged hybrid robots are developed, a novel energy based criterion is proposed to evaluate the locomotion performance of the rolling and walking locomotion mode, a new rule to determine the threshold values of the locomotion transition criterion is derived, and two walking gaits to negotiate steps with different heights for quadruped wheel/track-legged hybrid robots are proposed.

The autonomous locomotion mode transition method is proposed. It's first proposed based on the energy performance knowledge of the simplified rolling and walking locomotion evaluations of ground hybrid robots. Then, the method is refined by the work on the Cricket robot. Simulated case study results are presented to illustrate that the autonomous locomotion mode transition method is able to switch between the Cricket's rolling and walking locomotion modes when negotiating step style obstacles. Even though the proposed method is improved by

the work on the Cricket robot, the method is generally applicable to a wide range of wheel/track-legged hybrid robots.

## **ACKNOWLEDGEMENTS**

I would like to thank my supervisor Dr. Alex Ramirez-Serrano for the support of my study. His guidance helped me in all the time of research and writing of this thesis. I would like to thank my friends in the AR<sup>2</sup>S Lab at the University of Calgary: Krispin Davies, Graeme Wilson, Diego Ospina Latorre, Mahmoud Mustafa, and Marshall Staples for their help, advice, encouragement and support. I would like to thank my girlfriend Lei Zhao for her emotional support. I would like to thank my parents, for everything.

## **DEDICATION**

This thesis is dedicated to my beloved mother.

恭献此文给我最深爱的母亲。

## TABLE OF CONTENTS

|  |      |
|--|------|
| ABSTRACT .....   | ii   |
| ACKNOWLEDGEMENTS .....   | iv   |
| DEDICATION .....   | v    |
| TABLE OF CONTENTS .....  | vi   |
| LIST OF TABLES .....   | ix   |
| LIST OF FIGURES AND ILLUSTRATIONS .....                              | x    |
| LIST OF SYMBOLS, ABBREVIATIONS AND NOMENCLATURE .....                | xiii |
| <br>   |      |
| CHAPTER ONE: INTRODUCTION .....                                      | 1    |
| 1.1 Overview of Current Hybrid Robots .....                          | 3    |
| 1.2 Cricket Robot Platform .....                                     | 4    |
| 1.3 Outline of The Thesis .....                                      | 7    |
| <br>   |      |
| CHAPTER TWO: LITERATURE REVIEW .....                                 | 9    |
| 2.1 Ground Hybrid Robots .....                                       | 9    |
| 2.1.1 Wheeled/tracked robots with Passively Articulated Frames ..... | 9    |
| 2.1.2 Wheeled/tracked robots with Actively Articulated Frames .....  | 10   |
| 2.2 Autonomous Locomotion Mode Transition .....                      | 13   |
| 2.3 Observations .....   | 17   |
| <br>   |      |
| CHAPTER THREE: PROPOSED WORK .....                                   | 18   |
| 3.1 Problem Statement .....  | 18   |
| 3.2 Assumptions and Constraints .....                                | 19   |
| 3.2.1 Assumptions .....  | 20   |
| 3.2.2 Constraints .....  | 20   |
| 3.3 Proposed Approach .....  | 22   |
| 3.3.1 Outline of the Proposed Work .....                             | 23   |
| 3.3.2 Summary .....  | 26   |
| 3.4 Proposed Contributions .....                                     | 27   |
| <br>   |      |
| CHAPTER FOUR: ROLLING LOCOMOTION MODELING .....                      | 29   |
| 4.1 Preparatory Definitions .....                                    | 32   |
| 4.2 Stage 1 .....  | 36   |
| 4.3 Stage 2 .....  | 38   |
| 4.4 Stage 3 .....  | 41   |
| 4.5 Summary .....  | 42   |
| <br>   |      |
| CHAPTER FIVE: WALKING LOCOMOTION MODELING .....                      | 43   |
| 5.1 Dynamics Modeling Methods .....                                  | 43   |
| 5.1.1 Parameters Definition .....                                    | 46   |
| 5.1.2 DeNOC Matrices .....   | 48   |
| 5.1.3 Uncoupled Newton-Euler Equations .....                         | 51   |
| 5.1.4 Coupled Equations of Motion .....                              | 52   |
| 5.1.5 Recursive Inverse Dynamics Equations .....                     | 54   |
| 5.1.5.1 Step 1: Forward Recursion (Kinematic Equations) .....        | 54   |

|  |            |
|--|------------|
| 5.1.5.2 Step 2: Backward Recursion (Dynamic Equations) .....                     | 54         |
| 5.1.6 Recursive Forward Dynamic Equations .....                                  | 55         |
| 5.1.6.1 Step 1 .....   | 56         |
| 5.1.6.2 Step 2 .....   | 56         |
| 5.1.6.3 Step 3 .....   | 57         |
| 5.2 Modeling of the Walking Locomotion Mode .....                                | 57         |
| 5.3 Summary .....  | 62         |
| <b>CHAPTER SIX: TENTATIVE AUTONOMOUS LOCOMOTION MODE TRANSITION METHOD .....</b> | <b>63</b>  |
| 6.1 Energy Consumption Evaluations .....   | 63         |
| 6.2 Tentative Method .....   | 70         |
| 6.3 Summary .....  | 72         |
| <b>CHAPTER SEVEN: SIMULATION MODEL .....</b>                                     | <b>73</b>  |
| 7.1 Physical Model Building .....  | 73         |
| 7.1.1 Pure Shape Components.....   | 74         |
| 7.1.2 Mass and Inertia Tensor Import .....                                       | 75         |
| 7.1.3 Joint Constraints .....  | 76         |
| 7.2 Rolling Locomotion Configuration .....                                       | 78         |
| 7.3 Walking Locomotion Model Calculations.....                                   | 79         |
| 7.3.1 Leg Kinematics Calculation .....   | 79         |
| 7.3.2 Kinematics and Dynamics Calculation Modules in V-REP.....                  | 84         |
| 7.4 Environment Friction Parameters Tuning.....                                  | 86         |
| 7.5 Summary .....  | 87         |
| <b>CHAPTER EIGHT: STEP CLIMBING GAITS .....</b>                                  | <b>88</b>  |
| 8.1 Step-climbing Gaits of Wheel-legged Robot.....                               | 88         |
| 8.2 The Whole Body Climbing Gait .....   | 90         |
| 8.3 The Rear Body Climbing Gait .....  | 98         |
| 8.4 Summary .....  | 99         |
| <b>CHAPTER NINE: RESULTS AND VERIFICATION.....</b>                               | <b>100</b> |
| 9.1 Simulation Settings .....  | 100        |
| 9.2 Autonomous Locomotion Mode Transition Method .....                           | 101        |
| 9.3 Walking Locomotion Energy Evaluation .....                                   | 103        |
| 9.4 Threshold Values .....   | 106        |
| 9.5 Simulation Results .....   | 107        |
| 9.6 Summary .....  | 110        |
| <b>CHAPTER TEN: CONCLUSION AND FUTURE WORK .....</b>                             | <b>112</b> |
| 10.1 Conclusion .....  | 112        |
| 10.2 Future work .....   | 113        |
| <b>REFERENCES .....</b>  | <b>115</b> |
| <b>APPENDIX A: THE STANDARD AND MODIFIED D-H METHOD.....</b>                     | <b>120</b> |

|  |     |
|--|-----|
| A.1. Standard D-H method .....   | 120 |
| A.2. Standard D-H method .....   | 122 |
| A.3. D-H Method of DeNOC Algorithm .....   | 123 |
| <b>APPENDIX B: ANALYTICAL EXPRESSIONS OF THE DENOC DYNAMIC EQUATIONS OF MOTION VARIABLES .....</b> |     |
| B.1. Generalized Inertia Matrix (GIM).....   | 125 |
| B.2. Matrix of Convective Inertia (MCI).....   | 126 |
| B.3. Vector of Convective Inertia (VCI) .....  | 129 |
| B.4. Generalized Forces.....   | 130 |
| <b>APPENDIX C: INVERSE KINEMATICS CALCULATION METHOD SUMMARY</b>                                   |     |
| C.1. The Leg Inverse Kinematics Calculation.....   | 132 |
| C.2. Inverse Kinematics Calculation Steps Summary .....  | 133 |

## **LIST OF TABLES**

|  |     |
|--|-----|
| Table 5-1. Symbol Summary in the DeNOC Method.....         | 47  |
| Table 5-2. Model and Step Parameters Definition.....       | 60  |
| Table 7-1. D-H Parameters of the Front Leg of Cricket..... | 82  |
| Table B. Parameters of Standard D-H Method.....            | 121 |

## LIST OF FIGURES AND ILLUSTRATIONS

|   |    |
|---|----|
| Figure 1-1. a) DRC-HUBO from KAIST [7], b) CHIMP from Carnegie Mellon University [8], c) Momaro from University of Bonn [9], and d) RoboSimian from JPL [10], Respectively..... | 3  |
| Figure 1-2. a) Robot (Cricket) Prototype and b) Its Leg Joints Layout [26]. .....   | 5  |
| Figure 1-3. Cricket Leg Mechanical Design Layout. ....  | 6  |
| Figure 1-4. Locomotion Modes of Cricket in Different Configurations [27].....   | 7  |
| Figure 1-5. Body Titling Configurations to Overcome Small Confined Spaces [27]. .....   | 7  |
| Figure 2-1. a) Spirit and Opportunity Mars Rover [30], b) SOLERO [31], and c) CRAB II Mars Rover [32], Respectively. ....   | 10 |
| Figure 2-2. a) Robhaz DT3 [33] and b) Gunryu [34]. .....  | 10 |
| Figure 2-3. Epi.q-TG Mechanical Hybrid Robot [38]. .....  | 12 |
| Figure 2-4. Quattroped Mobile Hybrid Robot [35]. .....  | 12 |
| Figure 3-1. Schematics of Ground Quadruped Wheel/track-legged Hybrid Robots.....  | 21 |
| Figure 3-2. Work Flowchart Steps to be Performed in this Research. ....   | 24 |
| Figure 4-1. One Wheel-terrain Modeling Method using the Point Contact Terramechanics Model in Horizontal and Vertical Directions.....   | 30 |
| Figure 4-2. Three Motion Stages of One Wheel-Step Negotiation Model.....  | 31 |
| Figure 4-3. Obstacle Height Explanation.....  | 37 |
| Figure 4-4. Calculations of the Initials of Stage 2. ....   | 41 |
| Figure 5-1. Generalized Model of a Serial-link System with Fixed Base. ....   | 46 |
| Figure 5-2. Adjacent Links (Link i and i + 1) Parameter Definitions. ....   | 49 |
| Figure 5-3. Step Climbing Gait of the Walking Locomotion Mode.....  | 58 |
| Figure 5-4. Joint Trajectory of Joint 1 and 2 of the Wheel Stepping Phase. ....   | 61 |
| Figure 5-5. Joint Trajectory of Joint 1 and 2 of the Body Moving Phase.....   | 61 |
| Figure 6-1. Energy Evaluation Result of Rolling Locomotion in x-y-z Plane. ....   | 65 |
| Figure 6-2. Energy Evaluation Result of Walking Locomotion in x-y-z Plane.....  | 65 |

|   |    |
|---|----|
| Figure 6-3. Energy Evaluation Result of Rolling Locomotion in x-z Plane.....                        | 66 |
| Figure 6-4. Energy Evaluation Result of Walking Locomotion in x-z Plane.....                        | 67 |
| Figure 6-5. Energy Evaluation Result of Rolling Locomotion in y-z Plane.....                        | 68 |
| Figure 6-6. Energy Evaluation Result of Walking Locomotion in y-z Plane.....                        | 68 |
| Figure 6-7. Energy Evaluation Result of Rolling Locomotion in x-y Plane. ....                       | 69 |
| Figure 6-8. Energy Evaluation Result of Walking Locomotion in x-y Plane.....                        | 70 |
| Figure 6-9. Autonomous Locomotion Mode Transition Flowchart.....                                    | 71 |
| Figure 7-1. The Pure Shape Model of Cricket's Individual Component.....                             | 75 |
| Figure 7-2. Parameters from SolidWorks Mass Properties (a) to V-REP Dynamics Properties<br>(b)..... | 76 |
| Figure 7-3. One Leg Chain V-REP Model of Cricket. ....  | 77 |
| Figure 7-4. Cricket Dynamic Respondable V-REP Model.....  | 78 |
| Figure 7-5. Home Configuration of Rolling Locomotion Mode and Leg Joints' Position.....             | 79 |
| Figure 7-6. Front Left Leg of Cricket Kinematics Calculations.....                                  | 81 |
| Figure 7-7. Kinematics Calculation of Cricket in V-REP. ....  | 85 |
| Figure 7-8. Track-terrain Frictional Coefficient Tuning Process. ....                               | 87 |
| Figure 8-1. Top-down View of the Step-climbing Gait Using Leg Movement Strategy. ....               | 90 |
| Figure 8-2. Top-down View of the Step-climbing Gait Using Body Movement Strategy.....               | 90 |
| Figure 8-3. Initial Position of the Whole Body Climbing Gait.....                                   | 91 |
| Figure 8-4. Sub-phase 1 a: Move Body Backward, Move Front Legs Up. ....                             | 92 |
| Figure 8-5. Sub-phase 1 b: Move Body Forward, Move Front Legs Forward. ....                         | 93 |
| Figure 8-6. Sub-phase 1 c: Move Body Up and Forward, Move Front Legs Forward.....                   | 93 |
| Figure 8-7. Sub-phase 2 a: Move Body Forward, Moves Rear Legs Forward. ....                         | 94 |
| Figure 8-8. Sub-phase 2 b: Move Body Backward, Moves Front Legs Forward. ....                       | 94 |
| Figure 8-9. Sub-phase 2 c: Move Body Forward, Moves Rear Legs Forward.....                          | 95 |

|  |     |
|--|-----|
| Figure 8-10. Sub-phase 2 d: Move Body Backward, Moves Front Legs Forward.....                      | 95  |
| Figure 8-11. Sub-phase 2 e: Move Body Forward, Moves Rear Legs Forward.....                        | 95  |
| Figure 8-12. Phase 3: Move Body Forward, Steps Rear Legs Forward.....                              | 96  |
| Figure 8-13. Phase 3: Move Body Forward and Sideways, Steps Rear Legs Forward.....                 | 96  |
| Figure 8-14. The Foot and Body Displacement of the Whole Body Step Climbing Gait.....              | 97  |
| Figure 8-15. Rear Body Climbing Gait of Step Negotiation.....                                      | 98  |
| Figure 9-1. Overall Hierarchical Scheme of the Autonomous Locomotion Mode Transition Control ..... | 100 |
| Figure 9-2. The Refined Decision Making Process Flowchart.....                                     | 102 |
| Figure 9-3. Step Negotiation Power Comparison of the Rolling and Climbing Locomotion ...           | 104 |
| Figure 9-4. Energy Evaluations of the Step Negotiations using the Whole Body Climbing Gait.....    | 105 |
| Figure 9-5. Energy Evaluations of the Step Negotiations using the Rear Body Climbing Gait.         | 105 |
| Figure 9-6. Energy Consumption of Step Negotiation with $h_t$ height.....                          | 108 |
| Figure 9-7. Energy Consumption of Step Negotiation with $2h_t$ height. ....                        | 109 |
| Figure 9-8. Energy Consumption of Step Negotiation with $3h_t$ height. ....                        | 110 |
| Figure I. Standard D-H Method .....  | 121 |
| Figure J. Modified D-H Method .....  | 122 |
| Figure K. D-H Method in DeNOC Algorithm.....   | 124 |

## LIST OF SYMBOLS, ABBREVIATIONS AND NOMENCLATURE

| <b>Acronym</b>                   | <b>Definition</b>  |
|----------------------------------|--|
| AAF                              | Actively Articulated Frames  |
| COM                              | Center of Mass   |
| COG                              | Center of Gravity  |
| DARPA                            | Defense Advanced Research Projects Agency  |
| DeNOC                            | Decoupled Natural Orthogonal Complement  |
| DOF                              | Degree of Freedom  |
| DRC                              | DARPA Robotics Challenge   |
| EL                               | Euler-Lagrange   |
| EMF                              | Back Electromotive Force   |
| FD                               | Forward dynamics   |
| FK                               | Forward Kinematics   |
| GIM                              | Generalized inertia matrix   |
| ID                               | Inverse dynamics   |
| IK                               | Inverse Kinematics   |
| MCI                              | Matrix Convective inertia  |
| MSD                              | Mass Spring Damper   |
| NE                               | Newton-Euler   |
| NOC                              | Natural Orthogonal Complement  |
| PAF                              | Passively Articulated Frames   |
| PD                               | Proportional-Derivative  |
| USAR                             | Urban Search and Rescue  |
| VCI                              | Vector Convective Inertia  |
| V-REP                            | Virtual Robot Experimentation Platform   |
| <b>Roman Symbols</b>             | <b>Definition</b>  |
| $a_r, a_\phi$                    | Radial and transverse accelerations for stage 2 of the wheel model                           |
| $B_{i,i-1}, \dot{B}_{i+1,i}$     | Propagation matrix of twist and twist rate from link $i - 1$ to link $i$                     |
| $\mathcal{C}$                    | MCI  |
| $c_{i,i-1}$                      | Position vector from $C_i$ to $C_{i-1}$  |
| $d$                              | Step horizontal distance   |
| $d_{i-1}$                        | Position vector from $O_{i-1}$ to $C_{i-1}$  |
| $d_{comp}, \dot{d}_{comp}$       | Wheel deformation and its derivation   |
| $e_i$                            | Unit vector along the $i^{th}$ joint axis  |
| $E_r, E_w$                       | Energy consumption of the rolling and walking locomotion                                     |
| $E_{RW}, E_{Rr}$                 | Energy consumption of the whole body and rear body rolling                                   |
| $E_{CW}, E_{Cr}$                 | Energy consumption of the walking using the whole body climbing and rear body climbing gaits |
| $F_{h_{other}}$                  | The horizontal forces the other part of the vehicle exert on the modeled wheel               |
| $F_{fx}, F_{fy}, F_{Nx}, F_{Ny}$ | Frictional forces and Normal forces in $x$ and $y$ axis for wheel-terrain interaction model  |
| $F_{EX_r}, F_{EX_\theta}$        | Resultant forces of radial and transverse directional component                              |
| $f_i$                            | Resultant force applied at $C_i$   |

|                    |  |
|--------------------|--|
| $h$                | Step height  |
| $\mathbf{h}$       | VCI  |
| $h_t$              | Track height   |
| $h_B$              | Body height of the walking model   |
| $I$                | Inertia tensor of the wheel  |
| $\mathbf{I}$       | GIM  |
| $I_a$              | Motor armature current   |
| $I_i$              | Inertia tensor about $C_i$ of the $i^{th}$ link  |
| $k, c$             | Spring and damper coefficient of wheel model   |
| $K_{emf}$          | Back electromotive force constant of motor   |
| $K_p$              | Proportional coefficient   |
| $K_t$              | Torque constant of motor   |
| $l_1, l_2$         | Leg link 1 and 2 length of the walking model   |
| $M$                | One wheel mass of the simplified wheel model   |
| $M_i$              | Mass matrix of the $i^{th}$ link   |
| $M$                | Generalized mass matrix  |
| $\tilde{M}$        | Composite mass matrix  |
| $\tilde{M}_l$      | $\tilde{M}_l = N_l^T M \dot{N}_l$  |
| $\tilde{M}_\omega$ | $\tilde{M}_\omega = \tilde{M} \Omega$  |
| $\tilde{M}_e$      | $\tilde{M}_e = N_l^T W M N_l$  |
| $m_i$              | Mass of the $i^{th}$ link  |
| $N$                | NOC matrix of the velocity constraints   |
| $N_l, N_d$         | Decoupled matrix of NOC  |
| $n_i$              | Vectors of the resultant moment applied about $C_i$  |
| $P$                | Wheel center   |
| $p_i$              | Joint rate propagation vector  |
| $r_{i-1}$          | Position vector from $C_{i-1}$ to $O_i$  |
| $r_c$              | Step corner radius   |
| $r_w$              | Wheel radius for simplified wheel model  |
| $R_a$              | Electrical resistance of the motor   |
| $t_i$              | Twist of the rigid link $i$ in 3-dimensinal Cartesian space  |
| $t$                | Generalized twist vector   |
| $T_t$              | Threshold values of the proposed method  |
| $T_{wb}, T_{rb}$   | Threshold values determined by the walking locomotion using the whole body climbing and rear body climbing gaits |
| $U_a$              | Motor applied voltage  |
| $v_i$              | Linear velocity of the center of gravity ( $C_i$ ) of the $i^{th}$ link  |
| $\dot{v}_i$        | Linear acceleration of the center of gravity ( $C_i$ ) of the $i^{th}$ link                                      |
| $v_{contact}$      | Contact velocity between wheel and terrain   |
| $W_i$              | Angular velocity matrix of the $i^{th}$ link   |
| $W$                | Generalized angular velocity matrix  |
| $w_i$              | Wrench acting on rigid link $i$  |
| $w$                | Generalized wrench vector  |
| $w^E$              | External wrench  |
| $w^C$              | Constraint wrench  |

|                                       |  |
|---------------------------------------|--|
| $x, \dot{x}, \ddot{x}$                | Wheel position, velocity and acceleration with respect to $x$ axis                                 |
| $\dot{x}_d$                           | Wheel desired velocity   |
| $y, \dot{y}, \ddot{y}$                | Wheel position, velocity and acceleration with respect to $y$ axis                                 |
| <b>Greek Symbol</b>                   | <b>Description</b>   |
| $\gamma, \dot{\gamma}, \ddot{\gamma}$ | Position, velocity and acceleration with respect to radial axis for stage 2 of the wheel model     |
| $\theta_i, \dot{\theta}_i$            | Revolute joint angle, angular velocity of the joint $i$ for walking model                          |
| $\dot{\theta}$                        | Generalized joint rate vector  |
| $\mu_{static}, \mu_{dynamic}$         | Static and dynamic frictional coefficient  |
| $\tau$                                | Motor torque output  |
| $\phi, \dot{\phi}, \ddot{\phi}$       | Position, velocity and acceleration with respect to transverse axis for stage 2 of the wheel model |
| $\omega_i, \dot{\omega}_i$            | Angular velocity and acceleration of the $i^{th}$ link   |

## Chapter One: INTRODUCTION

Mobile robotics is a relatively young field when compared to the field of industrial robot arms, or robot manipulators which have already achieved enormous success in industrial manufacturing. However, all the major robotics institutions such as International Federation of Robotics and European Robotics Research Network predict that the world market of mobile service robotics is expected to increase dramatically over the next twenty years, surpassing the market of industrial robotics in terms of units and sales [1]. In contrast to robot manipulators which are typically fixed to the ground, a mobile robot can move through the given environment to fulfill its task. Thus, the first challenge in mobile robotics is locomotion itself. “How should a robot move? Why a particular locomotion style (e.g. walking, rolling, swimming, and flying etc.) is more appropriate than another alternative locomotion for a given mission? [2]” are some of the questions that a robot needs to determine while moving through any homogeneous or heterogeneous (rough or smooth, static or dynamic, etc.) environment.

Mobile robotic systems typically include three components: *i*) mechanisms which are capable of exerting forces and torques on the environment, *ii*) a perception system for sensing the world, and *iii*) a decision and control system which modulates the robot's behavior to achieve the desired ends [3]. The goal of the mechanisms design within the scope of this work is to gain superior locomotion characteristics and high mobility for robots to operate in either terrestrial, aquatic, or aerial domains or a combination of them. In the terrestrial or ground robots area, two most commonly employed mechanical designs for locomotion are wheels/tracks and legs [1, 4]. Powered wheels are a great human invention that can achieve extreme efficiency in terms of velocity and energy on flat hard terrains, but suffer on uneven, rough, and soft terrains. Articulated leg, on the other hand is the simplest bionic approach that can be used to transverse a

wide variety of rough environments over a wide range of terrains. The efficiency of wheeled locomotion vehicles depends significantly on the terrain's environmental quality, especially the flatness and hardness of the terrain surface properties. In contrast, the efficiency of legged locomotion systems depends on leg and body mass rather than on the robot's interaction with the terrain, however, legged locomotion suffers from its inherent greater mechanical complexity when compared to wheeled locomotion due in part of the higher Degrees of Freedom (DOF) required for walking locomotion [5].

Robots, however are often required to operate in situations where wheels and legs are required. For robots used in Urban Search and Rescue (USAR), for example, operation environments include both flat ground such as concrete/wooden floors as well as rough terrains such as steps/stairs as well as unstructured surfaces such as rubble. Legged robots offer good maneuverability in rough terrain but are inefficient on flat ground and need sophisticated control for any type of walking gait needed to be used. Wheeled/tracked robots are very efficient to move around on flat surfaces, but are inefficient and in some cases incapable of negotiating rough terrains.

Hybrid solutions, combining the adaptability of legs with the efficiency of wheels/tracks, offer a fascinating compromise. In the 2015 DARPA Robotics Challenge finals (DRC, a ground robot competition aiming to executing complex tasks in dangerous, degraded, human-engineered environments [6]), four of the five top teams robot designs combined legged and wheeled/tracked locomotion (Figure 1-1). Within the context of this thesis, robots having more than one locomotion mode are referred to as "Hybrid Robots". Although not guaranteed, the use of hybrid mobile robots indicate a superiority over non-hybrid mobile robots for challenging tasks.



a

b

c

d

**Figure 1-1.** a) DRC-HUBO from KAIST [7], b) CHIMP from Carnegie Mellon University [8], c) Momaro from University of Bonn [9], and d) RoboSimian from JPL [10], Respectively.

## 1.1 Overview of Current Hybrid Robots

Despite a number of research and development in designing mobile robots for locomotion in diverse environments (ground, air and water) has been conducted for decades, there is no current system that can operate with the fluidity and agility of animals in the real world. In an attempt to improve this researchers are looking into multi-modal (mechanical and control) locomotion [5]. Multi-modal locomotion aims to extend the mobility of the robots to operate and transition within multiple environment domains, and thus enabling robots to have multiple locomotion styles.

Multi-modal locomotion is gaining increasing interest in robotics research as it improves the robots' environmental adaptability, the locomotion versatility, and operational flexibility [11]. Prior research includes locomotion mode transition between flying and terrestrial locomotion modes [12], swimming and terrestrial locomotion modes [13] , as well as transition between different terrestrial locomotion modes [5]. Within terrestrial multi-locomotion robots, and due to their excellence in both locomotive efficiency (in terms of velocity and energy) and rough terrain negotiation abilities [14], the majority of the proposed hybrid robots in the past decades are wheel/track-legged systems [1].

In general, hybrid robots have three main technical complexities [15]: *i*) locomotion control needed to perform appropriate motions within each of their individual locomotion mode [14, 16-18], *ii*) Transition phase control to enable the change from one locomotion mode to another [14, 16, 17, 19], and *iii*) Decision-making process to facilitate the selection of the most appropriate locomotion mode available in the current conditions [15, 20, 21].

The main advantage of hybrid robots stems from their multiple (two or more) locomotion modes, among which robots can select from depending on the encountered terrain conditions. However a proper locomotion mode transition control needs to be available to take full advantage of the expected hybrid robots' locomotion mobility. Unlike modular robots [22], where reconfiguration control indicates a method that transforms a given robotic configuration to a desired configuration via a sequence of module detachments and reattachments [23], the locomotion mode transition control of hybrid robots typically refers to the decision-making process that select the most appropriate locomotion mode among the multi-locomotion modes available to the robot. Locomotion transition can either be realized by “supervised autonomy” [24], where transition decisions are made by operators; or autonomously where robots switch between locomotion styles automatically based on pre-determined criteria and mechanisms [21]. The supervised locomotion transition control requires continuous human-robot interaction, which is not always available or reliable [25], especially when robots are used in confined and complex environments such as those encountered in USAR tasks and other purposes where operators don't have a complete situational awareness to make effective decisions.

## 1.2 Cricket Robot Platform

In this thesis, work on autonomous locomotion mode transition of ground hybrid robots is conducted. The goal of this thesis is to enable robots to effectively switch between locomotion

modes when needed. Even the goal of the proposed locomotion mode transition method will be applicable to diverse hybrid robots, the research reported in this thesis will be based on a hybrid robot shown in Figure 1-2 that has been being developed at the University of Calgary since 2009 [26, 27]. In this section, the robot, named Cricket, is to be described from a locomotion perspective point of view.

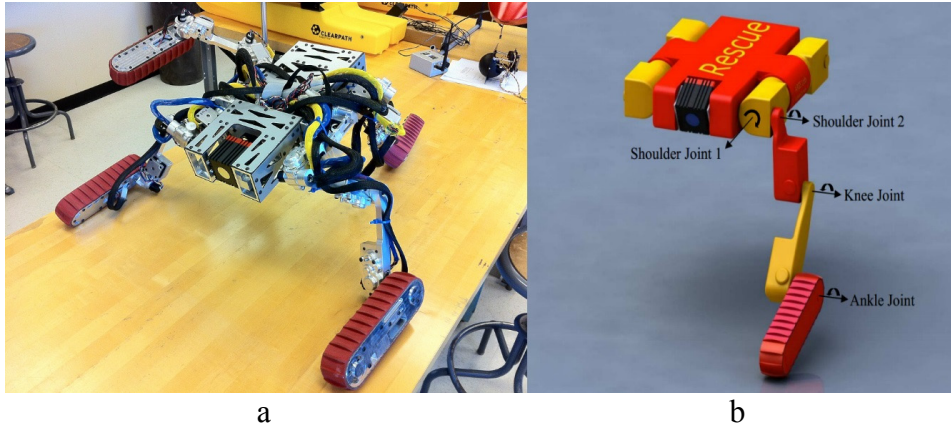


**Figure 1-2. a) Robot (Cricket) Prototype and b) Its Leg Joints Layout [26].**

As shown in Figure 1-2, the robot's locomotion system resembles a hybrid quadruped robot with four revolute joints in each leg. The tracks on the original robot design can be replaced with wheels or any other feet configurations, if desired. Each leg comprises four component, i.e. shoulder, proximal, distal, and track shown in Figure 1-3. The leg joints are arranged as a pair of shoulder joints, a knee joint, and an ankle joint shown in Figure 1-2b. In addition to the four revolute joints, each leg features a drivable track encircling the outermost leg segment, which allows the robot to drive in similar fashion to conventional skid-steer tank robots. Furthermore, the robot is capable to perform sophisticated maneuvers not possible by traditional tracked vehicles such as walking in diverse gait patterns and ladder climbing [28].

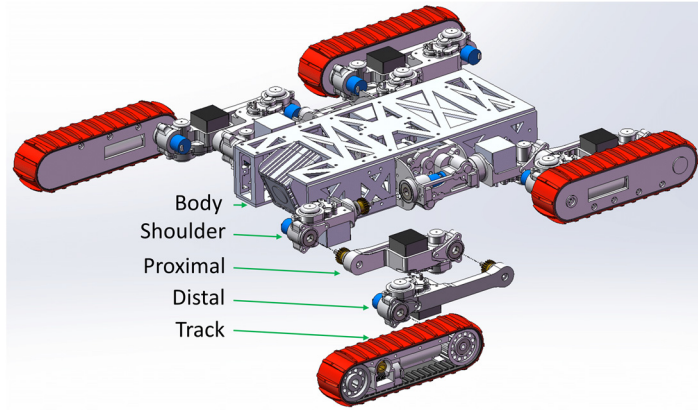


**Figure 1-3. Cricket Leg Mechanical Design Layout.**

The locomotion system of the Cricket robot enables two main forms of movement, walking for traversing complex rough terrain, and rolling using treads or wheels for efficient travel on open semi-flat terrains. These two locomotion modes are referred as walking and rolling locomotion within the context of this thesis. Besides, the robot can also perform vertical climbing activities, but these aren't considered within the framework of this research. Different possible locomotion geometries that can be executed by the robot are shown in Figure 1-4. In Figure 1-4a, the robot moves in a hybrid locomotion style combining walking and rolling simultaneously. Figures 1-4b and 1-4c show examples of different leg configurations that can be executed during rolling locomotion. Figure 1-4d illustrates a case when the front left leg is changing its locomotion mode from rolling to walking. Figure 1-4e shows a vertical climbing locomotion example while Figure 1-4f illustrates a case of a challenging rough terrain and obstacle negotiation ability which the robot is theoretically capable to achieve.

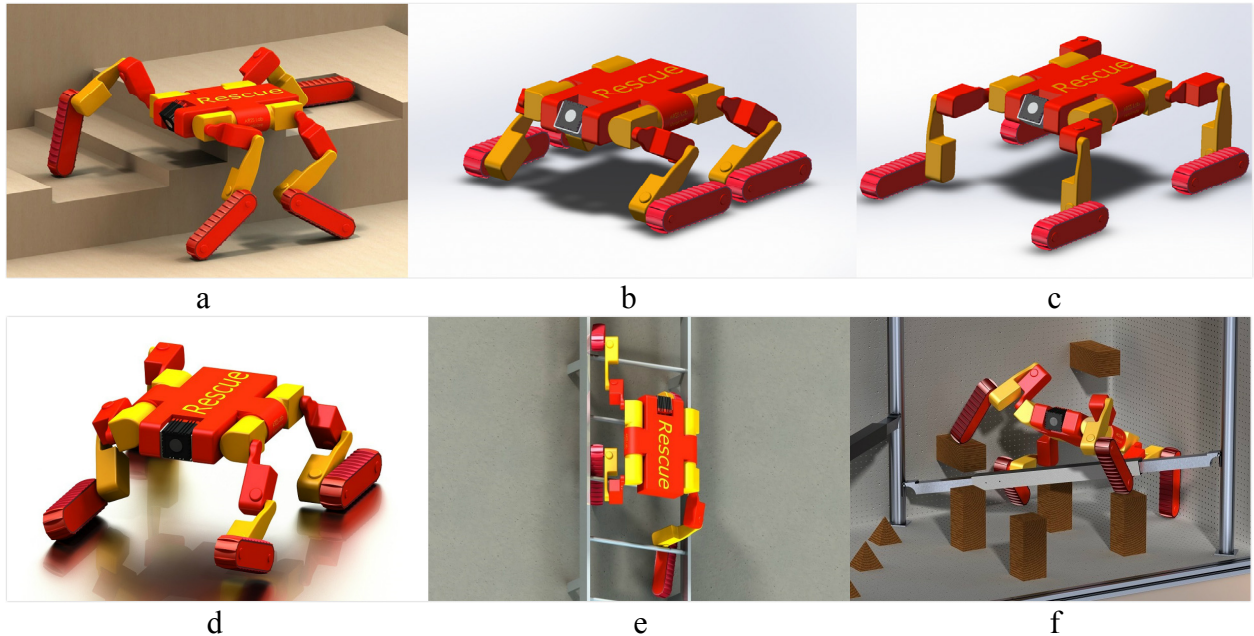


**Figure 1-4. Locomotion Modes of Cricket in Different Configurations [27].**

From these locomotion examples, it can be seen that the robot has the capability to raise or lower its center of mass (COM) to enhance its stability during its motion. Other capabilities include tilting of the body as shown in Figure 1-5 to overcome challenging spaces including small confined spaces.

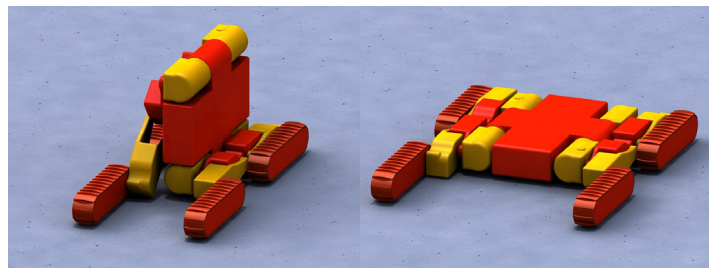


**Figure 1-5. Body Titling Configurations to Overcome Small Confined Spaces [27].**

### 1.3 Outline of The Thesis

This thesis is organized in four parts: The first part including Chapter 1, 2 and 3 is the introduction, literature review and proposed work, in which the state-of-the-art research overview, problem statement, proposed solution, and the proposed contribution are specified.

The second part consisting Chapter 4, 5, and 6, presents the simplified dynamics modeling methods of the rolling locomotion mode, the walking locomotion mode of ground hybrid robots, and the energy evaluations of the two locomotion modes, respectively. The third part including Chapter 7, 8, and 9 explains the physical modeling process of Cricket and environment parameters setting in a robotics simulation package, the development of two climbing gaits to negotiate steps with different height, and simulation results of Cricket using the proposed autonomous locomotion mode transition method, respectively. The final part is conclusion and future work summarized in Chapter 10.

## Chapter Two: LITERATURE REVIEW

Terrestrial or ground hybrid robots are systems developed to move on the top of diverse surfaces including homogenous and heterogeneous terrains which present different challenges. This chapter surveys related work of locomotion mode selection/transition of ground hybrid robots where all available locomotion modes enable the given robot to move on-top of ground surfaces. Hybrid robots in aquatic or aerial domains, although interesting, are out of this research scope.

### 2.1 Ground Hybrid Robots

This section sets out to review the state-of-the-art of the locomotion mechanical designs of ground hybrid robots. The focus is on robots having a combined wheel/track plus leg systems used to negotiate uneven terrains and to overcome complex environment such as step/stair obstacles.

Wheeled/tracked robots with articulated frames can be separated into two categories: those having passively and actively articulated frames. If the wheels/tracks can perform actuated relative motions with respect to the main body, then such wheel/track mechanisms are considered as legs, as a result these vehicles are considered wheel/track-legged hybrid robots.

#### 2.1.1 Wheeled/tracked robots with Passively Articulated Frames

Robots with wheels/tracks having passively articulated frames (PAF) are not typically considered hybrid robots. However, due to mobility of their passive joints, these robots can adapt their configuration to the encountered ground, thus significantly reducing resistance when overcoming obstacles and traversing rough terrains when compared with traditional wheeled robots having non-articulated frames [29]. These type of robots are quite common and have been used in space robot designs. Figure 2-1 shows examples of this type of robots include the rocker-

bogie type rovers Spirit and Opportunity (Figure 2-1a) developed by NASA [30] for Mars exploration, SOLERO (Figure 2-1b) based on the original Shrimp robot design [29], and CRAB (Figure 2-1c) developed by the European Space Agency [31, 32] for planetary exploration.



**Figure 2-1. a) Spirit and Opportunity Mars Rover [30], b) SOLERO [31], and c) CRAB II Mars Rover [32], Respectively.**

PAF robot designs are also commonly used to improve negotiation of uneven terrains and steps/stairs climbing abilities of non-articulated tracked robots. Examples of such robots include the Robhaz DT3 and DT5 (Figure 2-2a) developed by the KIST Intelligent Robotics Research Center [33], and Gunryu (Figure 2-2b) developed by the Hirose-Fukushima Robotics Lab [34].



**Figure 2-2. a) Robhaz DT3 [33] and b) Gunryu [34].**

### ***2.1.2 Wheeled/tracked robots with Actively Articulated Frames***

Plenty and diverse wheeled/tracked robots with Actively Articulated Frames (AAF) designs have been proposed in recent years [1, 4, 35]. Thus, instead of merely reviewing AAF

robots by their mechanical design category, i.e. wheel-legged, track-legged, wheel-tracked, and wheel-track-legged, this section will survey wheel/track-legged hybrid robots in the locomotion mode transition perspective. The four robots described in Figure 1-1 that participated in the DRC finals in 2015 are the latest designs in this category. However, due to the complexities associated with their locomotion control for all these state-of-the-art AAF robots, their locomotion mode transition has been realized by the supervised autonomy approach [7, 24, 36, 37].

In an effort to extend supervised autonomy, several solutions have been proposed to increase the locomotion mode transition autonomy by utilizing particular mechanical designs such as the Epi.q-TG robot [38]. The Epi.q-TG (Figure 2-3) is a quadruped wheel-legged robot equipped with a wheeled locomotion unit comprising three wheels on each leg. The front unit is actuated by a single motor via a customized epicyclic gearing system that is designed to suitably switch between wheeled and legged locomotion mode [38]. When the robot bumps against an obstacle, if the friction between the front wheel and obstacle is sufficient to stop the wheel, the epicyclic gearing starts to work in such a way switching the robot to overcome the obstacle in a pre-specified automatic walking mode. Thus the robot automatically changes locomotion mode from rolling on wheels (advancing mode) to stepping on legs (automatic climbing mode) passively according to local friction and system conditions without any active sensing and control.



**Figure 2-3. Epi.q-TG Mechanical Hybrid Robot [38].**

Quattroped hybrid robot [35] is another mechanical design example that improves the locomotion mode transition autonomy (Figure 2-4). In contrast to most hybrid platforms that have separate mechanisms for wheels and legs, the Quattroped robot is implemented with a unique designed transformation mechanism that directly switches the morphology of the driving mechanism between the wheels and the two DOF leg. Switching between wheeled and legged modes is achieved by a particular designed mechanism that alters the shape of the circular rim of the driving mechanism as illustrated in the bottom part of Figure 2-4.

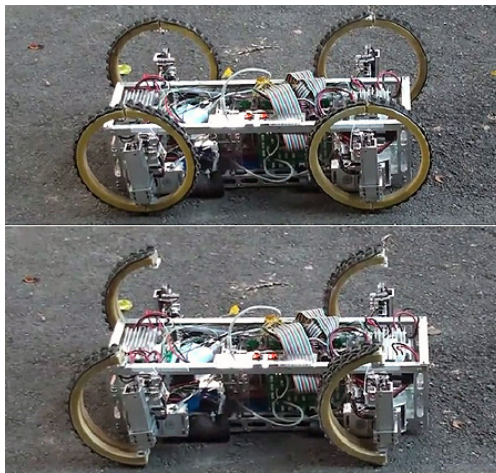


**Figure 2-4. Quattroped Mobile Hybrid Robot [35].**

## **2.2 Autonomous Locomotion Mode Transition**

Very limited research and development has been done in the area of ground hybrid robots' autonomous locomotion mode transition via on-board decision-making techniques. However, works on autonomous gait transition using criterion based decision-making method of legged locomotion has been extensively investigated [39, 40]. Their changing gait criteria are derived based on diverse criteria such energy, time efficiency, and the robot's stability margin [41-43]. Although walking locomotion (bipedal, quadruped, hexapod, etc.) systems have many difference to hybrid robots, their works provide references to design locomotion transition criteria of hybrid robots.

Within the reviewed literature, one of the first automatic locomotion transition research is the development of the Russian Moon Rover wheel-walking robot [44]. In their study, Russian and European robotic engineers faced the challenge of developing an automatic locomotion mode module to switch between rolling and walking. They proposed three solutions with different level of automation: mechanics-only, pre-programmed, and an autonomous feedback solutions using sensors' information for the automatic locomotion mode transition [21]. In the former two solutions, the locomotion switch is a pre-determined process with no decision-making module involved, while in the autonomous feedback solution, the vehicle executes the locomotion switch based on onboard sensors' feedback that measure the terrain characteristics and the robot's internal states [21]. For example, when an obstacle is found to be non-traversable via rolling locomotion or when wheel slippage is excessive, the locomotion system automatically switches from rolling to walking mode.

Although mechanics and pre-programmed solutions have improved the autonomy of the robot's locomotion mode transition, the complete autonomous solution is far behind and it's still

in the initial stage of development. One of the significant challenges to realize the automatic locomotion transition is the requirement of an effective sensing method to evaluate the vehicle-terrain interaction characteristics (also known as terramechanics) and terrain parameters reliably and efficiently. The terramechanics methods for modelling wheel-soil or vehicle-terrain interaction are based on identification of soil properties, which requires significant in-place measurements of soil characteristics prior to robot being deployed [45, 46]. Moreover, the terramechanics model methods that try to predict the robot-terrain interaction are heavily computational expensive [47]. So terramechanics based vehicle-terrain interaction evaluation are inadequate to be used for autonomous locomotion mode transition directly [21], especially when robots are required to operate at high speed such as in USAR operations.

One of the earliest and essential research of locomotion mode transition of hybrid robots has been reported in [48, 49], where the performance of three locomotion modes of a quadruped wheel-legged robot named HyLoS, purely rolling, rolling with reconfiguration, and peristaltic walking mode on different soils are evaluated and compared using the grade-ability (i.e., the maximum slope that a vehicle can climb without compromising the vehicle's stability or its ability to move forward) and the power consumption criterion. These two criteria have been developed with terramechanics models assuming that the vehicle-ground mechanic properties as well as the digital evaluation maps of the terrain (from a stereovision system) are known [50]. Based on the grade-ability and power consumption performance of three locomotion modes, a hierarchical control scheme was developed to conduct the locomotion mode selection (external loop) and each locomotion motion control (internal loop). However, despite its potential, no continued work related to decision-making of the autonomous locomotion mode transition using the grade-ability and power consumption criterion has been conducted. Even though

effectiveness of performance evaluations of locomotion mode using the propose criteria was showed, it is very difficult, if not impossible, to identify if the criteria are applicable to perform the locomotion mode transition control without verification, especially the grade-ability criterion was developed based on a terramechanics model [49].

Autonomous locomotion mode transition research of a humanoid robot with biped walking, quadruped walking, and ladder climbing locomotion modes reported in [19, 20] is very enlightening for hybrid robots. In their work, researchers have successfully realized autonomous locomotion transition between bipedal and quadruped walking. The locomotion selection method has been developed based on a cost function to evaluate the locomotion reward [15]. The locomotion reward is defined as an evaluation of the falling risk and the robot's moving velocity. With such evaluation the robot selects its locomotion mode based on the locomotion reward values. The falling risk was proposed as an indicator to evaluate system stability using Bayesian Network theory which combines environmental information (via force and laser range sensors) and sensing errors estimation [15, 20]. However, unnecessary locomotion mode transitions have been observed due to minor robot states disturbance that hasn't been resolved [19, 20]. These aspects have prevented efficient autonomous selection application of locomotion mode. As a result, such proposed locomotion mode transition method can't be directly applied to hybrid robots which have greater locomotion challenges.

Within the reviewed literature, WorkPartner [51] is the only publication that presents a mechanism with the ability to switch between two different locomotion modes automatically, i.e. rolling and rolking (rolling and walking simultaneously). Such proposed mechanism is based on criteria derived using the concept of power consumption, wheels slippage, and wheel-terrain interaction resistance forces [21]. The technique can be implemented using either a single

criterion or a combination of weighted criteria. When the decision-making is made based on a single criterion, a time or a distance window is used to confirm the actual need of locomotion mode transition to reduce some unnecessary transition because of system noise. For example, when the power consumption pass over the threshold value for more than two seconds in rolling locomotion mode, the robot switches from rolling to rolking; when the robot travels one vehicle length in rolking locomotion mode, the robot transform from rolking to rolling. Here, two second is the time window and one vehicle length is the distance window. When the decision-making is made based on a weighted sum of several criteria, the mode change occurs immediately when the weighted sum is bigger than a certain pre-determined value. The proposed approach allows weights to be customized depending on the task the robot is going to perform. The biggest contribution of this approach is that it integrates individual criterion into a cost function as the decision-making part of the locomotion mode transition control system. However, a number of challenges remain to be solved in determining the threshold values for each proposed criterion and the weights of each criterion for their integration as the decision-making cost function.

When determining each criterion weight of the cost function, no method has been proposed [21], so the selection of the weights has been left to the users which is not pragmatic for a system. The most important parameter, the threshold value of each criterion, has been “set to” a value based on experimental data collected by moving the robot through limited different terrain conditions where rolling and rolking locomotion styles are both needed to effectively transverse over the various terrains. As a result, the threshold value varies between different vehicles and terrains, and these numbers have to be determined beforehand in order to perform the transition control. All above mentioned developments and associated issues and challenges

indicate the complexities associated to realize an autonomous locomotion mode transition of hybrid robots.

### **2.3 Observations**

From this literature review it is concluded that improved criterion is needed to realize the fully autonomous locomotion mode transition of hybrid robots. Following previous developments, such criterion can continue to be developed based on various parameters including external environment information such as texture maps of the terrain, and internal states of the robots such as stability, energy consumption, and velocity.

Within the reviewed literature, WorkPartner [51] is the only one successfully realized automatic locomotion mode transition between two different locomotion modes: rolling and walking. Current methods can't be used without a priori conducting extensive experiment tests on the targeted terrain with afterward threshold values tuning work. More importantly, the proposed criteria found in the literature are derived based on the internal states of robot without considering any external environment information. This causes in diverse instances serious troubles such as the local minima [52], which don't account that the decision-making process needs to be made considering the encountered terrain parameters faced by the robot.

## Chapter Three: **PROPOSED WORK**

### **3.1 Problem Statement**

The ultimate goal of autonomous locomotion mode transition research of hybrid ground robots is to enable robots to transverse terrains using the fullest of their hybrid locomotion advantages, i.e. each individual leg determines its most appropriate locomotion mode during their motion. Due to its efficiency and simplicity, rolling is the default locomotion mode of the majority of hybrid ground robots [53]. So ground hybrid robots start to move in rolling locomotion mode, switch to walking locomotion mode when needed, and transform back to rolling locomotion mode when challenging terrain negotiation is finished. From the literature review, it was observed that there are a number of problems that have to be solved in order to fully realize autonomous locomotion mode transition of ground hybrid robots. Some of such problems include:

- 1) New Locomotion control strategies to improve the rolling locomotion mobility by changing the chaise (articulated legs) configuration of ground hybrid robots,
- 2) New Locomotion control strategies to improve the walking locomotion mobility by developing various walking gaits to negotiate homogeneous or heterogeneous environments,
- 3) Solve the complexities associated with the locomotion transition phase to enable smooth changes from one to another locomotion mode,
- 4) Novel transformation mechanical mechanism design customized to different hybrid robots,
- 5) Solve the complexities associated with sensor data analysis to evaluate the surrounding environment conditions of hybrid robots,

- 6) Novel locomotion mode transition strategy to enable the automatic selection of the most appropriate locomotion mode based on current environment situations,
- 7) New criteria to evaluate the locomotion performance of hybrid robots efficiently and generically.
- 8) Etc.

It must be noted that many other challenges exist, but not mentioned herein to keep the problem bounded/focus to a few manageable aspects while still being able to enable ground hybrid robots locomotion mode transition automatically. Due to the large scope of problems in the arear of locomotion mode transition of ground hybrid robots, in this thesis the focus is on problem 6 and 7. The reason why such aspects were considered and no the other ones is due to the fact that a solution for these two aspects provide a generic solution that can be applied to different hybrid robots to realize the autonomous locomotion mode transition as well as provide a stepping stone what will lead to help resolve the rest of other challenges. Thus, the specific problem to be solved in this thesis is described as follows:

***Develop a generic criterion based decision making mechanism to enable autonomous locomotion mode transition of ground hybrid robots.***

The following sections provide a brief outline of the proposed solutions that have been conducted to solve this problem.

### **3.2 Assumptions and Constraints**

Due to the diverse challenges associated to fully solve the specified problem, a set of assumptions and constraints are made in order to achieve a reachable contribution.

### ***3.2.1 Assumptions***

1. Robot is considered as a rigid body. In the multibody dynamics modeling for the robot of interest, the body and legs are considered to be 100% rigid. It's only considered that wheels/tracks of the robot can deform (elastically).
2. It's assumed that all terrains when the robot transverses don't deform. That is, only hard and solid surfaces are considered.
3. All needed terrain geometric data is available. This research won't deal with any perception technology. All required geometry data of the environment obtained by the perception system is assumed to be available.
4. Sensor data is 100% accurate. The data obtained from sensors is always accurate, sensor errors and their potential effects/management is outside the scope of this research topic. Thus, uncertainties faced due to sensor errors won't be dealt with.
5. It's assumed that during the robot motion, the front and rear legs always negotiate the same terrain conditions. That is, the front two legs and rear two legs are only allowed to be in contact with surfaces having the same properties (e.g. roughness), and the surface properties of front and rear legs can be different.

### ***3.2.2 Constraints***

1. This research focus on the ground quadruped wheel/track-legged hybrid robots. This thesis researches ground hybrid robots with the mechanical design that the outermost leg segment of each leg is a drivable wheel/track, which allows robots to drive in similar fashion to conventional car/tank robots as well as perform sophisticated walking maneuvers not possible by traditional wheeled/tracked vehicles. The schematics of these

robots are shown in Figure 3-1. Figure 3-1a represents a quadruped wheel-legged hybrid robot while Figure 3-1b denotes a quadruped track-legged hybrid robot.

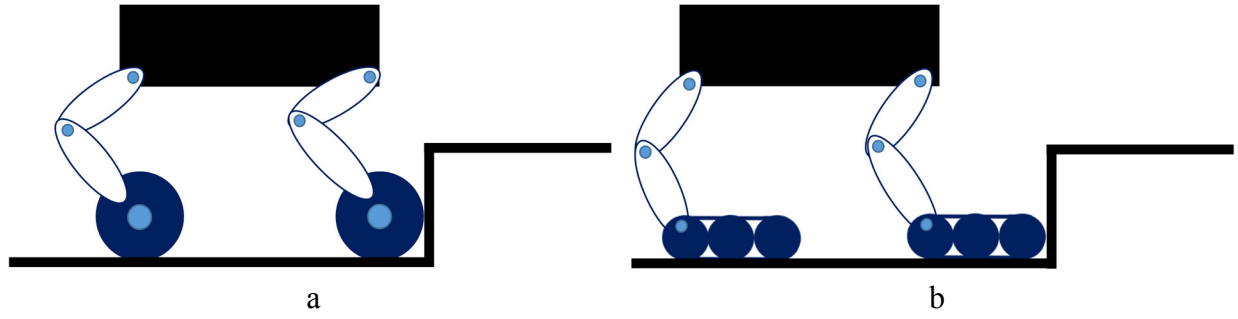


**Figure 3-1. Schematics of Ground Quadruped Wheel/track-legged Hybrid Robots.**

2. This work will only deal with locomotion mode transition between rolling and walking. The research won't dealing with combined locomotion mode (e.g. rolling, simultaneous rolling and walking locomotion mode).
3. This research will address the rolling locomotion via a fixed configuration. Thus, the configuration of the robot during the rolling locomotion won't change, i.e. the link joints of all legs are fixed, thus the robot will move (roll) as a traditional wheeled/tracked vehicle with its body (chassis) fixed on a given configuration. No strategies by changing the chassis configuration to gain more locomotion motility in rolling locomotion mode will be researched.
4. This research won't consider body-terrain interactions such as collisions. All vehicle-terrain interactions will be constrained to wheel/track-terrain interactions. Thus, the interaction or collision between the robot's body and terrains are out of the research scope.
5. The research will only consider locomotion mode transition application where steps' climbing up negotiation are handled as illustrated in Figure 3-1. The steps/stairs are a

commonly challenging terrain in human made environment. Moreover, heterogeneous terrain profiles such as slopes can be approximated by step shaped terrains. In other words, this research won't consider stepping down from steps as it's assumed that pure rolling locomotion is able to overcome such situations safely.

6. This research won't work on walking gaits optimization. The walking gaits to be proposed will follow the static stable method. Even the to be proposed walking gaits will be able to negotiate steps with different heights properly, no technique will be applied to optimize the proposed walking gait with respect to any criterion (e.g. minimum torque, leg displacement, and power etc.).

### **3.3 Proposed Approach**

Under above assumptions and constraints, the proposed approach to the specified problems is divided into four specific tasks that is described below:

1. An energy consumption criterion is proposed to evaluate locomotion modes' performance of hybrid robots. Rather than particular mechanical designs [35, 38], and the use of criterion only applicable to evaluate one locomotion mode of the multi-locomotion modes of hybrid robots (e.g. slippage of wheels/tracks can only evaluate rolling locomotion performance [21], falling risk can only evaluate walking locomotion performance properly [15]), the criterion used as the decision-making process in this research is to generic enough to evaluate the performance of multiple locomotion modes, including rolling, walking, climbing, and even jumping locomotion modes of various hybrid robots. Thus, an energy evaluation based criterion is proposed to meet the desired genericity.

2. The rolling locomotion mode performance is to be developed. This performance can be evaluated either by
  - i. Predicting energy consumption of rolling locomotion mode using the terramechanics models solution, or
  - ii. Measuring energy consumption to reflect the locomotion performance of rolling locomotion mode.

In this research, the second method has been selected due to the reason explained in the literature review.

3. The walking locomotion mode performance evaluation is to be developed and used in cooperation with the rolling performance to guide the locomotion mode transition. The proposed approach need to
  - i. Use proper walking gaits to negotiate steps with different heights, and
  - ii. Predict energy consumption of walking locomotion mode by developing dynamics model of the robot with a high computational efficiency.
4. The last task is to determine threshold values of criterion to be used in the locomotion mode transition method rather than using the traditional empirical values. In the proposed energy based locomotion mode transition criterion, the threshold values will be determined by the energy performance of walking locomotion mode.

### ***3.3.1 Outline of the Proposed Work***

In order to solve the problem stated in section 2.1 within above assumptions and constraints, the work will be performed in a series of four steps where each one provides the stepping stone and information needed by the subsequent steps as shown in the flowchart in Figure 3-2.

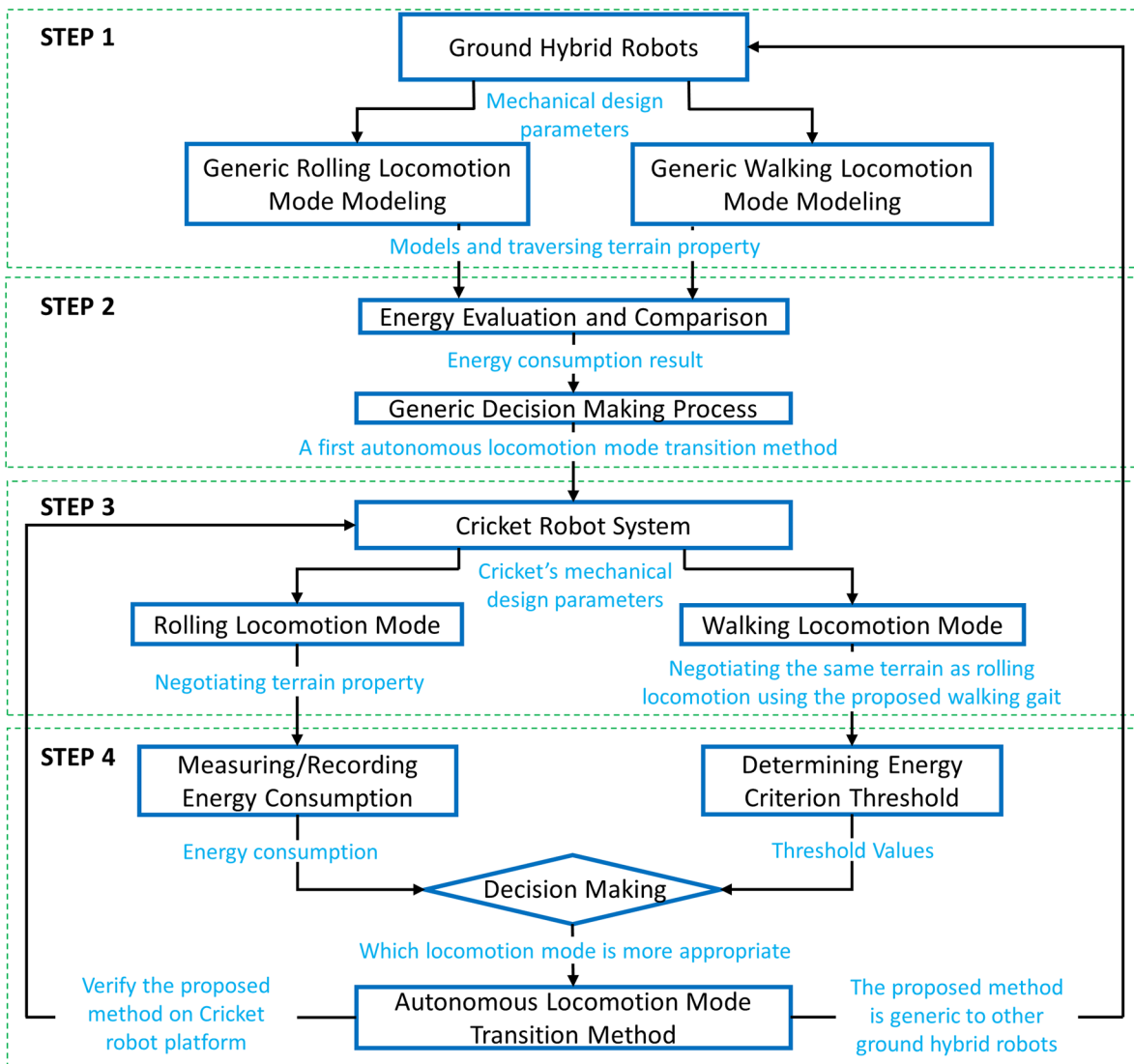


**Figure 3-2. Work Flowchart Steps to be Performed in this Research.**

STEP 1) Simplified dynamics modeling methods of rolling and walking locomotion modes of ground hybrid robots will be developed. The mechanical design of ground hybrid robots shown in Figure 3-1a will be used to develop the dynamic models. Due to the complexity of the wheel-terrain interaction modeling, only the basic fundamental properties, i.e. friction and deformation of wheels, will be considered in the rolling locomotion mode modeling. Here, the modeling method of the rolling locomotion mode

developed in this research aims to provide a fundamental energy evaluation of the generalized rolling locomotion mode. Even though the wheel-terrain interaction evaluation method using the terramechanics models have a higher accuracy, it's an ongoing academic challenge, and it can't be directly used for autonomous locomotion mode transition due to the reason specified in the literature review, thus it isn't the topic of this thesis. This part will be explained in Chapter Four.

For the walking aspects, a recursive multibody dynamics modeling algorithm will be employed with the goal to enable the walking locomotion model applicable to predictive calculations of energy evaluations efficiently and accurately. This will be explained in Chapter three. This part will be described in Chapter Five.

STEP 2) In the second step, energy evaluations between rolling and walking locomotion are characterized for ground hybrid robots. For this, the models developed in step 1 are used to negotiate steps shown in Figure 3-1. With the energy evaluation results, a first autonomous locomotion mode transition method is then proposed. This tentative method will be applied to the Cricket robot and be refined based on the results of steps 3 and 4. This step is to be explained in Chapter Six.

STEP 3) The research follows with simulation tests on the Cricket system. Due to the complexity of the vehicle-terrain interaction modeling and collision dynamics, a robotics simulation software is used to evaluate the proposed locomotion performances generated in step 2. A model of Cricket will be developed in the robotics simulator based on the real mechanical design parameters. The goal of this work is to make the rolling locomotion mode energy evaluation more reliable as well as to reduce the motion control (kinematics and dynamics) complexity of the walking locomotion mode (to be described in Chapter

Seven). Two walking gaits are proposed to negotiate steps with different heights. These gaits are then used to generate a proper step negotiation locomotion and to evaluate the energy consumption of the walking locomotion mode (to be explained in Chapter Eight).

STEP 4) In the fourth and final step of this research, the energy consumption of a step negotiation process where different step heights in the walking locomotion mode are evaluated. Then, a set of threshold values of the locomotion mode transition criterion are determined. A decision making process will be employed to determine which locomotion mode is more appropriate based on the energy criterion. Finally, the envisioned autonomous locomotion mode transition method is completed and refined. This work will be employed the Cricket robot as a test bench without losing genericity for the proposed approach to be applied to other type of hybrid robots as the ones shown in Figure 3-1 and Figure 1-1. This step will be described in Chapter Nine.

### **3.3.2 *Summary***

The proposed energy performance will be developed and used as the criterion to evaluate which locomotion mode of hybrid robots' multi-locomotion modes is more appropriate to the encountering terrain conditions, with such approach a decision making process will be developed to realize an autonomous locomotion mode transition between tow locomotion modes (rolling and walking). The energy evaluation of the rolling locomotion mode is intended to be performed in real time as the robot moves. This will be achieved by measuring motors' voltage and current. However, in contrast to no predictive evaluations of rolling locomotion mode will be made, the walking locomotion energy performance will be either a beforehand or predictive evaluation.

On the one hand, the energy evaluation results of the walking locomotion mode will be obtained by performing case studies of robots' terrain negotiation. The obtained results will be

used to determine a set of energy threshold values to be employed during the decision making process for the autonomous locomotion mode transition realization. On the other hand, the energy evaluation of the walking locomotion mode will be realized by predictive calculations employing the developed multibody dynamics models of robots. Due to the complexity of the intended goal, such calculations will be conducted using a specific set of designed walking gaits generated based on the encountering terrain conditions.

### **3.4 Proposed Contributions**

The goal of this research is to propose a criterion based method to realize the locomotion mode transition of ground hybrid robots automatically. To achieve this goal, the proposed contributions of this thesis are:

1. Develop a simplified dynamic modeling method for the rolling locomotion mode of wheel/track-legged hybrid robots. The developed method is a general dynamics model of the wheel-terrain interaction without being specific to one particular robot. Thus, the method can be used to provide a fundamental dynamics evaluation of the rolling locomotion mode of hybrid ground robots.
2. Develop a generalized dynamic model for the walking locomotion mode of wheel/track-legged hybrid robots employing an efficient multibody dynamics algorithm, Decoupled Natural Orthogonal Complement (DeNOC). The model will be developed based on the general mechanical structure of wheel/track-legged robots as shown in Figure 3-1, thus it's applicable to the walking locomotion modeling of all these wheel/track-legged robots.
3. Propose a novel criterion to evaluate the locomotion performance of ground hybrid robots efficiently. The contribution of the proposed energy criterion to evaluate the locomotion

performance of the ground hybrid robots is that it considers both the internal states of the robot and the external environment information.

4. Propose a new rule to determine the criterion threshold values for locomotion mode transition. In the energy criterion, the threshold value is determined by the energy performance of the walking locomotion mode instead of being defined as an empirical number.
5. Propose step negotiation gaits of the walking locomotion mode to realize a proper locomotion performance. The gaits are generated considering the step height information. Even though these gaits are proposed based on the Cricket robot, they can be used for a wide range of quadruped wheel/track-legged robots.
6. Develop a generic method to realize the autonomous locomotion mode transition of ground hybrid robots for the step negotiation. This work is one of the pioneering researches in realizing the autonomous locomotion mode transition of ground hybrid robots, thus the method is a contribution by itself.

## Chapter Four: ROLLING LOCOMOTION MODELING

This Chapter develops a simplified model for the rolling locomotion mode of hybrid wheel/track-legged robots. The purpose of the simplified wheel-terrain model, together with the generalized walking locomotion model in Chapter Five, are to provide preliminary energy evaluations in Chapter Six, is not to contribute an accurate terramechanics modeling method.

When hybrid robots transverse over terrains in rolling locomotion mode, the vehicle-terrain interaction indicates wheel/track-terrain interaction. In terramechanics models, tracks are commonly modeled as several neighboring wheels with a rubber track wrapped around them [54] as represented in Figure 3-1b. Thus, for simplicity, a one-wheel modeling method is developed to calculate the fundamental dynamics of the rolling locomotion mode of hybrid wheel/track-legged robots. In the modeling method development, an assumption that the vehicle's load is distributed evenly on all wheels is made. In the one wheel modeling method, the deformation of the wheel due to gravity as well as collisions is evaluated by the most extensively used terramechanics method, the point contact method [55] as shown in Figure 4-1. As illustrated in Figure 4-1, the point contact method is generally represented as a spring and damper in parallel, i.e. a mass-spring-damper (MSD) system, resulting in fairly good approximations of the forces developed as the wheel passes over smooth and flat ground profiles [56]. This approach is suitable to evaluate steps negotiation environment. In the wheel-step negotiation, the wheel motion resistance [57] due to the combined effect of the axle's friction and friction at the rim is assumed to be negligible; only the rolling resistance due to the wheel deformations is considered.

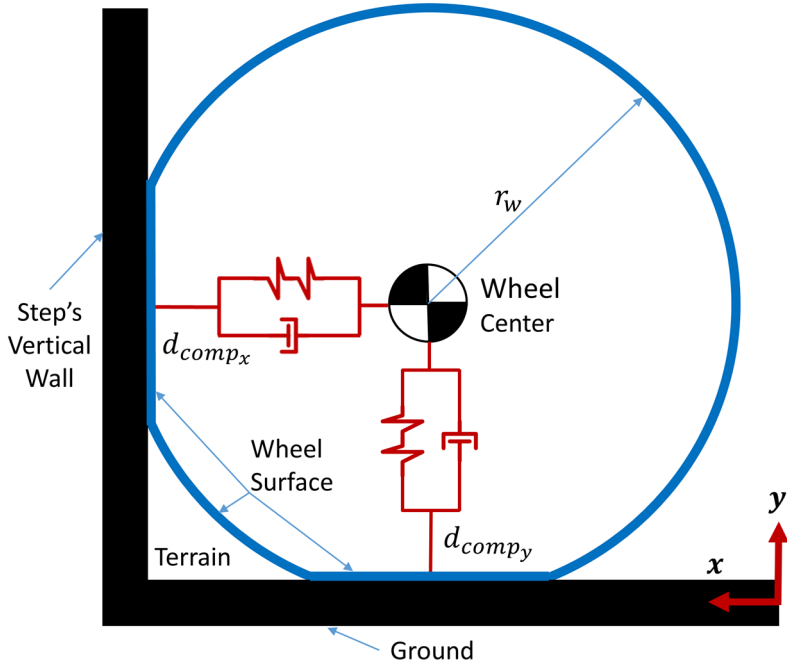


**Figure 4-1. One Wheel-terrain Modeling Method using the Point Contact Terramechanics Model in Horizontal and Vertical Directions.**

The rolling locomotion mode of track/wheel-legged to negotiate steps thus can be modeled as a one wheel-step negotiation process. The step negotiation of one wheel model is developed in three stages and illustrated in Figure 4-2. Stage 1: rolling towards the step, Stage 2: crossing over the step, and Stage 3: rolling on top of the step. The step negotiation process is divided into three stages due to the wheel-terrain forces evaluation complexity at the step corner in Stage 2. The direction of the wheel-terrain normal forces changes immediately at the top step corner (the connecting perpendicular point between vertical and horizontal part of the step as indicated in Figure 4-2), which will loss continuous of the computational calculation. The solution used to solve the sudden force direction changes at the step corner is assuming an arc (with radius  $r_c$ ) to make the force direction change gradually. Due to the fact that the wheel isn't in contact with the bottom step corner during the negotiation process, no assuming arc is needed at the bottom corner.

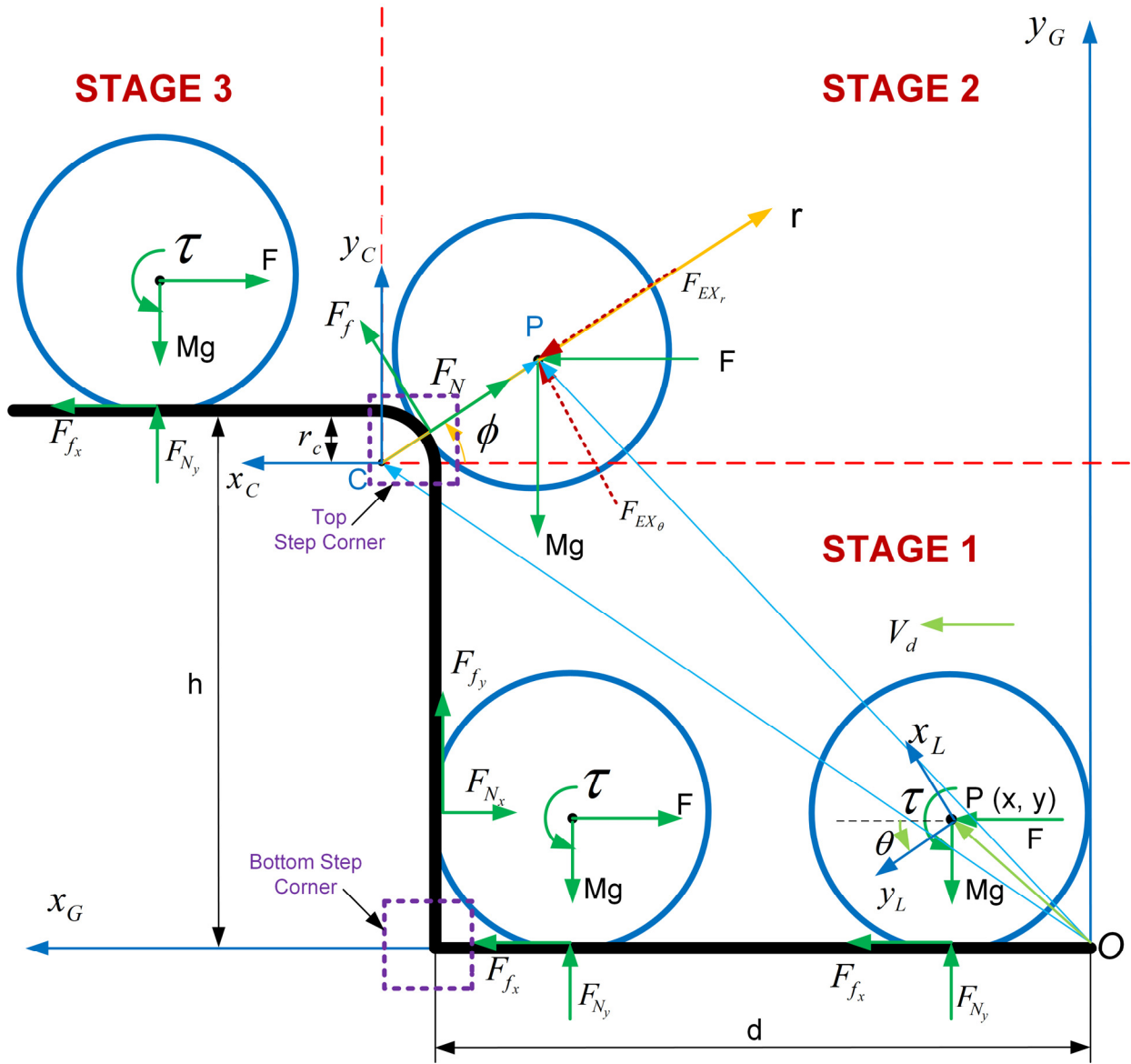


**Figure 4-2. Three Motion Stages of One Wheel-Step Negotiation Model.**

Thus, the three stages in Figure 4-2 are divided by the relative positions between the wheel center (denoted as  $P$  in Figure 4-2) and arc center (denoted as  $C$  in Figure 4-2) as follows.

- Stage 1: when  $x \leq h - r_c$ ,
  - Stage 2: when  $y > h - r_c$  &  $x < d + r_c$ , and
  - Stage 3: when  $x \geq d + r_c$ .

Here,  $x$  and  $y$  denotes the wheel center positon  $P$  in  $x$  and  $y$  axis of the global coordinates frame  $x_G O y_G$  respectively,  $h$  and  $d$  represents the step height and the horizontal distance between  $G$  and the step respectively shown in Figure 4-2.

In Figure 4-2,  $F_N$  and  $F_f$  denote the normal and frictional forces between the wheel and ground, respectively,  $T$  and  $F$  represent the output torque of the wheel actuator and the external horizontal forces exerted on the wheel by the rest part of the robot, respectively. The wheel rotation angle is represented by  $\theta$ , the wheel mass is denoted as  $M$ , and the radius of step corner arc  $r_c$  is defined as  $0.01h$ . The arc radius of the step corner  $r_c$  is defined relative to the step height, this number is an appropriate value for the modeling calculation. It's big enough to make sure the continuous of the computational calculation as well as to simplify the complexity of the modeling process, at the same time, it isn't too big to lose genericity of the step style terrain profiles. The parameters used in Stage 2 will be specified in the following modeling section.

#### 4.1 Preparatory Definitions

The initial states of the wheel-terrain dynamics model will be defined first. These initial states includes initial values of positon and velocity of the center of the wheel  $P$  in the  $x$  and  $y$  axis with respect to the global coordinates frame  $x_G O y_G$ , as well as the wheel rotation angle and the angular velocity shown in Figure 4-2. Similarly, the final states indicate the final values of the positon and velocity of the center of the wheel  $P$  and wheel's rotation angle and angular velocity. In this chapter, without specific mention, all analysis is conducted with respect to the global frame of reference  $x_G O y_G$ .

In the  $x$  direction, the initial position and velocity values of the center of the wheel  $P$  are  $x(0) = r_w$  and  $\dot{x}(0) = \dot{x}_d$ , in which  $r_w$  denotes the wheel radius, and  $\dot{x}_d$  represents the desired reference linear velocity of the wheel.

In the  $y$  direction, the wheel deformation  $d_{comp_y}$  is computed by analysing the MSD system in Figure 4-1:

$$\sum F_y = -Mg + kd_{comp_y} + c\dot{d}_{comp_y} \quad (4.1)$$

Here,  $k$  represents the spring coefficient, and  $c$  denotes the damping ratio of the wheel deformation model shown in Figure 4-1. Because the resultant forces in the  $y$  direction is zero, and  $\dot{d}_{comp_y} = 0$ , then  $d_{comp_y} = \frac{Mg}{k}$ . Thus the initial position and velocity values of the center of the wheel  $P$  in  $y$  direction are  $y(0) = r_w - \frac{Mg}{k}$ ,  $\dot{y}(0) = 0$  by solving Equation (4.1).

The initial wheel rotation angle  $\theta$  is defined as  $\theta(0) = 0$ , and the initial angular velocity is calculated by  $\dot{\theta}(0) = -\frac{\dot{x}_d}{r_w - \frac{Mg}{k}}$  with defining counter-clockwise as the positive rotation direction.

In modeling the wheel's motor, the motor's applied voltage is defined by multiplying the velocity difference between the desired velocity  $\dot{x}_d$  and the computed velocity by integrating the acceleration gained by the dynamic equations of motion with a combination gain of a proportional coefficient  $K_p$  and the height of the obstacle  $h$  as:

$$U = -(K_p + 300h^2) * (\dot{x}_d - \sqrt{\dot{x}^2 + \dot{y}^2}) \quad (4.2)$$

where  $\dot{x}$  and  $\dot{y}$  denotes the calculated horizontal and vertical linear velocity of the wheel center respectively.

Next, torque outputs of the wheel's motor shaft is calculated. For a DC motor, the energy  $E_i$  consumed during a time  $T_i$  can be evaluated by [58]:

$$E_i = \int_0^{T_i} U_a I_a dt = \int_0^{T_i} \tau \dot{\theta} dt + \int_0^{T_i} I_a^2 R_a dt \quad (4.3)$$

where  $U_a$  and  $I_a$  denote the applied voltage and armature current, respectively.  $\tau$  indicates the motor shaft output torque,  $\dot{\theta}$  represents the motor shaft output angular velocity, and  $R_a$  is the armature resistance. Moreover,  $I_a$  can be calculated by:

$$U_a = K_{emf} \dot{\theta} + I_a R_a \quad (4.4)$$

where  $K_{emf}$  represents the back electromotive force (*emf*) constant. Moreover, the motor torque  $\tau$  can be derived as:

$$\tau = K_t I_a \quad (4.5)$$

where  $K_t$  denotes the torque constant.

In Equation (4.3), the first term denotes the mechanical energy and the second part calculates the energy loss due to the heat emissions. Due to the fact that if there is no specific designed electrical system to store energy (which is true to the research focused wheel/track-legged robots), a negative value for the first part doesn't result in a gain of energy [58]. Therefore, the energy consumed by a DC motor during a time  $T$  is calculated as:

$$E_i = \int_0^{T_i} [f(\tau \dot{\theta})] dt + \int_0^{T_i} I_a^2 R_a dt \quad (4.6)$$

$$\text{where } f(\tau \dot{\theta}) = \begin{cases} \tau \dot{\theta} & \text{when } \tau \dot{\theta} > 0 \\ 0 & \text{when } \tau \dot{\theta} \leq 0 \end{cases}$$

The torque output of the wheel's motor  $\tau$  can be derived using Equations (4.4) and (4.5),  $\tau = K_t I_a = K_t * \frac{U_a - K_{emf} \dot{\theta}}{R}$  as:

$$\tau = K_t * \frac{U_a - K_{emf} \dot{\theta}}{R} \quad (4.7)$$

Hence, for quadruped hybrid robots, the horizontal forces that the other part of the vehicle exert to the wheel can be derived as:

$$F_{h_{other}} = -3 * \frac{\tau}{r_w - \frac{Mg}{k}} \quad (4.8)$$

The torque output of the other three wheels' motors is assumed to be as same as the modeled wheel torque output  $\tau$  in (4.7). Thus, the resultant forces the other part of the vehicle exert on the modeled wheel can be derived. Here, the forces expressed in Equation (4.8) shows the calculation only for the horizontal direction as  $F_{h_{other}}$  without dealing with forces in the vertical direction. However, the forces in the vertical direction still can be considered in the modeling process by adjusting the spring-damper coefficients. These coefficients can be changed due to the fact that the developed model doesn't represent for one specific particular vehicle, thus any coefficients provide a reasonable model behavior works.

The spring coefficient  $k$  and damping ratio  $c$  in Figure 4-1 are defined separately in  $x$  and  $y$  direction depending on different wheel-terrain interaction conditions. For example, when  $x < d - r_w$ , i.e. the wheel is still in the horizontal ground rolling phase without contact with the vertical part of the step, only the MSD in the  $y$  direction exerts forces to the wheel, thus the MSD parameters in  $x$  direction are defined as zero.

$$\text{In the } x \text{ direction, } k_x = \begin{cases} 0, & x < d - r_w \\ k, & d - r_w \leq x \leq d \\ 0, & x > d \end{cases}; c_x = \begin{cases} 0, & x < d - r_w \\ c, & d - r_w \leq x \leq d \\ 0, & x > d \end{cases} \quad (4.9)$$

$$\text{In the } y \text{ direction, } k_y = \begin{cases} k, & y \leq r_w \\ 0, & r_w < y \leq h \\ k, & h < y \end{cases}; c_y = \begin{cases} c, & y \leq r_w \\ 0, & r_w < y \leq h \\ c, & h < y \end{cases} \quad (4.10)$$

where  $k_x$  and  $c_x$ ,  $k_y$  and  $c_y$  are the spring coefficient and damping ratio of MSD in  $x$  and  $y$  direction, respectively.

The normal forces because of wheel deformations during the step negotiation can be calculated as:

$$F_{N_x} = k_x d_{comp_x} + c_x \dot{d}_{comp_x}; F_{N_y} = k_y d_{comp_y} + c_y \dot{d}_{comp_y} \quad (4.11)$$

Here, in Figure 4-1,  $d_{comp_x}$  and  $d_{comp_y}$  represent the wheel deformation in  $x$  and  $y$  direction, respectively.

During the wheel's rolling motion analysis, static and dynamic friction coefficients is used respectively to calculate the friction forces depending on if the wheel-terrain slippage happens or not. In the wheel-terrain modeling computation, for simplification, maximum friction force rules are always assumed when calculate the friction forces as:

$$F_{f_x} = \mu F_{N_y}, F_{f_y} = \mu F_{N_x} \quad (4.12)$$

where  $\mu$  is defined as:

$$\mu = \begin{cases} \mu_{static}, & \text{No slippage} \\ \mu_{dynamic}, & \text{Slippage occurs} \end{cases} \quad (4.13)$$

In the modeling calculations, which friction coefficient was used was determined by the contact velocity  $v_{contact}$  between the wheel and terrain. No slippage was defined when  $v_{contact}$  is smaller than 0.001 (a relatively small value compared with the wheel radius).

## 4.2 Stage 1

In Stage 1, analyzing the wheel forces as shown in Figure 4-2, dynamic equations of motion can be derived as:

$$M\ddot{x} = F_{f_x} - F_{N_x} + F \quad (4.14)$$

$$M\ddot{y} = F_{f_y} + F_{N_y} - Mg \quad (4.15)$$

$$I\ddot{\theta} = T + F_{f_x}(r_w - d_{comp_y}) + F_{f_y}(r_w - d_{comp_x}) \quad (4.16)$$

where  $I$  represents the inertia tensor of the wheel. The wheel deformations,  $d_{comp_x}$  and  $d_{comp_y}$ , in  $x$  and  $y$  directions are calculated respectively as:

$$d_{comp_x} = r_w - (d - x), d_{comp_y} = r_w - y \quad (4.17)$$

$$\dot{d}_{comp_x} = \dot{x}, \dot{d}_{comp_y} = -\dot{y} \quad (4.18)$$

The contact velocity  $v_{contact}$  between wheel and terrain in  $x$  and  $y$  directions can be calculated by adding the linear velocity of the wheel and the rotation velocity of the wheel rim as:

$$v_{contact_x} = \dot{x} + \dot{\theta}y; v_{contact_y} = \dot{y} + \dot{\theta}(d - x) \quad (4.19)$$

During the wheel-step negotiation, the step height  $h$  is a variable (external environment information) and defined to range from zero. When the step height  $h \leq r_w - \frac{Mg}{k} + r_c$  as shown in Figure 4-3, once the wheel touches the step, the motion starts Stage 2 immediately. So in this case, the spring stiffness and damper coefficients in  $x$  direction,  $k_x$  and  $c_x$  are set to zero instead of  $k$  and  $c$  in Equation (4.9). When the step height  $h \leq r_w - \frac{Mg}{k} + r_c$ , the horizontal ground still exerts forces to the wheel at the beginning of Stage 2 negotiation, which will be explained in the next Stage 2 modeling part.

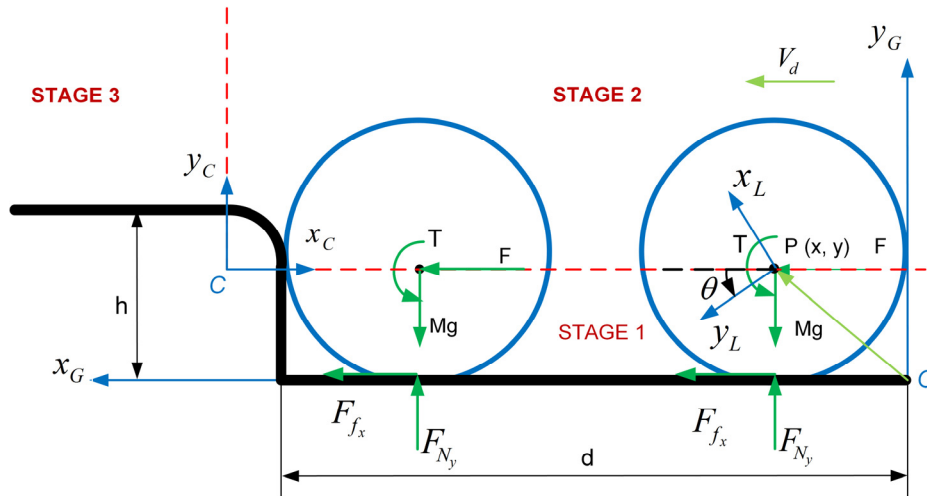


Figure 4-3. Obstacle Height Explanation.

### 4.3 Stage 2

For Stage 2 (Figure 4-2), the wheel-terrain interaction analysis is more complex than Stage 1. Due to the complex wheel deformation and the sudden direction change of the normal forces at the step corner, an arc is added to reduce the modeling complexity by making sure that the normal forces acting on the wheel always go through the center of the wheel  $P$ . Thus the normal forces' direction changes gradually with the wheel rotating around the step arc corner, this arc corner assumption was made to simplify the modeling complexity and to keep computation consistent. In this case, it is convenient to model the wheel's motion in a local polar coordinates  $r$  and  $\phi$  frame of reference as shown in Figure 4-2.

The direction of polar coordinate  $r$  can be calculated by the radial vector  $\overrightarrow{CP} = \overrightarrow{OP} - \overrightarrow{OC}$ , in which  $\overrightarrow{OP}$  is the vector between the origins of global frame of reference  $O$  and wheel center  $P$  and  $C$  is the center of the step arc (quadrant) corner. Vector  $\overrightarrow{OC}$  is fixed in frame  $x_G O y_G$ ,  $\overrightarrow{OP}$  can be computed by integrating wheel accelerations in both  $x$  and  $y$  directions. Furthermore, in Figure 4-2,  $F_{EX_r}$  and  $F_{EX_\phi}$  denotes the resultant forces of radial and transverse directional component. As a result, Stage 2 was modeled in the polar frame as:

$$Ma_r = F_{EX_r}; Ma_\phi = F_{EX_\phi} \quad (4.20)$$

$$a_r = \ddot{r} - r\dot{\phi}^2, a_\phi = r\ddot{\phi} + 2\dot{r}\dot{\phi} \quad (4.21)$$

In Equations (4.20) and (4.21),  $a_r$  and  $a_\phi$  denote the radial and transverse accelerations, respectively.

As mentioned in Stage 1, when the obstacle height satisfies the following relationship  $h \leq r_w - \frac{Mg}{k} + r_c$  shown in Figure 4-3, there is no step climbing process after the horizontal rolling in Stage 1, and Stage 2 starts immediately when the wheel contacts the step. In such

cases, from the beginning of Stage 2 until the position satisfying  $(rsin\phi + h - r_c) \geq r_w$ , the wheel has interactions with the horizontal ground, thus there are forces acting on the wheel form the horizontal ground. Thus,

$$F_{EX_r} = -Fcos\phi - Mgsin\phi + F_N + F_{Ny}sin\phi - F_{fx}cos\phi \quad (4.22)$$

$$F_{EX_\theta} = -Mgcos\phi + Fsin\phi + F_f + F_{Ny}cos\phi + F_{fx}sin\phi \quad (4.23)$$

where

$$F_{Ny} = kd_{comp_y} + cd_{comp_y}; F_{fx} = \mu F_{Ny} \quad (4.24)$$

$$d_{comp_y} = r_w - h + r_c - rsin\phi; \dot{d}_{comp_y} = r\dot{\phi}cos\phi + \dot{r}sin\phi \quad (4.25)$$

$$F_N = kd_{comp} + cd_{comp}; F_f = \mu F_N \quad (4.26)$$

$$d_{comp} = r_w - (r - r_c), d_{comp} = -\dot{r} \quad (4.27)$$

In frame  $x_c Cy_c$  (the local frame of reference), the velocity of the wheel center is negative based on the right hand rule, so the contact velocity between the wheel and terrain is derived as:

$$v_{contact} = -r\dot{\phi} + (r - r_c)\dot{\theta} \quad (4.28)$$

In Stage 2, the desired velocity is defined in a similar fashion as in Stage 1. The wheel actual velocity  $v_c$  determined by the dynamic equations of motion is calculated as:

$$v_c = \sqrt{\dot{r}^2 + (r\dot{\phi})^2} \quad (4.29)$$

In Stage 2, because the dynamic equations of motion are developed with respect to the local polar coordinates  $r$  and  $\phi$ , the initial states (similar definitions as in Stage 1) are calculated by the final states of Stage 1, and the final states of Stages 2 are used to calculate the initial states of Stage 3. The initial values of polar coordinate  $r$  can be derived as:

$$r_{i_{S2}} = \sqrt{r_{c_x}^2 + r_{c_y}^2} \quad (4.30)$$

In which  $r_{c_x}$  and  $r_{c_y}$  is the components of polar coordinate  $r$  with respect to  $x$  and  $y$  axis of the local frame of reference  $x_c Cy_c$  respectively. They can be derived by the final position values of Stage 1 as:

$$r_{c_x} = -(x - d - r_c); r_{c_y} = y - h + r_c \quad (4.31)$$

The initial values of the transverse coordinate  $\phi$  are derived as:

$$\phi_{i_{S2}} = \arctan \frac{r_{c_y}}{r_{c_x}} \quad (4.32)$$

The initial values of  $\dot{r}$  and  $\dot{\phi}$  can be calculated by the equality between the final resultant velocity of Stage 1  $v_{f_{S1}}$  and the initial resultant velocity of Stage 2  $v_{i_{S2}}$  as shown in Figure 4-4.

$$v_{f_{S1}} = \sqrt{\dot{x}_{f_{S1}}^2 + \dot{y}_{f_{S1}}^2}; \alpha = \arctan\left(\frac{\dot{y}_{f_{S1}}}{\dot{x}_{f_{S1}}}\right) \quad (4.33)$$

$$v_{i_{S2}} = v_{f_{S1}} \quad (4.34)$$

$$\dot{r}_{i_{S2}} = v_{i_{S2}} \cos(\alpha - \phi_{i_{S2}}); \dot{\phi}_{i_{S2}} = \frac{v_{i_{S2}} \sin(\alpha - \phi_{i_{S2}})}{r_{i_{S2}}} \quad (4.35)$$

Here,  $\alpha$  denotes the angular between  $\dot{x}_{f_{S1}}$  and  $v_{f_{S1}}$ ,  $\dot{x}_{f_{S1}}$  and  $\dot{y}_{f_{S1}}$  is the final velocity component in  $x$  and  $y$  direction of Stage 1 respectively. The initial values of wheel rotation angle and angular velocity can be calculated as:

$$\theta_{i_{S2}} = -\pi - \theta_{f_{S1}}; \dot{\theta}_{i_{S2}} = -\dot{\theta}_{f_{S1}} \quad (4.36)$$

where  $\theta_{f_{S1}}$  and  $\dot{\theta}_{f_{S1}}$  represent the final rotation angle and angular velocity of Stage 1, respectively. Furthermore,  $\theta_{i_{S2}}$  and  $\dot{\theta}_{i_{S2}}$  denote the initial rotation angle and angular velocity of Stage 2, respectively.

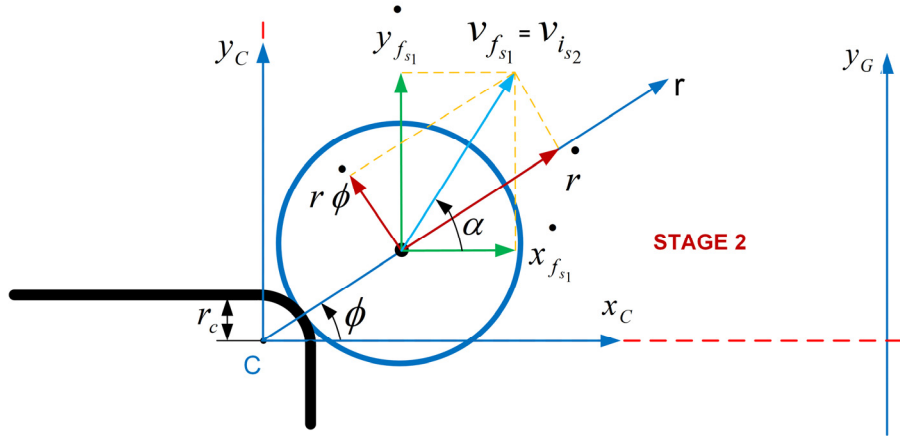


**Figure 4-4. Calculations of the Initials of Stage 2.**

The initial states of Stage 3 can be calculated by the final states of Stage 2 as:

$$x_{i_{S3}} = -r_{f_{S2}} \cos\phi + d + r_c; \quad y_{i_{S3}} = -r_{f_{S2}} \sin\phi + h + r_c \quad (4.37)$$

$$\dot{x}_{i_{S3}} = -\dot{r}_{f_{S2}} \cos\phi + \dot{\phi} r_{f_{S2}} \sin\phi; \quad \dot{y}_{i_{S3}} = -\dot{r}_{f_{S2}} \sin\phi - \dot{\phi} r_{f_{S2}} \cos\phi \quad (4.38)$$

$$\theta_{i_{S3}} = -\theta_{f_{S2}}; \quad \dot{\theta}_{i_{S3}} = -\dot{\theta}_{f_{S2}} \quad (4.39)$$

Here, the parameters definitions are as same as the ones of the initial states calculations of Stage 2 with only subscripts difference.

#### 4.4 Stage 3

The Stage 3 shown in Figure 4-2 has the same dynamics characteristics as Stage 1 in the horizontal ground motion phase, so the dynamic equations of motion of Stage 3 are as same as Stage 1. The dynamics modeling differences between Stage 1 and 3 are their intermediate variables calculations of the wheel deformation  $d_{comp}$  and the wheel-terrain contact velocity  $v_{contact}$ . Thus, the dynamics equations of Stage 3 are:

$$M\ddot{x} = F_{fx} - F_{Nx} + F \quad (4.40)$$

$$M\ddot{y} = F_{fy} + F_{Ny} - Mg \quad (4.41)$$

$$I\ddot{\theta} = T + F_{fx}(r_w - d_{comp_y}) + F_{fy}(r_w - d_{comp_x}) \quad (4.42)$$

The wheel deformation,  $d_{comp_x}$  and  $d_{comp_y}$ , in  $x$  and  $y$  directions are calculated respectively as:

$$d_{comp_x} = 0, d_{comp_y} = r_w - (y - h) \quad (4.43)$$

$$\dot{d}_{comp_x} = 0, \dot{d}_{comp_y} = -\dot{y} \quad (4.44)$$

The contact velocity  $v_{contact}$  between wheel and terrain in  $x$  and  $y$  directions can be calculated as:

$$v_{contact_x} = \dot{x} + \dot{\theta}(y - h); v_{contact_y} = 0 \quad (4.45)$$

## 4.5 Summary

In this chapter, a dynamic modeling method of the wheel-step negotiation is developed. Due to the complexity of the wheel-terrain interaction modeling, only the basic fundamental properties, i.e. friction and deformation of the wheel, have been considered in the modeling process. The control input for the developed model is the desired velocity, thus the motion time for rolling locomotion step negotiation is governed by the equations of motion. The method provides a simplified model for the rolling locomotion mode of the wheel/track-legged hybrid robots, which can be employed for the energy evaluations of the rolling locomotion in Chapter Six.

## Chapter Five: WALKING LOCOMOTION MODELING

In this Chapter, a model for the generalized walking locomotion mode of hybrid wheel/track-legged robots is presented. Different with the rolling locomotion mode modeling method that only considered essential dynamics properties, the walking locomotion mode modeling process employs an efficient multi-body dynamics modeling algorithm named the Decoupled Natural Orthogonal Complement (DeNOC) method that can provide accurate and efficient evaluation results of locomotion performance. This chapter starts with the description of DeNOC, continues with the explanation of the recursive inverse and forward dynamics algorithm developed by DeNOC method, then follows with the development of a generalized walking locomotion mode model, i.e. 3-link leg with the outermost segment is a drivable wheel, to be used in the locomotion energy consumption evaluations.

### 5.1 Dynamics Modeling Methods

An accurate dynamics model of the system is essential to realize the proposed energy consumption evaluations of locomotion modes [59], and computational efficiency is equally important for the simulation and real-time control of hybrid robots with highly articulated legs (with degrees of freedom (DOF) equal or more than three) such as the Cricket used as the experimental test platform in this research. Robots' dynamics modeling consists of three major computations [60]:

- Forward dynamics (FD) is the process in which the joint accelerations are determined by the specified applied joint actuators torques/forces and required for simulations.
- Inverse dynamics (ID) is the process in which the required joint actuator torques/forces are computed from a given specification of the manipulator's trajectory (position, velocity, and acceleration) and used in the robots' feedforward control.

- Inertia (mass) matrix is used to map the joint accelerations to joint forces (derived in FD and ID computations), which is fundamental in the analysis and corresponding feedback control to linearize the dynamics as well as an integral part of the forward dynamics formulations.

The Newton-Euler (NE) and Euler-Lagrange (EL) equations are the two most commonly used methods in developing robots' dynamics model. The former method is good for control, due to the fact that it derives all physical equations of motion of each part using the free body diagram method, which include the constraint forces due to the kinematic pair between the neighbouring links. For an open loop multi-body systems, e.g. lifting legs of hybrid robots, these constraints along with the driving forces can be solved recursively. For a closed loop system, e.g. supporting legs of hybrid robots, on the other hand, the NE equations generally need to be solved simultaneously to obtain the driving and constraint forces at the same time. When all feet are in contact with the ground, the robot system is in a closed-loop form, thus the use of the NE equations of motion are not as efficient as for the open loop cases [61].

On the other side of the coin, the EL method uses the generalized coordinates concept instead of the Cartesian coordinates [62]. For an open loop system, the number of generalized coordinates typically equals the DOF of the system, and the constraint forces don't appear in the equations of motion. For the closed loop system case, the constraint forces appear as Lagrange's multipliers [63]. Thus, the dynamic models developed using the EL method are good for forward dynamics simulations because of its energy based nature without dealing with the constraints forces.

In order to take advantage of these two classic dynamics modeling methods in the modeling and control of robots' system, a series of methods based on orthogonal complements of

the velocity constraints have been proposed which enables the equations of motion derived in the EL form to be derived from the NE equations by multiplying a proper matrix to eliminate the constraint forces [64, 65]. One of such proposed methods is the DeNOC developed in recent years [61, 66].

The DeNOC is a method that allows constraint forces eliminations of the equations of motion derived in the NE form via multiplication of the uncoupled dynamic equations by a proper defined orthogonal complement of the linear velocity constraints matrix [66]. In the following sections, the DeNOC method is used to develop the mathematical model of a serial-link system with a fixed base, which represents one of the legs of the wheel/track-legged hybrid robots shown in Figure 3-1 focused in this thesis. To the best of the our knowledge, this is the first time that the DeNOC methodology is used to model wheel/track-legged hybrid robots with highly articulated legs.

In the following sections, the process that dynamic equations of motion of a  $n$ -link ( $n$  DOF) serial system, representing one leg of the hybrid robot, are derived using the DeNOC method is explained first. There are three main steps to obtain the robots' dynamic equations of motion using DeNOC method:

- 1) Derive the DeNOC matrices to relate the Cartesian velocities of the links with joints rates by expressing kinematics constraints between adjacent links due to joints,
- 2) Develop uncoupled Newton-Euler (NE) equations of motion of each link and write these equations in a compact matrix form, and
- 3) Pre-multiply the DeNOC matrices with the uncoupled NE equations to obtain a set of coupled independent equations of motion, which represent the same equations of motion as the Euler-Lagrange (EL) equations of the system.

### 5.1.1 Parameters Definition

A generalized serial-link with fixed base system can be represented as shown in Figure 5-1, in which the fixed body is denoted by link #0, followed by  $n$  moving rigid bodies representing the leg, indicated by #1, #2, ..., and # $n$  linkages, coupled by  $n$  one DOF joints numbered as 1, 2, ...,  $n$ , where  $n$  is the number of moving rigid links in the serial chain system. For the hybrid robots, link # $n$  represents the wheel. In order to keep things manageable in the following formulation, all joints of the robot are considered revolute and powered via revolute actuators. Thus, in what follows all equations of motion are derived of the revolute joint without considering prismatic joints scenario. This however can be easily extended to include other joint types, such as prismatic, spherical and cylindrical. This set of considerations are in line with the available experimental robot platform Cricket that only processes revolute joints.

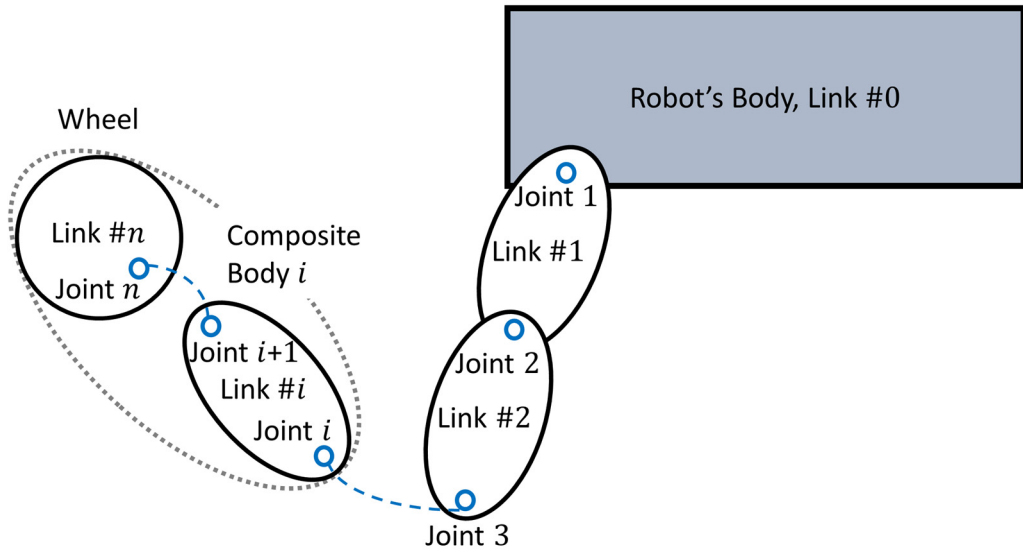


**Figure 5-1. Generalized Model of a Serial-link System with Fixed Base.**

To generate a mathematical model of hybrid robot via the DeNOC approach, parameters used throughout the DeNOC formulation are listed in Table 5-1.

**Table 5-1. Symbol Summary in the DeNOC Method**

| Roman Symbol       | Description   | Dimension      |
|--------------------|---|----------------|
| $B_{i,i-1}$        | Propagation matrix of twist or velocity from link $\#i - 1$ to link $\#i$   | $6 \times 6$   |
| $\dot{B}_{i+1,i}$  | Propagation matrix of twist rate  | $6 \times 6$   |
| $C$                | Convective inertia (MCI) terms matrix                                       | $n \times n$   |
| $c_{i,i-1}$        | Position vector from $C_i$ to $C_{i-1}$ , $c_{i,i-1} = -d_i - r_{i-1}$      | $3 \times 1$   |
| $d_{i-1}$          | Position vector from $O_{i-1}$ to $C_{i-1}$                                 | $3 \times 1$   |
| $e_i$              | Unit vector along the $i^{th}$ joint axis                                   | $3 \times 1$   |
| $f_i$              | Resultant force applied at $C_i$  | $3 \times 1$   |
| $h$                | Convective inertia (VCI) terms vector                                       | $n \times 1$   |
| $I$                | Generalized inertia matrix (GIM)  | $n \times n$   |
| $I_l$              | Inertia tensor about $C_i$ of the $i^{th}$ link                             | $3 \times 3$   |
| $M_i$              | Mass matrix of the $i^{th}$ link  | $6 \times 6$   |
| $M$                | Generalized mass matrix   | $6n \times 6n$ |
| $\tilde{M}$        | Composite mass matrix   | $6n \times 6n$ |
| $\tilde{M}_l$      | $\tilde{M}_l = N_l^T M \dot{N}_l$   | $6n \times 6n$ |
| $\tilde{M}_\omega$ | $\tilde{M}_\omega = \tilde{M}\Omega$  | $6n \times 6n$ |
| $\tilde{M}_e$      | $\tilde{M}_e = N_l^T W M N_l$   | $6n \times 6n$ |
| $m_i$              | Mass of the $i^{th}$ link   | $1 \times 1$   |
| $N$                | Natural Orthogonal Complement (NOC) matrix of the velocity constraints      | $6n \times n$  |
| $N_l$              | Decoupled NOC, $N = N_l N_d$  | $6n \times 6n$ |
| $N_d$              | Decoupled NOC   | $6n \times n$  |
| $n_i$              | Vectors of the resultant moment applied about $C_i$                         | $3 \times 1$   |
| $p_i$              | Joint rate propagation vector   | $6 \times 1$   |
| $r_{i-1}$          | Position vector from $C_{i-1}$ to $O_i$                                     | $3 \times 1$   |
| $t_i$              | Twist of the rigid link $i$ in 3-dimensinal Cartesian space                 | $6 \times 1$   |
| $t$                | Generalized twist vector  | $6n \times 1$  |
| $v_i$              | Linear velocity of the center of gravity ( $C_i$ ) of the $i^{th}$ link     | $3 \times 1$   |
| $\dot{v}_i$        | Linear acceleration of the center of gravity ( $C_i$ ) of the $i^{th}$ link | $3 \times 1$   |
| $W_i$              | Angular velocity matrix of the $i^{th}$ link                                | $6 \times 6$   |
| $W$                | Generalized angular velocity matrix   | $6n \times 6n$ |
| $w_i$              | Wrench acting on rigid link $i$   | $6 \times 1$   |
| $w$                | Generalized wrench vector   | $6n \times 1$  |
| $w^E$              | External wrench   | $6n \times 1$  |
| $w^C$              | Constraint wrench   | $6n \times 1$  |
| Greek Symbol       | Description   | Dimension      |
| $\theta$           | Revolute joint angle of the joint $i$                                       | $3 \times 1$   |
| $\dot{\theta}_i$   | Revolute joint angular velocity of the joint $i$                            | $3 \times 1$   |
| $\ddot{\theta}$    | Generalized joint rate vector   | $n \times 1$   |

|                  |                                       |              |
|------------------|---------------------------------------|--------------|
| $\tau$           | Generalized forces                    | $n \times 1$ |
| $\omega_i$       | Angular velocity of the $i^{th}$ link | $3 \times 1$ |
| $\dot{\omega}_i$ | Acceleration of the $i^{th}$ link     | $3 \times 1$ |

Four essential generalized parameters will be defined first of all. The twist ( $t_i$ ) and wrench ( $w_i$ ) vectors acting on rigid link  $i$  are defined in 3-dimensional Cartesian space as:

$$t_i = \begin{bmatrix} \omega_i \\ v_i \end{bmatrix} \text{ and } w_i = \begin{bmatrix} n_i \\ f_i \end{bmatrix} \quad (5.1)$$

where  $\omega_i$  is the angular velocity vector of the  $i^{th}$  link, and  $v_i$  is the linear velocity vector of the center of gravity ( $C_i$ ) of the leg's  $i^{th}$  link. Moreover,  $n_i$  and  $f_i$  are the vectors of the resultant moment applied about  $C_i$  and the resultant force at  $C_i$  respectively.

The mass matrix  $M_i$  and the angular velocity matrix  $W_i$  of the leg's  $i^{th}$  link are defined as:

$$M_i = \begin{bmatrix} I_i & \mathbf{0} \\ \mathbf{0} & m_i \mathbf{1} \end{bmatrix} \text{ and } W_i = \begin{bmatrix} \omega_i \times \mathbf{1} & \mathbf{0} \\ \mathbf{0} & \mathbf{0} \end{bmatrix} \quad (5.2)$$

where  $\omega_i \times \mathbf{1}$  is the  $3 \times 3$  cross-product tensor associated with the angular velocity  $\omega_i$  which is defined as  $(\omega_i \times \mathbf{1})x = \omega_i \times x$ . Moreover,  $\mathbf{1}$  and  $\mathbf{0}$  in Equation (4.1) are  $3 \times 3$  identity and zero matrices respectively, and  $I_i$  and  $m_i$  are the  $3 \times 3$  inertia tensor about  $C_i$  and the mass of the  $i^{th}$  link respectively.

### 5.1.2 DeNOC Matrices

The robot's kinematics constraints of the two neighbouring links, link  $\#i - 1$  and link  $\#i$ , coupled by a revolute joint (joint  $\#i$ ) are illustrated in Figure 5-2. In Figure 5-2, the coordinate frame of reference  $i$  ( $x_i y_i z_i$ ) and  $i + 1$  ( $x_{i+1} y_{i+1} z_{i+1}$ ) is attached to the link  $i - 1$  and link  $i$  respectively following a modified traditional Denavit-Hartenberg (D-H) method. The

explanation of the D-H method used in the DeNOC and comparison of traditional D-H method can be found in Appendix A.

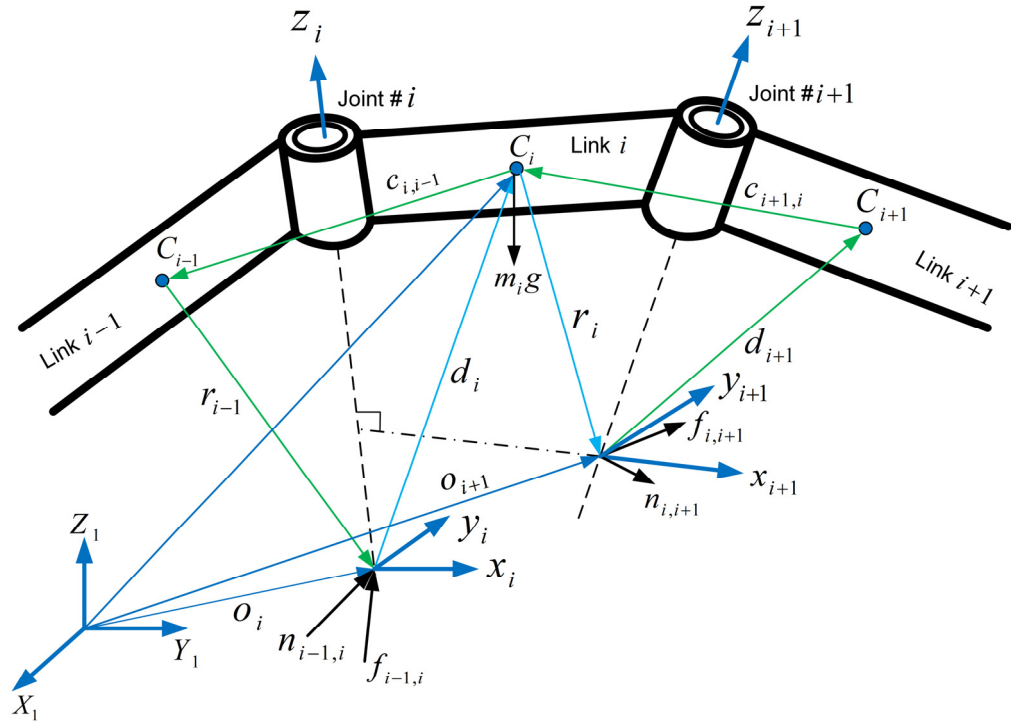


**Figure 5-2. Adjacent Links (Link  $i$  and  $i + 1$ ) Parameter Definitions.**

The kinematic equations of link  $i - 1$  and  $i$  in terms of velocity (angular and linear velocities) are written as:

$$\omega_i = \omega_{i-1} + \dot{\theta}_i e_i \quad (5.3)$$

$$v_i = v_{i-1} + \omega_{i-1} \times r_{i-1} + \omega_i \times d_i \quad (5.4)$$

Here,  $\dot{\theta}_i$  represents the joint rate of the joint  $i$ ,  $e_i$  denotes the unit vector along the  $i^{th}$  joint axis ( $e_i = [0, 0, 1]$  based on the D-H method),  $r_{i-1}$  is the position vector from  $C_{i-1}$  to  $O_i$ , and  $d_i$  is the position vector from  $O_{i-1}$  to  $C_i$  shown in Figure 5-2.

The above Equations (5.3) and (5.4) can be written in a more compact form as:

$$t_i = B_{i,i-1} t_{i-1} + p_i \dot{\theta}_i \quad (5.5)$$

where  $B_{ij}$  and  $p_i$  are defined as:

$$B_{i,i-1} = \begin{bmatrix} \mathbf{1} & \mathbf{0} \\ c_{i,i-1} \times \mathbf{1} & \mathbf{1} \end{bmatrix} \text{ and } p_i = \begin{bmatrix} e_i \\ e_i \times d_i \end{bmatrix} \quad (5.6)$$

In Equation (5.6),  $c_{i,i-1}$  is the position vector from  $C_i$  to  $C_{i-1}$  defined as  $c_{i,i-1} = -d_i - r_{i-1}$  in Figure 5-2, and  $c_{i,i-1} \times 1$  is the cross-product tensor associated with vector  $c_{i,i-1}$ , which is defined in a similar fashion as  $\omega_i \times 1$ . Then, the kinematic equations of the serial chain system comprising  $n$  links can be derived to a compact matrix form as:

$$t = N\dot{\theta} \quad (5.7)$$

in which,

$$\begin{bmatrix} t_1 \\ t_2 \\ \vdots \\ t_{n-1} \\ t_n \end{bmatrix} = \begin{bmatrix} p_1 & \mathbf{0} & \mathbf{0} & \cdots & \mathbf{0} \\ B_{21}p_1 & p_2 & \mathbf{0} & \cdots & \mathbf{0} \\ \vdots & \vdots & \vdots & \ddots & \vdots \\ B_{n-1,1}p_1 & B_{n-1,2}p_2 & \cdots & B_{n-1,n-2}p_{n-2} & B_{n,n-1}p_{n-1} \\ B_{n1}p_1 & B_{n2}p_2 & \cdots & B_{n,n-1}p_{n-1} & p_n \end{bmatrix} \begin{bmatrix} \dot{\theta}_1 \\ \dot{\theta}_2 \\ \vdots \\ \dot{\theta}_{n-1} \\ \dot{\theta}_n \end{bmatrix} \quad (5.8)$$

Thus, the generalized twist  $t$  is expressed as a linear transformation of the n-dimensional joint rate vector  $\dot{\theta}$  in Equation (5.8), in which the vector  $t$  is defined as  $t = [t_1 \ t_2 \ \dots \ t_{n-1} \ t_n]^T$ , the vector  $\dot{\theta}$  is defined as  $\dot{\theta} = [\dot{\theta}_1, \dots, \dot{\theta}_n]^T$ , and the Natural Orthogonal Complement (NOC) matrix  $N$  is defined as:

$$N = \begin{bmatrix} p_1 & \mathbf{0} & \mathbf{0} & \cdots & \mathbf{0} \\ B_{21}p_1 & P_2 & \mathbf{0} & \cdots & \mathbf{0} \\ \vdots & \vdots & \vdots & \ddots & \vdots \\ B_{n-1,1}p_1 & B_{n-1,2}p_2 & \cdots & B_{n-1,n-2}p_{n-2} & B_{n,n-1}p_{n-1} \\ B_{n1}p_1 & B_{n2}p_2 & \cdots & B_{n,n-1}p_{n-1} & p_n \end{bmatrix} \quad (5.9)$$

The NOC matrix  $N$  can be decoupled as:

$$N = N_l N_d \quad (5.10)$$

in which the matrix  $N_l$  and the matrix  $N_d$  are defined as the Decoupled Natural Orthogonal Complement of a serial chain system and can be derived as:

$$N_l = \begin{bmatrix} \mathbf{1} & \mathbf{0} & \mathbf{0} & \cdots & \mathbf{0} \\ B_{21} & \mathbf{1} & \mathbf{0} & \cdots & \mathbf{0} \\ B_{31} & B_{32} & \mathbf{1} & \cdots & \mathbf{0} \\ \vdots & \vdots & \vdots & \ddots & \vdots \\ B_{n1} & B_{n2} & B_{n3} & \cdots & \mathbf{1} \end{bmatrix} \text{ and } N_d = \begin{bmatrix} p_1 & \mathbf{0} & \mathbf{0} & \cdots & \mathbf{0} \\ \mathbf{0} & p_2 & \mathbf{0} & \cdots & \mathbf{0} \\ \mathbf{0} & \mathbf{0} & p_3 & \cdots & \mathbf{0} \\ \vdots & \vdots & \vdots & \ddots & \vdots \\ \mathbf{0} & \mathbf{0} & \mathbf{0} & \cdots & p_n \end{bmatrix} \quad (5.11)$$

where  $\mathbf{0}$  and  $\mathbf{0}$  are the  $6 \times 6$  matrix of zeros and the 6-dimensional vector of zeros respectively.

### 5.1.3 Uncoupled Newton-Euler Equations

Dynamic equations of motion of each link of the serial chain system shown in Figure 5-1 are derived in this section. Equations are first derived without considering the kinematic constraints in section 5.1.2 of each link. These equations without considering kinematics constraints are uncoupled or unconstrained Newton-Euler equations. The uncoupled NE equations of motion of the  $i^{th}$  link (Figure 5-2) can be derived as:

$$\text{Euler's Equation:} \quad I_i \dot{\omega}_i + \omega_i \times I_i \omega_i = n_i \quad (5.12)$$

$$\text{Newton's Equation:} \quad m_i \dot{v}_i = f_i \quad (5.13)$$

where  $\omega_i$  and  $\dot{\omega}_i$  are the vectors of angular velocity and acceleration of the  $i^{th}$  link respectively.

Furthermore,  $\dot{v}_i$  is the vector of linear acceleration of the center of mass  $C_i$ . The Equations (5.12) and (5.13) can be written in a compact form as:

$$M_i \dot{t}_i + W_i M_i t_i = w_i \quad (5.14)$$

In above equation,  $\dot{t}_i$  is the time derivative of the twist of the  $i^{th}$  link, i.e.  $\dot{t} = [t_1 \ t_2 \ \dots \ t_{n-1} \ t_n]^T$ . For the serial-link system with  $n$  rigid links, the equations can thus be written as:

$$M\dot{t} + WMt = w \quad (5.15)$$

Equation (5.15) constitutes a set of  $6n$  uncoupled equations, where  $M$  and  $W$  are the generalized mass and generalized angular velocity matrix respectively defined as:

$$M = \begin{bmatrix} M_1 & \cdots & O \\ \vdots & \ddots & \vdots \\ O & \cdots & M_n \end{bmatrix} \text{ and } W = \begin{bmatrix} W_1 & \cdots & O \\ \vdots & \ddots & \vdots \\ O & \cdots & W_n \end{bmatrix} \quad (5.16)$$

As described previously in Equation (5.1),  $w_i$  and  $t_i$  are the vectors of generalized wrench and twist of link  $i$  respectively as:

$$t = [t_1^T, \dots, t_n^T]^T \text{ and } w = [w_1^T, \dots, w_n^T]^T \quad (5.17)$$

#### 5.1.4 Coupled Equations of Motion

The dynamics model of the serial chain system (Figure 5-1) are obtained by introducing the kinematics constraints into the uncoupled NE equations of motion derived as Equation (5.15). The exerting wrench  $w$  of the serial chain system can be expressed as:

$$w = w^E + w^C \quad (5.18)$$

where  $w^E$  and  $w^C$  is the external and constraint wrench respectively. The external wrench  $w^E$  is contributed by the moments and forces due to the joint actuators, gravity, and environment effects; whereas the constraint wrench  $w^C$  is due to the presence of the joints that deliver the reaction moments and forces at the joints. Due to the fact that the constraint wrench  $w^C$  doesn't do any useful work towards the motion of the leg links, thus the power consumption of the constraint wrench  $w^C$  equals zero and can be expressed as:

$$P^C = t^T w^C = 0 \quad (5.19)$$

Substituting Equation (5.7) and (5.10) into Equation (5.19) as:

$$(N\dot{\theta})^T w^C = \dot{\theta}^T N^T w^C = 0 \quad (5.20)$$

For a serial chain system with  $n$  links, the  $n$ -dimensional joint rate vector  $\dot{\theta}$  is independent. Hence, in order to satisfy Equation (5.20), the following equation must hold as:

$$N^T w^C = 0 \quad (5.21)$$

Thus, by pre-multiplying the transpose of NOC matrix  $N^T$  with both sides of Equation (5.15) as:

$$N^T(M\dot{t} + WMt) = N^T(w^E + w^C) \quad (5.22)$$

Then, substituting  $t$  and its time derivative  $\dot{t} = N\ddot{\theta} + \dot{N}\dot{\theta}$  to Equation (5.22), we can get  $n$  independent dynamic equations of motion as:

$$I\ddot{\theta} + C\dot{\theta} = \tau \quad (5.23)$$

In which,

$$\text{The generalized inertia matrix (GIM) terms: } I = N^T MN \quad (5.24)$$

$$\text{The matrix for convective inertia (MCI) terms: } C = N^T(M\dot{N} + WMN) \quad (5.25)$$

$$\text{The vector of convective inertia (VCI) terms: } h = C\dot{\theta} \quad (5.26)$$

The generalized forces due to driving torques/forces,

$$\text{and those resulting from the gravity, environment and } \tau = N^T w^E \quad (5.27)$$

dissipation:

The variables of the dynamic equations of motion in Equation (5.23) derived by DeNOC method, i.e. the GIM, MCI, VCI, and the generalized forces defined by Equation (5.24), (5.25), (5.26), and (5.27) respectively can be expressed analytically, which allows further physical interpretations and computational simplification [59]. These analytical expressions can be found in Appendix B.

### 5.1.5 Recursive Inverse Dynamics Equations

The inverse dynamics of a serial chain system is defined as the process of determining the joint forces/torques when the joint motions of the system are known [67]. Based on the dynamic equations of motion derived in previous sections, the inverse dynamics algorithm calculates the joint torques,  $\tau_i$  for  $i = 1, \dots, n$ , in two recursive steps, i.e. forward and backward formulations. The two recursive step process is described below.

#### 5.1.5.1 Step 1: Forward Recursion (Kinematic Equations)

First, the twist ( $t_i$ ) and twist-rate ( $\dot{t}_i$ ) vectors of each link are calculated for  $i = 1, 2, \dots, n$  as follows:

$$t_1 = p_1 \dot{\theta}_1; \quad \dot{t}_1 = p_1 \ddot{\theta}_1 + \dot{p}_1 \dot{\theta}_1 + \rho_G \quad (5.28)$$

$$t_2 = B_{21} t_1 + p_2 \dot{\theta}_2 \quad \dot{t}_2 = B_{21} \dot{t}_1 + \dot{B}_{21} t_1 + p_2 \ddot{\theta}_2 + \dot{p}_2 \dot{\theta}_2 \quad (5.29)$$

$$\vdots \quad \vdots$$

$$t_i = B_{i,i-1} t_{i-1} + p_i \dot{\theta}_i \quad \dot{t}_i = B_{i,i-1} \dot{t}_{i-1} + \dot{B}_{i,i-1} t_{i-1} + p_i \ddot{\theta}_i + \dot{p}_i \dot{\theta}_i \quad (5.30)$$

where  $\rho_G$  represents gravity as  $\rho_G = [\mathbf{0}^T, -g^T]$ , in which  $\mathbf{0} = [0 \ 0 \ 0]$ .

#### 5.1.5.2 Step 2: Backward Recursion (Dynamic Equations)

With the results from Step 1, the joint torques are derived per Equations (5.31) to (5.33) for  $i = n, n-1, \dots, 1$  as:

$$w_n = M_n \dot{t}_n + W_n M_n t_n - w_n^W; \quad \tilde{w}_n = w_n; \quad \tau_n = p_n^T \tilde{w}_n \quad (5.31)$$

$$\begin{aligned} w_{n-1} &= M_{n-1} \dot{t}_{n-1} + W_{n-1} M_{n-1} t_{n-1}; & \tilde{w}_{n-1} &= w_{n-1} + B_{n,n-1}^T \tilde{w}_n; & \tau_{n-1} &= p_{n-1}^T \tilde{w}_{n-1} \\ & & & & & \end{aligned} \quad (5.32)$$

$$\vdots \quad \vdots \quad \vdots$$

$$w_1 = M_1 \dot{t}_1 + W_1 M_1 t_1; \quad \tilde{w}_1 = w_1 + B_{21}^T \tilde{w}_2; \quad \tau_1 = p_1^T \tilde{w}_1 \quad (5.33)$$

where  $w_n^W$  denotes the external wrench acting on the wheel (the  $n^{th}$  link of leg) by the interaction terrains, which can be calculated by the wheel-terrain interaction model developed in Chapter Four.

### **5.1.6 Recursive Forward Dynamic Equations**

Given the joint torques and forces along with the robot's physical parameters, the forward dynamics solves for the joint accelerations [68]. In this section, we solve the joint acceleration  $\ddot{\theta}$  from the dynamic equation of motion using Equation (5.23). Then the solutions of the joint acceleration  $\ddot{\theta}$  are used to obtain the joint velocities  $\dot{\theta}$  and positions  $\theta$  for a given initial set of joint rate  $\dot{\theta}(0)$  and position  $\theta(0)$ .

Conventionally, the joint acceleration are solved directly by using the Equation (5.23) as  $\ddot{\theta} = \mathbf{I}^{-1}\phi$ , in which  $\phi = \tau - \mathbf{C}\dot{\theta}$ . It will be seen that the approach requires order ( $n^3$ ) computations, where  $n$  is the leg's link numbers of hybrid robots. The dynamic algorithm derived next based on the DeNOC method solves  $\ddot{\theta}$  recursively with an order ( $n$ ) computational complexity. In order to realize this, the GIM  $\mathbf{I}$  of Equation (5.23) is decomposed as  $\mathbf{I} = UDU^T$  using the Reverse Gaussian Elimination (RGE) method [66, 69], where  $U$  and  $D$  are the upper triangular and diagonal matrices respectively.

Thus, for the development of the recursive forward dynamics algorithm, the constrained dynamic equations of motion, Equation (5.23) is rewritten as  $UDU^T\ddot{\theta} = \phi$ . Then, three recursive steps are developed to calculate the joint accelerations.

In the forward dynamics procedure to be described in this section, there is a need to introduce new intermediate variables (e.g.  $\hat{\phi}, \psi, \eta, \tilde{\phi}$ , and  $\mu$ ) due to the fact that the RGE method was utilized to perform the matrix factorization of the generalized inertia matrix  $\mathbf{I} = UDU^T$ . The

essential idea of doing so is to solve  $\ddot{\theta}$  recursively to reduce the computational complexity associated with alternative direct solutions as  $\ddot{\theta} = \mathbf{I}^{-1}\phi$ .

#### 5.1.6.1 Step 1

Solution for the  $\hat{\phi}$ , defined as  $\hat{\phi} = DU^T\ddot{\theta}$ , then  $\hat{\phi} = U^{-1}\phi$  is evaluated as:

$$\hat{\phi}_i = \phi_i - p_i^T \eta_{i,i+1}, \text{ for } i = n, \dots, 1 \quad (5.34)$$

Note that  $\hat{\phi} = \phi_n$ , and the 6-dimensional vector  $\eta_{i,i+1}$  can be computed as:

$$\eta_{i,i+1} = B_{i+1,i}^T \eta_{i+1} \text{ and } \eta_{i+1} = \psi_{i+1} \hat{\phi}_{i+1} + \eta_{i+1,i+2} \quad (5.35)$$

where  $\eta_{n,n+1} = 0$ , and the variable  $\psi_{i+1}$  is the  $6 \times 6$  matrix which can be derived by Equation (5.36):

$$\psi_i = \hat{\psi}_i / \hat{m}_i, \text{ where } \hat{\psi}_i = \hat{M}_i p_i \text{ and } \hat{m}_i = p_i^T \hat{\psi}_i \quad (5.36)$$

The matrix  $\hat{M}_i$  can be obtained recursively as:

$$\hat{M}_i = M_i + B_{i+1,i}^T \bar{M}_{i+1} B_{i+1,i}, \text{ where } \bar{M}_{i+1} = \hat{M}_{i+1} - \hat{\psi}_{i+1} \psi_{i+1}^T \quad (5.37)$$

For  $i = n-1, \dots, 1$ , and  $\hat{M}_n = M_n$ . The  $6 \times 6$  symmetric matrix  $\hat{M}_i$  is the mass matrix of the articulated body  $i$  defined as the links  $\#i, \dots, \#n$ , coupled by the joints  $i+1, \dots, n$ , which is exactly the same as the Articulated Body Inertia (ABI) defined in the Featherstone algorithm [70, 71].

#### 5.1.6.2 Step 2

Solution for  $\tilde{\phi}$ , where  $\tilde{\phi} = U^T \ddot{\theta} = D^{-1} \hat{\phi}$ . Due to the property of the RGE method to do the  $\mathbf{I} = UDU^T$  factorization, the matrix  $D^{-1}$  only has non-zero diagonal elements and is the reciprocal of the corresponding diagonal elements of the matrix  $D$ . The vector  $\tilde{\phi}$  is then obtained as follows, for  $i = 1, \dots, n$ ,

$$\tilde{\phi}_i = \hat{\phi}_i / \hat{m}_i \quad (5.38)$$

where the scalar  $\hat{m}_i$  is defined in Equation (5.36).

#### 5.1.6.3 Step 3

Solution for  $\ddot{\theta}_i$ , and  $\ddot{\theta} = U^{-T} \tilde{\phi}$  is calculated for  $i = 2, \dots, n$  as:

$$\ddot{\theta}_i = \hat{\phi}_i - \hat{\psi}_i^T \tilde{\mu}_{i,i-1} \quad (5.39)$$

where  $\ddot{\theta}_1 = \tilde{\phi}_i$ , and the 6-dimensional vector  $\tilde{\mu}_{i,i-1}$  is obtained as,

$$\tilde{\mu}_{i,i-1} = B_{i,i-1} \tilde{\mu}_{i-1} \text{ and } \tilde{\mu}_{i-1} = p_{i-1} \ddot{\theta}_{i-1} + \tilde{\mu}_{i-1,i-2} \quad (5.40)$$

in which  $\tilde{\mu}_{10} = 0$ .

## 5.2 Modeling of the Walking Locomotion Mode

A 3-link leg (the outermost segment is a wheel) model shown in Figure 5-3a is developed using the DeNOC method in this section. The model is developed to show the generalized walking locomotion mode modeling method of hybrid robots shown in Figure 3-1 using the DeNOC algorithm.

In contrast with the continuous motion property, i.e. wheels interact with terrains all the time, defined in the rolling locomotion mode of hybrid robots describe in Chapter Four, the motion of legs in the walking locomotion mode are discrete because legs are lifted up and down as well as forward and backward all the time. The rule for these legs movement together with the body movement is named as the walking gait, which the robots are controlled to follow to achieve a proper walking locomotion. One cyclic walking gait, peristaltic gait, of a hybrid wheel-legged robot [49] was adapted to step negotiation shown in Figure 5-3 as: lifting one wheel up to the step while maintaining the rest part of the robot still shown in Figure 5-3b (wheel stepping phase), then moving the corresponding one quarter of the body up and forward while keeping the

stepped wheel fixed shown in Figure 5-3c (body moving phase); repeating this movement until the whole robot transverse over the step. This peristaltic gait is the simplest step climbing gait, in which only one leg negotiates the step at a time, thus is generic enough to be applied to various walking gaits of wheel/track-legged robots.

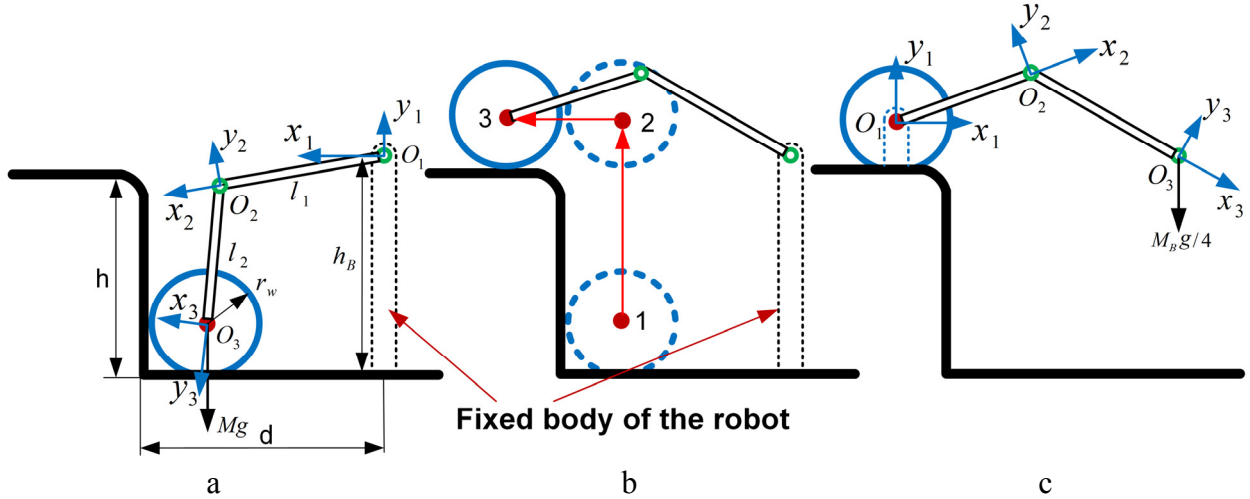


**Figure 5-3. Step Climbing Gait of the Walking Locomotion Mode.**

In Figure 5-3, the coordinate frames  $x_1O_1y_1$ ,  $x_2O_2y_2$  and  $x_3O_3y_3$  are attached to the body, link 1 and link 2 respectively following the modified traditional Denavit-Hartenberg (D-H) method used in DeNOC algorithm. In the wheel stepping phase of the peristaltic gait, the body is represented by a dotted link base attached on the ground shown in Figure 5-3a and b; in the body moving phase, the wheel is considered as a fixed base (dotted link base attached on the ground) as shown in Figure 5-3c.

In the wheel stepping phase of the peristaltic gait, the wheel trajectory is defined in a way that the wheel is first lifted from positon 1 (initial positon of wheel stepping phase) to 2, where the wheel is at the same height as the step, then is pushed forward from position 2 to 3, where is the final positon of wheel stepping phase. This stepping movement trajectory of the wheel can be shown as the red arrows in Figure 5-3b.

In order to achieve the defined trajectory for the wheel, joint trajectories must be defined properly to realize smooth joint motions. Thus, besides the initial and final positions of joint 1 and 2 obtained by solving the inverse kinematics problem using the algebra method, the joint velocity and acceleration should also be considered to define the joint trajectories. In this case, six conditions of the joint are controlled, i.e. position, velocity, and acceleration at the initial and final states, a fifth order polynomial is needed to produce a smooth trajectory for each joint. The fifth order polynomial is used to do the calculations for the joints from the Cartesian to the joint space. In general, a fifth-order polynomial is written as:

$$\theta(t) = a_0 + a_1 t + a_2 t^2 + a_3 t^3 + a_4 t^4 + a_5 t^5 \quad (5.41)$$

whose first two time derivatives are:

$$\dot{\theta}(t) = a_1 + 2a_2 t + 3a_3 t^2 + 4a_4 t^3 + 5a_5 t^4 \quad (5.42)$$

$$\ddot{\theta}(t) = 2a_2 + 6a_3 t + 12a_4 t^2 + 20a_5 t^3 \quad (5.43)$$

The initial and final states are expressed as:

$$\theta(t_i) = \theta_0; \dot{\theta}(t_i) = \dot{\theta}_0; \ddot{\theta}(t_i) = \ddot{\theta}_0 \quad (5.44)$$

$$\theta(t_f) = \theta_f; \dot{\theta}(t_f) = \dot{\theta}_f; \ddot{\theta}(t_f) = \ddot{\theta}_f \quad (5.45)$$

Substituting these initial and final states into above equations, six equations with six unknowns  $a_0, \dots, a_5$  are obtained as:

$$\theta(0) = \theta_0 = a_0 \quad (5.46)$$

$$\theta(t_f) = \theta_f = a_0 + a_1 t_f + a_2 t_f^2 + a_3 t_f^3 + a_4 t_f^4 + a_5 t_f^5 \quad (5.47)$$

$$\dot{\theta}(0) = a_1 \quad (5.48)$$

$$\dot{\theta}(t_f) = a_1 + 2a_2 t_f + 3a_3 t_f^2 + 4a_4 t_f^3 + 5a_5 t_f^4 \quad (5.49)$$

$$\ddot{\theta}(0) = 2a_2 \quad (5.50)$$

$$\ddot{\theta}(t_f) = 3a_2 + 6a_3 t_f + 12a_4 t_f^2 + 20a_5 t_f^3 \quad (5.51)$$

Thus a more compact matrix vector form can be written as  $\mathbf{Ax} = \mathbf{b}$ , where the  $6 \times 6$  matrix  $\mathbf{A}$ , the 6-dimensional unknown vector  $\mathbf{x}$  containing the polynomial coefficients, and the known 6-dimensional vector  $\mathbf{b}$  of the conditions is expressed respectively as:

$$\mathbf{A} = \begin{bmatrix} 1 & 0 & 0 & 0 & 0 & 0 \\ 1 & t_f & t_f^2 & t_f^3 & t_f^4 & t_f^5 \\ 0 & 1 & 0 & 0 & 0 & 0 \\ 0 & 1 & 2t_f & 3t_f^2 & 4t_f^3 & 5t_f^4 \\ 0 & 0 & 2 & 0 & 0 & 0 \\ 0 & 0 & 2 & 6t_f & 12t_f^2 & 20t_f^3 \end{bmatrix}, \mathbf{x} = \begin{bmatrix} a_0 \\ a_1 \\ a_2 \\ a_3 \\ a_4 \\ a_5 \end{bmatrix}, \text{ and } \mathbf{b} = \begin{bmatrix} \theta_0 \\ \theta_f \\ \dot{\theta}_0 \\ \dot{\theta}_f \\ \ddot{\theta}_0 \\ \ddot{\theta}_f \end{bmatrix} \quad (5.52)$$

Solutions of this set of linear algebraic equations can be obtained by  $\mathbf{x} = \mathbf{A}^{-1}\mathbf{b}$ .

For the 3-link leg system shown in Figure 5-3a, in order to do the joints trajectory planning and future energy evaluations of walking locomotion mode, the leg and step parameters are defined with respect to the wheel radius  $r_w$  shown in Table 5-2. Here,  $r_w = 0.098m$  based on Cricket's track design.

**Table 5-2. Model and Step Parameters Definition**

| Parameters | Definitions  | Values (meter) |
|------------|--|----------------|
| $r_w$      | Wheel radius   | $r_w$          |
| $l_1$      | Leg link 1   | $3r_w$         |
| $l_2$      | Leg link 2   | $3r_w$         |
| $h_B$      | Body height  | $5r_w$         |
| $d$        | Horizontal distance from the origin of Frame $G$ to the step | $4r_w$         |
| $h$        | Step height  | $2r_w$         |

For the wheel stepping phase, the trajectory of joint 1 and 2 can be plotted as shown in Figure 5-4. For the body moving phase, the trajectory of joint 1 and 2 can be plotted as shown in Figure 5-5.

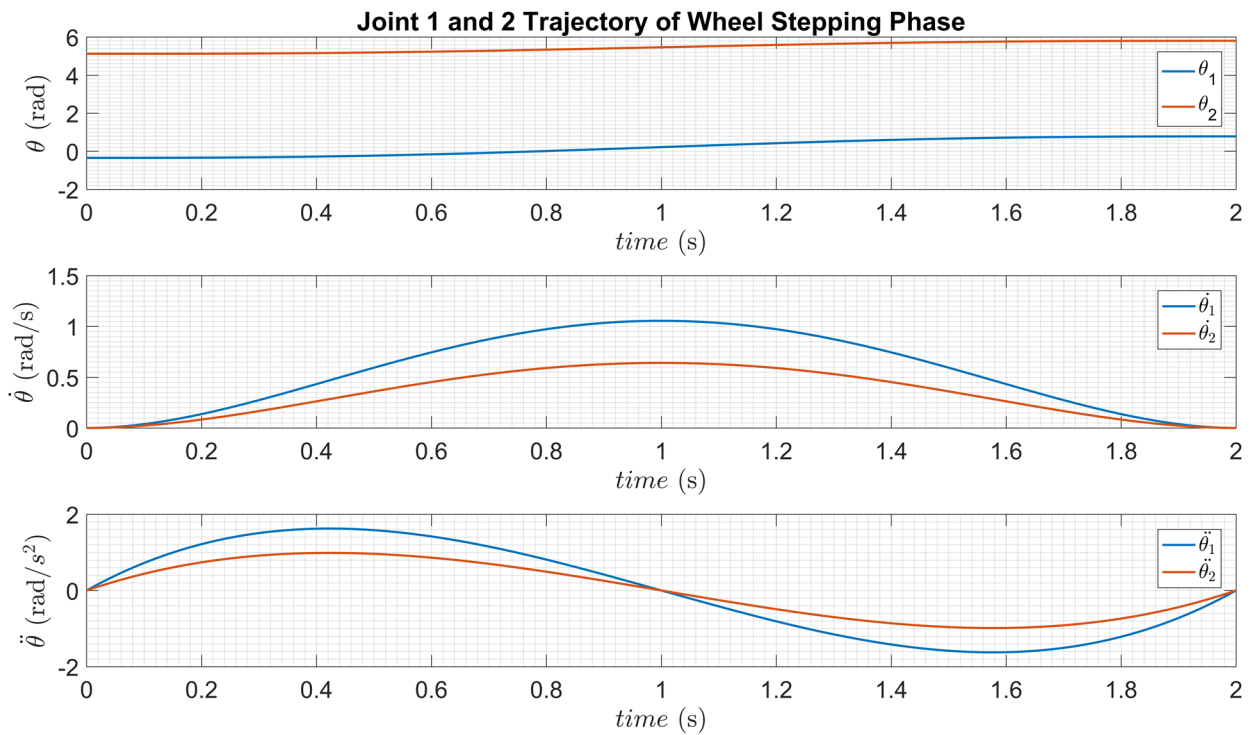


**Figure 5-4. Joint Trajectory of Joint 1 and 2 of the Wheel Stepping Phase.**

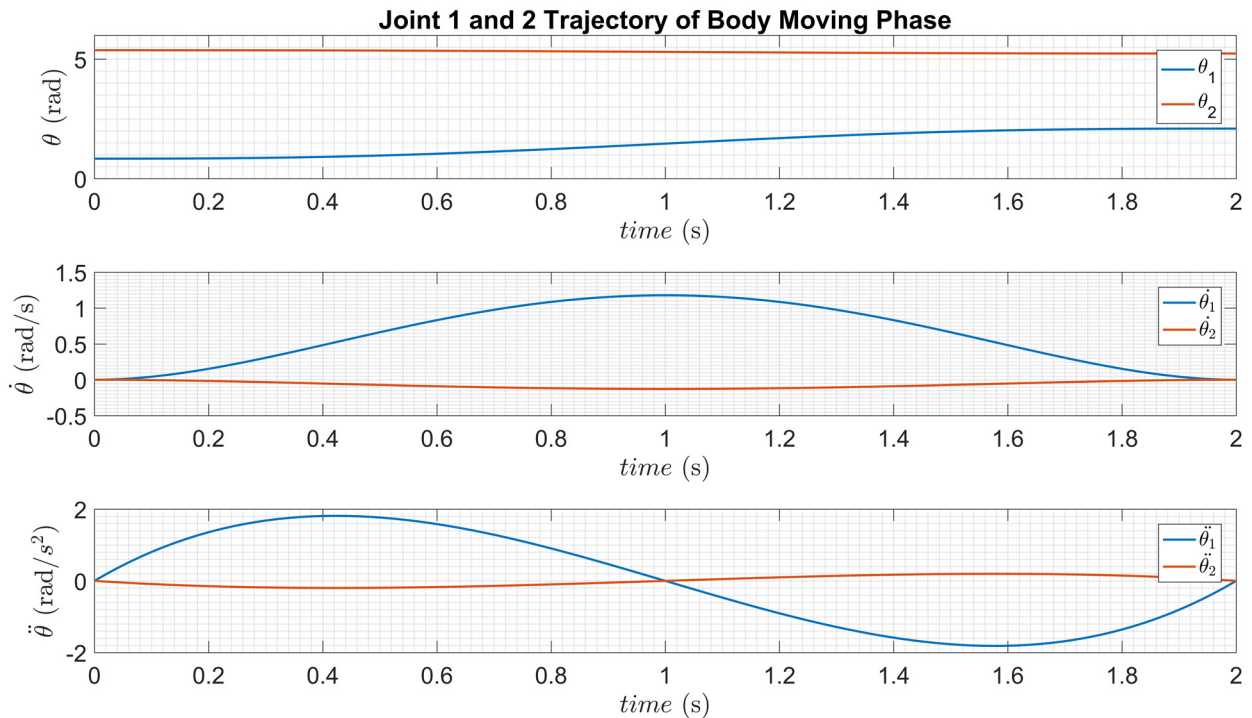


**Figure 5-5. Joint Trajectory of Joint 1 and 2 of the Body Moving Phase.**

### **5.3 Summary**

In this chapter, a recursive multibody dynamics modeling algorithm, DeNOC, is explained and then employed to develop the generalized dynamic model for the walking locomotion mode of wheel/track-legged hybrid robots. Different with the mathematical model developed for the rolling locomotion mode in Chapter Four, in which only the essential dynamics properties are considered due to the complexity of the wheel-terrain interaction evaluations, the developed walking locomotion model can provide accurate and efficient evaluation results for the walking locomotion. A 3-link leg with a drivable wheel as outermost segment is then developed representing the model of walking locomotion of the wheel/track-legged hybrid robots, together with the simplified rolling locomotion model developed in Chapter Four, will be used to conduct the energy evaluations for ground hybrid robots in Chapter Six.

The modeling method can also be extended to provide predictive evaluations for the walking locomotion mode of the ground hybrid robots. In order to achieve this goal, a complete dynamic model of the hybrid robot as well as adaptive walking gaits to realize the proper locomotion performance are needed.

## Chapter Six: TENTATIVE AUTONOMOUS LOCOMOTION MODE TRANSITION METHOD

The energy performances of rolling and walking locomotion modes of wheel/track-legged robots to negotiate step obstacle are evaluated in this chapter using the generalized locomotion mode models developed in Chapter Three and Four. A tentative autonomous locomotion mode transition method of wheel/track-legged robots is then proposed based on these energy performance knowledge.

### 6.1 Energy Consumption Evaluations

The energy consumption of the hybrid robots in both rolling and walking locomotion mode is the result of the energy consumption in the motor actuators. Other energy consumption due to on-board electronics sensors and ancillary equipment is negligible, thus weren't considered in the energy evaluations of the hybrid robot's locomotion modes. In general, the energy consumption of a DC motor can be calculated by Equation (3.5) and (3.6), which are reproduced here as:

$$\tau = K_t I_a \quad (6.1)$$

$$E_i = \int_0^{T_i} [f(\tau\dot{\theta})] dt + \int_0^{T_i} I_a^2 R_a dt \quad (6.2)$$

where  $\tau$  represents the motor shaft output torque,  $K_t$  denotes the torque constant,  $I_a$  represents the armature current; moreover,  $E_i$  represents the energy consumption of motor  $i$  during a time period  $T_i$ ,  $\dot{\theta}$  denotes the motor shaft output angular velocity, and  $R_a$  is the armature resistance.

The function  $f$  is defined as  $f(\tau\dot{\theta}) = \begin{cases} \tau\dot{\theta} & \text{when } \tau\dot{\theta} > 0 \\ 0 & \text{when } \tau\dot{\theta} \leq 0 \end{cases}$ , due to the fact that a negative value for the mechanical energy consumption ( $\tau\dot{\theta}$ ) doesn't result in a gain of energy of the motor without the specific designed electrical system to store energy. Substituting  $I_a$  derived by

Equation (6.1) into (6.2), then the energy consumption of motor  $i$  during a time period  $T_i$  can be evaluated as:

$$E_i = \int_0^{T_i} [f(\tau\dot{\theta})] dt + \int_0^{T_i} \frac{\tau^2 R_a}{K_t^2} dt \quad (6.3)$$

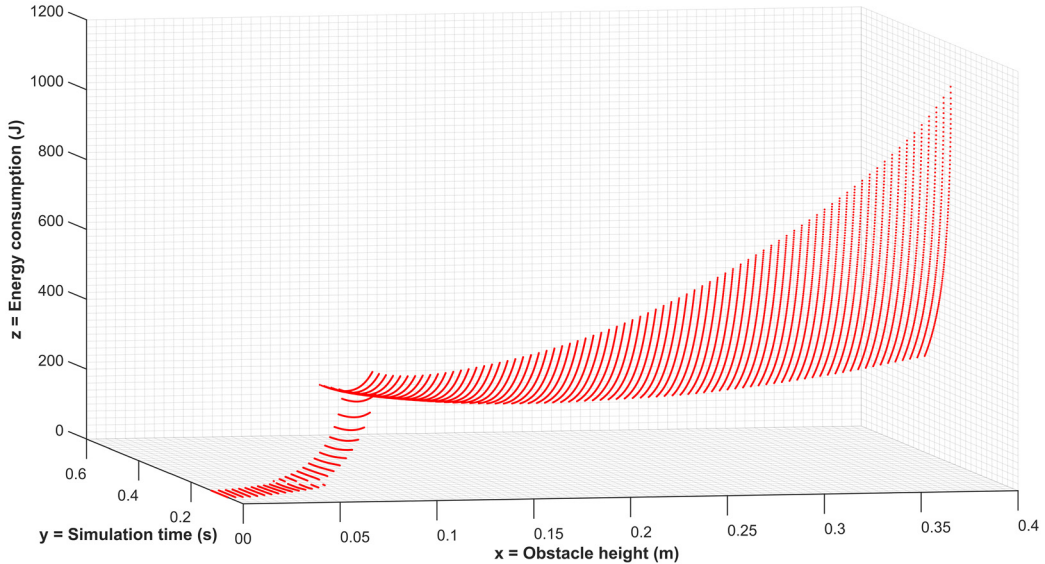
Here, the motor parameters including the armature resistance  $R_a$  and the torque constant  $K_t$  are specified based on the motor design of Cricket.

Both models of rolling and walking locomotion modes of wheel/track-legged robots were developed in MATLAB environment. Thus the energy performance evaluations of the two locomotion modes were also conducted in MATLAB. The energy consumption need to be compared in the same environment scenario (i.e. the same step height) and the same simulation time  $t$  (calculated time) for rolling and walking locomotion modes. For the rolling locomotion mode, the desired velocity of the vehicle  $v_d$  is the control input of the dynamics model, thus the simulation time  $t_r$  is calculated by the equations of motion; for the walking locomotion mode, the simulation time  $t_w$  is the control input to generate the leg trajectory, thus the simulation time  $t_w$  is defined to match the rolling simulation time  $t_r$ .

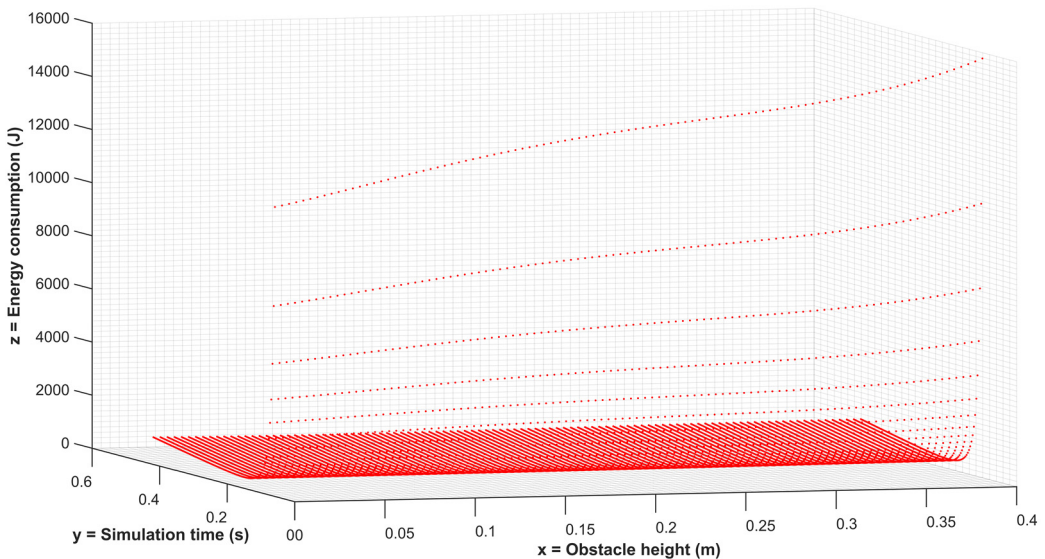
Despite the developed rolling and walking locomotion mode models aren't specified to one particular wheel/track-legged robot, the energy performances can only be evaluated through cases study by specifying parameters of the models. In the cases study, the step heights  $h$  was defined to range from 0 to 0.392m (4 times of the wheel radius  $r_w$ ), the desired velocity was defined to range between 3 m/s to 5 m/s.

The energy consumption of the two locomotion modes were calculated and compared under different step height  $h$  and simulation time  $t$  combinations. The obtained simulation results are shown in Figure 6-1 to Figure 6-8, in which  $x$ ,  $y$  and  $z$  axis represents the obstacle height

(meter), simulation time (second), and energy consumption (joule), respectively. In Figure 6-1 to Figure 6-8, each plotted dot represents an energy consumption value with respect to its step height and simulation time combination.

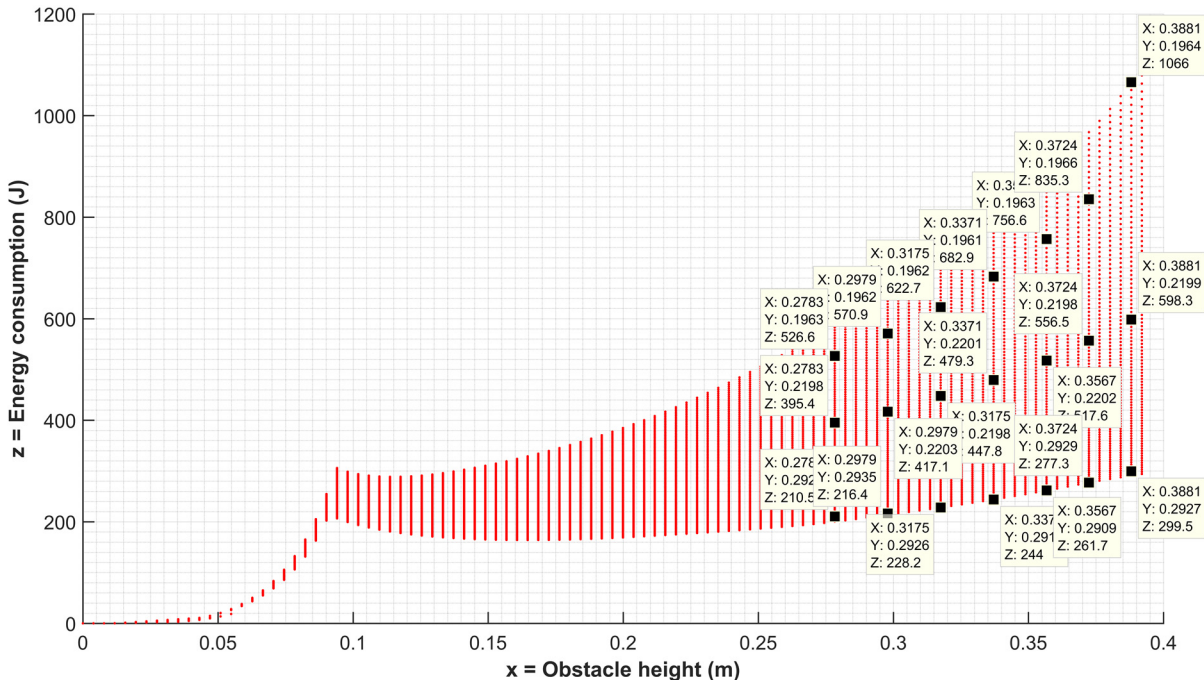


**Figure 6-1. Energy Evaluation Result of Rolling Locomotion in  $x$ - $y$ - $z$  Plane.**



**Figure 6-2. Energy Evaluation Result of Walking Locomotion in  $x$ - $y$ - $z$  Plane.**

For the rolling locomotion mode, it can be seen in Figure 6-3, when  $x$ , i.e. obstacle height is the same, energy consumption increases with  $y$ , i.e. simulation time decreases; it can be seen in Figure 6-5, when  $y$ , i.e. simulation time is the same, energy consumption increases with  $x$ , i.e. obstacle height increases.



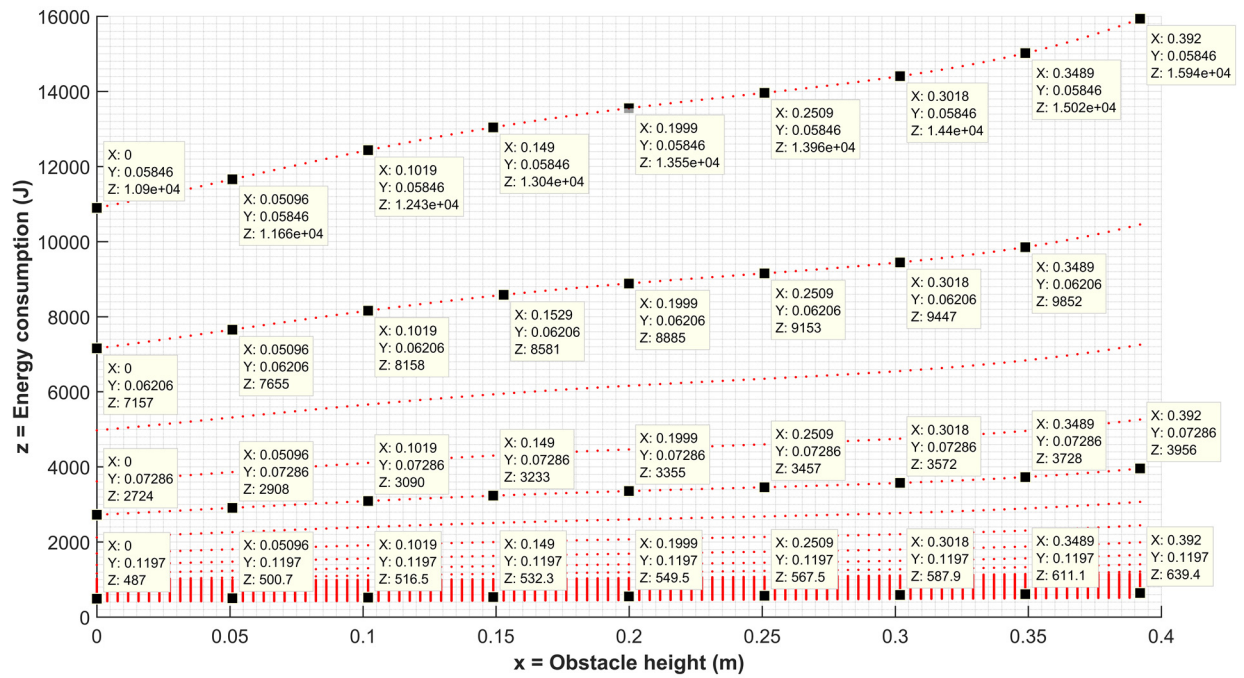


**Figure 6-4. Energy Evaluation Result of Walking Locomotion in  $x$ - $z$  Plane.**

For the walking locomotion mode, it can be observed in Figure 6-4, when  $y$ , i.e. simulation time is the same, energy consumption increases with  $x$ , i.e. obstacle height increases; it can be seen in Figure 6-6, when  $x$ , i.e. obstacle height is the same, energy consumption first decreases with  $y$ , i.e. simulation time decreases, then increases with  $y$  decreases after passing the lowest energy consumption point. This is because the back electromotive force (emf) effect of the motor that also can be seen in Figure 6-2. From these energy evaluation results, it is can be concluded that these simulation results are reliable to reflect the energy performances of rolling and walking locomotion modes.

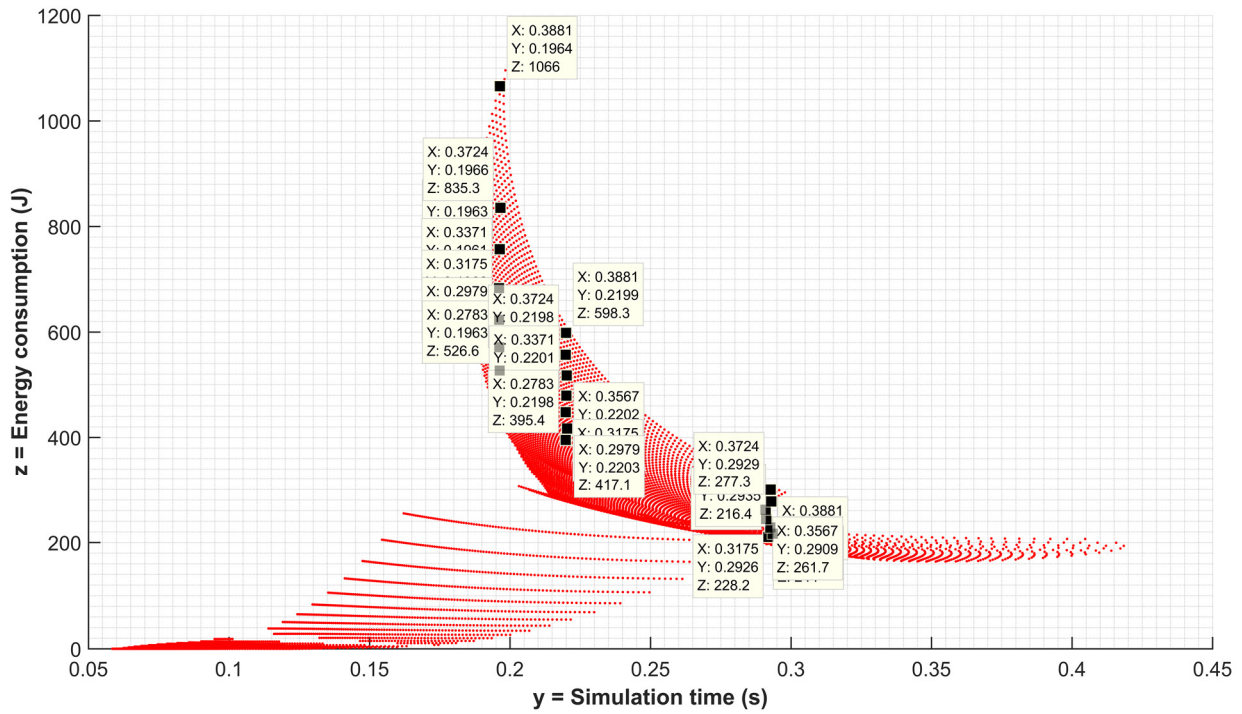


**Figure 6-5. Energy Evaluation Result of Rolling Locomotion in y-z Plane.**

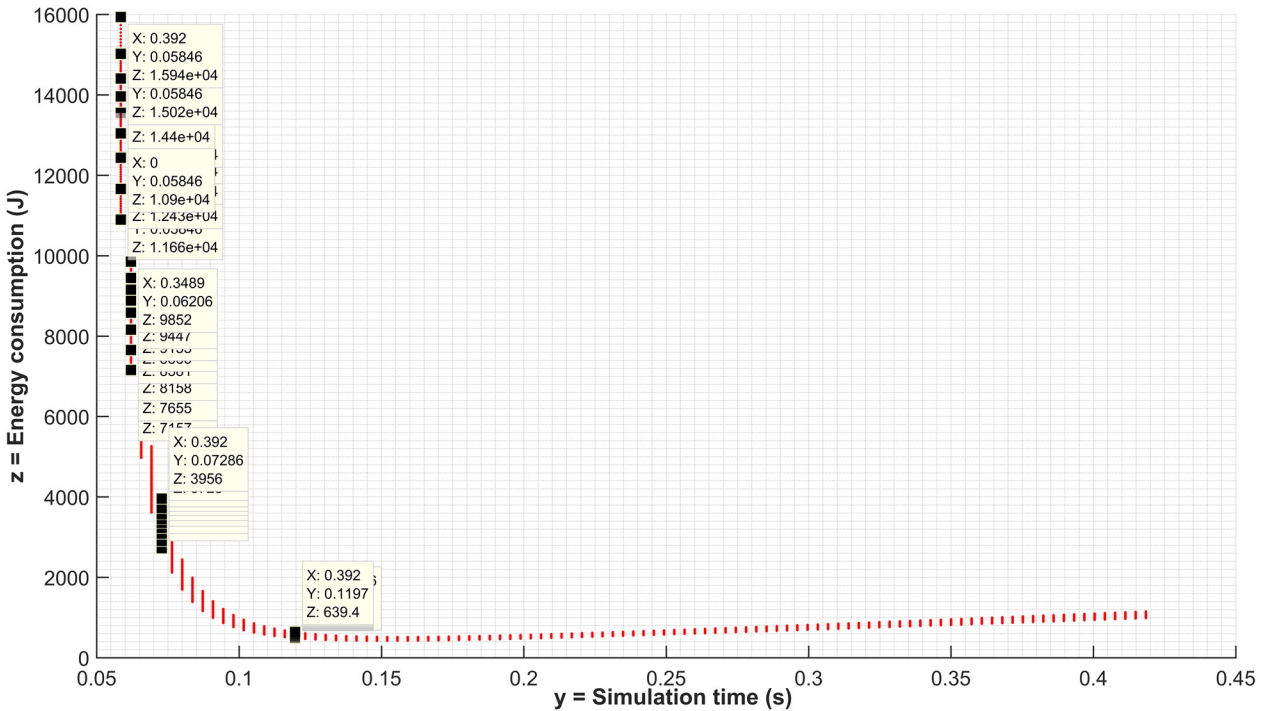


**Figure 6-6. Energy Evaluation Result of Walking Locomotion in y-z Plane.**

The energy performance of rolling and walking can be compared in the same negotiation environment, i.e. both locomotion mode are in the same step height shown in Figure 6-7 and Figure 6-8. It can be seen that within the blue squared data, when  $x$ , i.e. step heights are the same, walking locomotion consumes less energy ( $z$ ); at the same time, walking always takes less time. Within the green squared data, walking locomotion still consumes less energy for the same step height  $x$ . So based on the energy consumption criterion, walking is more appropriate compared with rolling locomotion mode in the green section area.

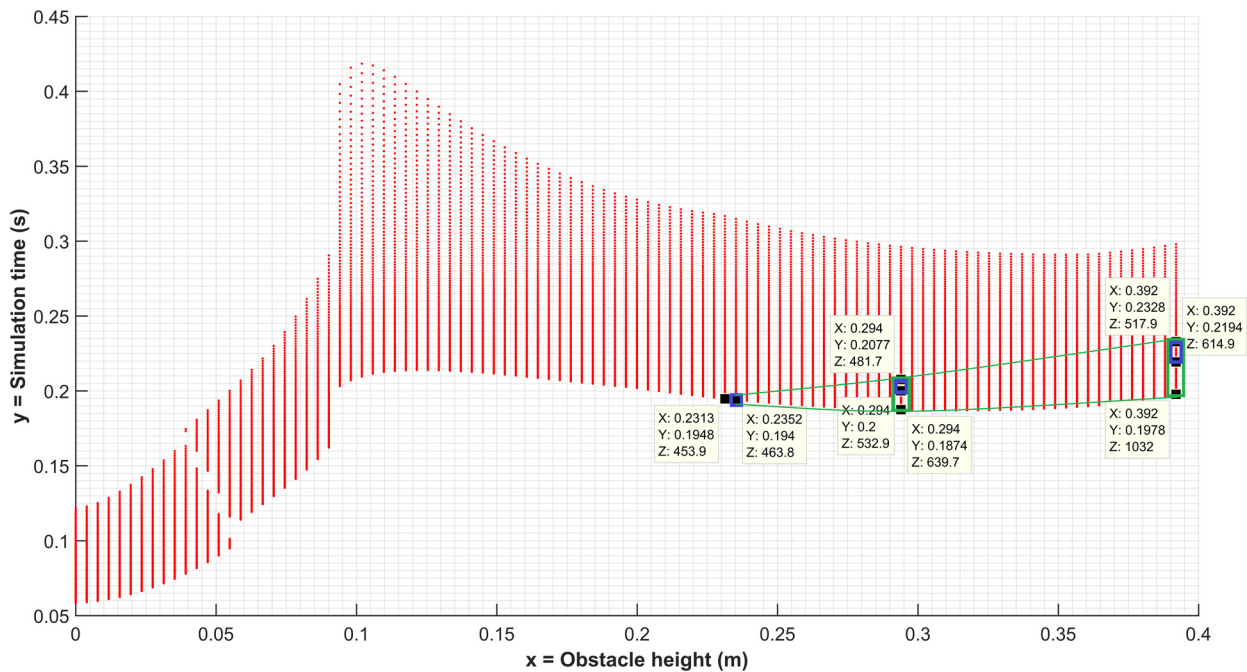


**Figure 6-7. Energy Evaluation Result of Rolling Locomotion in  $x$ - $y$  Plane.**

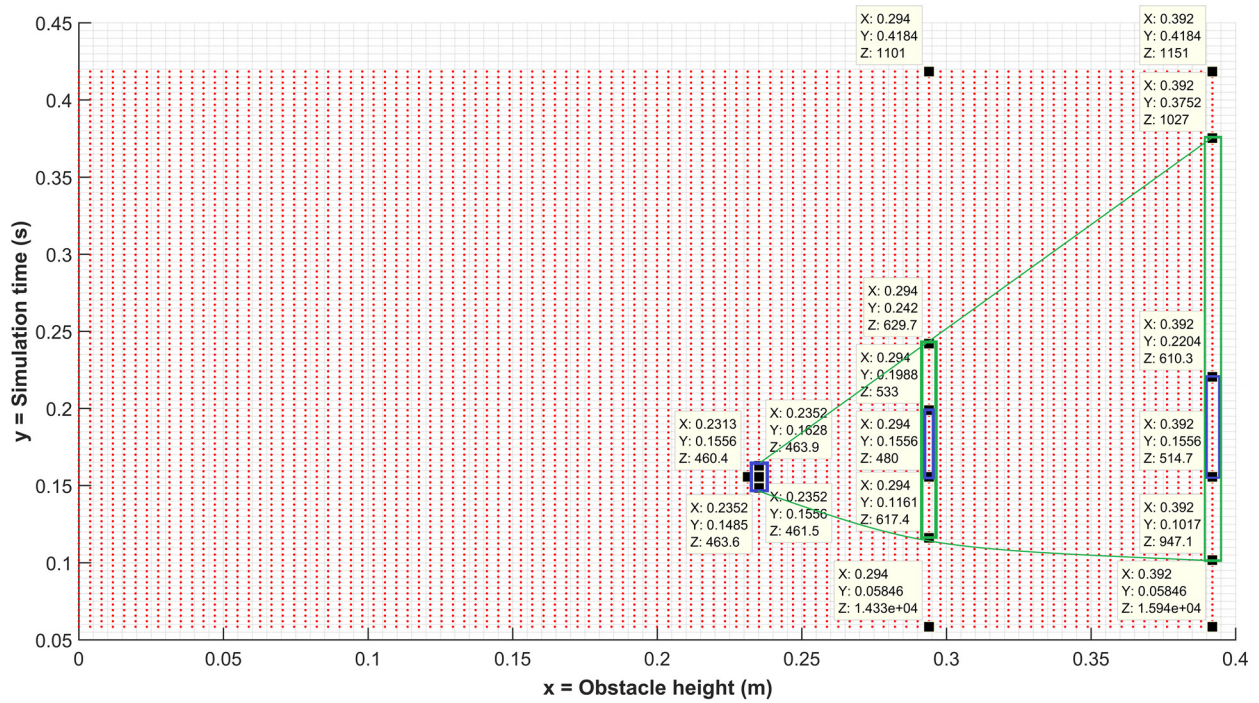


**Figure 6-8. Energy Evaluation Result of Walking Locomotion in  $x$ - $y$  Plane.**

From the obtained results, it can conclude that the energy consumption can be used as a criterion to realize the autonomous locomotion mode transition of wheel/track-legged robots because it can distinguish the locomotion performance of the two locomotion modes well. It can also be concluded that rolling locomotion is appropriate to negotiate low height steps, and walking locomotion is suitable to negotiate high height steps with respect to energy consumption criterion. So, it is necessary to conduct a locomotion mode transition from rolling to walking when negotiating steps with high height based on the energy consumption performance.

## 6.2 Tentative Method

The energy consumption performance knowledge of the two locomotion modes can be utilized to realize the locomotion mode transition. In above energy consumption evaluations, it can conclude that the walking locomotion may have more energy advantage in negotiating steps

with high height steps, so the locomotion transition need to be invoked to switch locomotion mode from default rolling to walking.

A tentative method to realize the locomotion mode transition automatically is then proposed and illustrated in Figure 6-9.

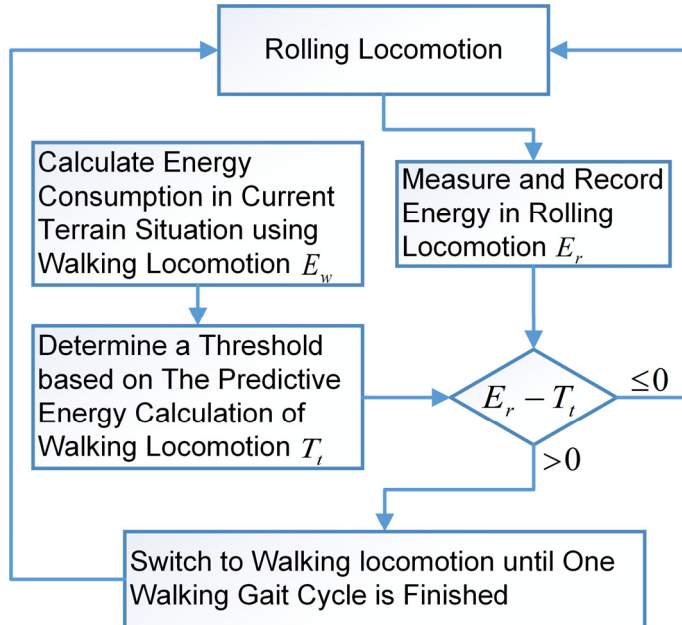


**Figure 6-9. Autonomous Locomotion Mode Transition Flowchart.**

The robot starts to negotiate the step in rolling locomotion mode, measuring and recording the consumed energy consumption since the negotiation start ( $E_r$ ); at the same time, calculating the energy consumption that the walking locomotion mode will consume to negotiate the step ( $E_w$ ); determining the threshold value ( $T_t$ ) based on the predictive energy consumption  $E_c$  ( $T_t$  was defined as same as  $E_c$  in this method); executing a decision-making process in a way that if  $E_r > T_t$ , the robot switches from rolling to walking locomotion until the designed one walking gait cycle is finished, then switches back to rolling locomotion; otherwise if  $E_r \leq T_t$ , the robot keeps in rolling locomotion mode.

The energy evaluation of the walking locomotion mode is an on-line predictive energy calculation based on one cycle of the designed step negotiation gait, the designed gait is generated based on the step height information  $h$  gathered by on-board sensors. So when the robot changes to walking locomotion, it keeps in walking locomotion mode until one gait cycle is finished.

### **6.3 Summary**

In this chapter, the energy evaluations between the rolling and walking locomotion modes are compared and characterized for the ground hybrid robots. For this, the models developed in Chapter Four and Five are used. With the energy evaluation results, a first autonomous locomotion mode transition method is proposed. This tentative method will be applied to the Cricket robot and be refined based on the continuing work. It can be concluded that the energy criterion provides a good locomotion performance evaluations for the ground hybrid robots, thus can be used to continue the work to realize the autonomous locomotion mode transition of ground hybrid robots.

## Chapter Seven: SIMULATION MODEL

From Chapter Six to Eight, the proposed autonomous locomotion mode transition method will be applied to the quadruped track-legged robot platform Cricket introduced in Chapter 1.2. This Chapter explains the physical model development of Cricket in a robotics simulation package. The physical model is created based on the mechanical design of Cricket. The kinematics calculation of the created model is the focus topic of this chapter, which is also the groundwork of the walking gait design in Chapter Seven.

### 7.1 Physical Model Building

This section elaborates the physical modeling process of Cricket in a virtual robot experimentation platform (V-REP) [9]. The robot simulator V-REP has a modular simulation architecture combined with a distributed control mechanism [72, 73]. The modular simulation architecture means each object/model can be individually controlled via an embedded script, a plugin, a ROS node, or a remote API client. The distributed control mechanism enables multitude of different programming techniques (i.e. C/C++, Python, Java, Lua, MATLAB, Octave and Urbi) for controllers. Moreover, efficient simulation performance is realized by powerful calculation modules including the kinematics module, dynamics module, collision detection module, and path/motion planning module embedded in V-REP. Especially in the dynamics module, there are four physical engines, i.e. Bullet Physics Library [74], Open Dynamics Engine [10], Vortex Dynamics [11], and Newton Dynamics [12] available to choose, which has a great advantage in validating simulation results than only relies on one single physics engine.

The modeling process includes creating “pure shape” of robot components, refining mass and inertia tensor parameters, and adding joints constraints to the model.

### ***7.1.1 Pure Shape Components***

The first step to build the physical model is to create pure shape approximations of every individual component of Cricket. In V-REP, shapes are rigid mesh objects that are composed of triangular faces and can be edited. Pure shapes include primitive shapes, i.e. cuboid, cylinder or sphere, and a group of primitive shapes. Pure shapes are best suited for all dynamics related calculations, since they perform fast and are stable. Besides pure shapes, convex shapes are convex meshes that are optimized for dynamics collision response calculation. Different with pure shape approximation of system components have to be created manually, convex shapes can be automatically created by built-in function with a better geometrical approximation of the original mechanical design. However, pure shapes are still recommended prior to convex shapes due to their better calculation speed and stable properties. In V-REP simulations, it is the model composed of pure shapes and convex shapes perform respondable and dynamic motions.

V-REP uses triangular meshes to describe and display shapes. The URDF file (\*.urdf) [3] is a format that describes objects as triangular meshes and is supported for import operations via a plugin function of V-REP. The URDF file can be obtained from SolidWorks file format (\*.SLDPRT and \*.SLDASM) by installing a software add-in named as SolidWorks to URDF Exporter [2]. The exporter creates a ROS-like package that contains a directory for meshes, textures and robots (\*.urdf files).

For Cricket specifically, a track-legged hybrid robot with highly articulated legs shown in Figure 1-2, the dynamics calculation of the V-REP model need to be both fast and stable. Thus, the body, the shoulder, and the proximal were approximated as pure shapes. The distal was created as convex shapes for its assembly geometry complexity with the track that needs higher approximation accuracy. The track part was modeled as five parallel cylinder pure shapes. These

V-REP respondable and dynamic models of each individual component are shown in Figure 7-1.

In Figure 7-1, the upper row are URDF files exported from SolidWorks, the lower row are respondable models created in V-REP. And from left to right is the body, shoulder, proximal, distal and track, respectively.

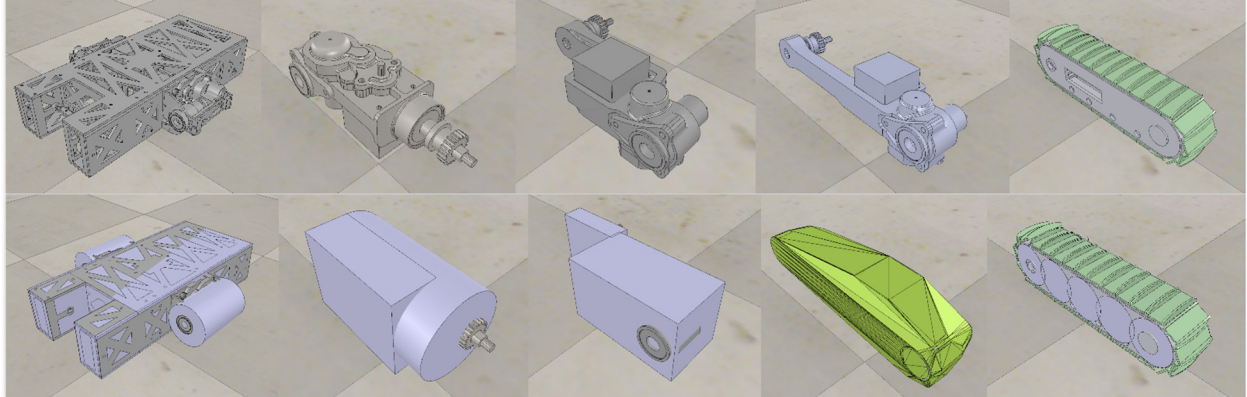


**Figure 7-1. The Pure Shape Model of Cricket's Individual Component.**

### 7.1.2 Mass and Inertia Tensor Import

The next step is to set the dynamics properties of each respondable model component. For all created dynamic models of the robot's individual component, these parameters including mass, principal moments of inertia, and the inertia tensor expressed relative to the center of mass. Since the mechanical design of Cricket was conducted in SolidWorks, these dynamics properties parameters can be obtained by mass properties evaluation shown in Figure 7-2 a.

For the mass and principal moments of inertia, it is pretty straightforward to transfer the values from mass properties evaluation of SolidWorks. When setting the inertia tensor parameters in V-REP, it should be noted that the moment of inertia in SolidWorks mass properties evaluations is mere values without signs. The matrix signs need be added referred to the canonical form of the tensor of inertia formula (written in matrix form) about the center of mass  $G$  with respect to the  $xyz$  axes [75] as:

$$I_G = \begin{pmatrix} I_{xx} & -I_{xy} & -I_{xz} \\ -I_{yx} & I_{yy} & -I_{yz} \\ -I_{zx} & -I_{zy} & I_{zz} \end{pmatrix} \quad (7.1)$$

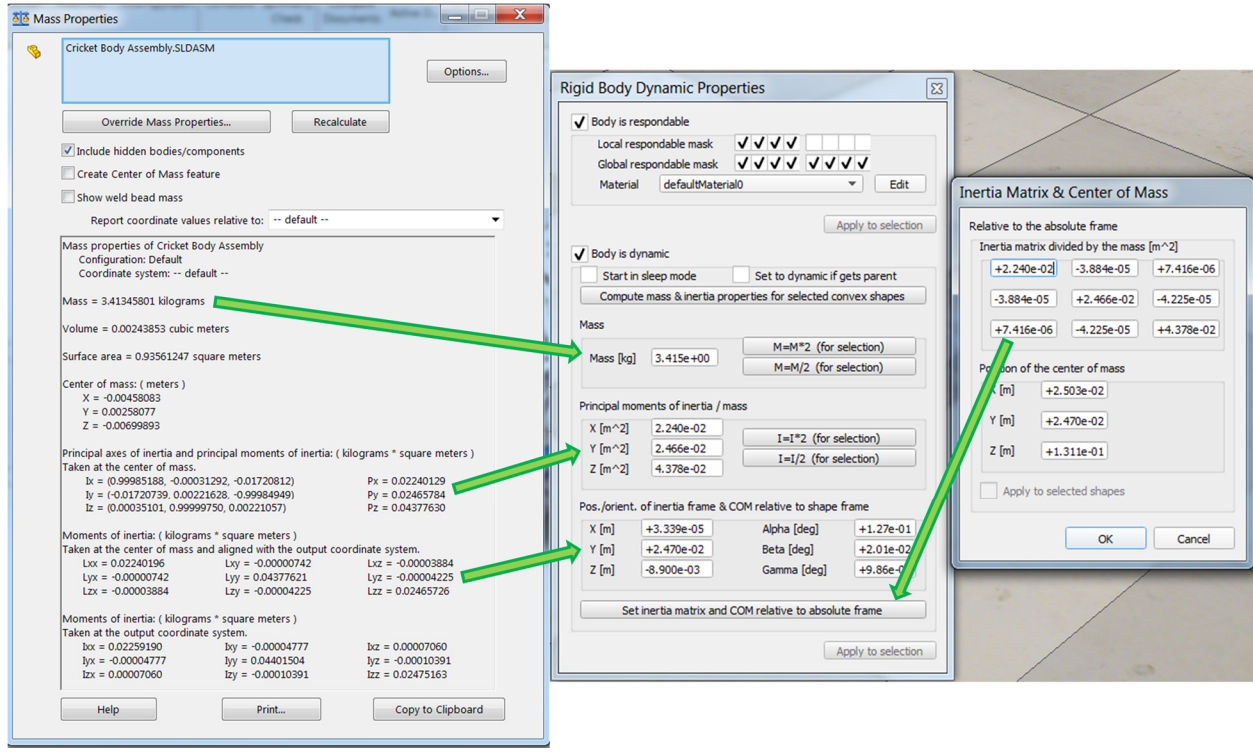


**Figure 7-2. Parameters from SolidWorks Mass Properties (a) to V-REP Dynamics Properties (b).**

### 7.1.3 Joint Constraints

The following step is to assemble each created individual objects by adding joint constraints. The joint positions are determined first by importing the urdf format file of the leg, then each individual object is made the child of corresponding joint. Thus objects are connected by joints, joints constraints are added between neighbor objects. Next, the leg kinematics chain was created shown in Figure 7-3, it can be seen that the respondable objects are the children of the corresponding joints, the imported SolidWorks components (only for visual purposes without respondable and dynamics reactions) are the children of the respondable objects, and joints are

the children of their previous link objects. In fact, the respondable objects and the visual objects can be defined and categorized in different layers, thus only the respondable object layer need to be activated during the simulations.

As mentioned above, the track was modeled as five rollers as shown in Figure 7-3 b. The tricky issue is the first roller joint need to function as both a link joint (walking locomotion mode) and roller joint (rolling locomotion mode). Because only one kinematic constraint, including joints, force sensors, etc., can be added between two respondable objects in V-REP, the proposed solution is to add one additional joint and roller (i.e. TrackJoint6 and TrackDynamics\_roller6 in Figure 7-3) at exactly the same position of the first joint and set the additional added roller mass as zero. Thus, TrackJoint1 is used in walking locomotion mode only as same as other leg joints, the other track joints are used in rolling locomotion mode.

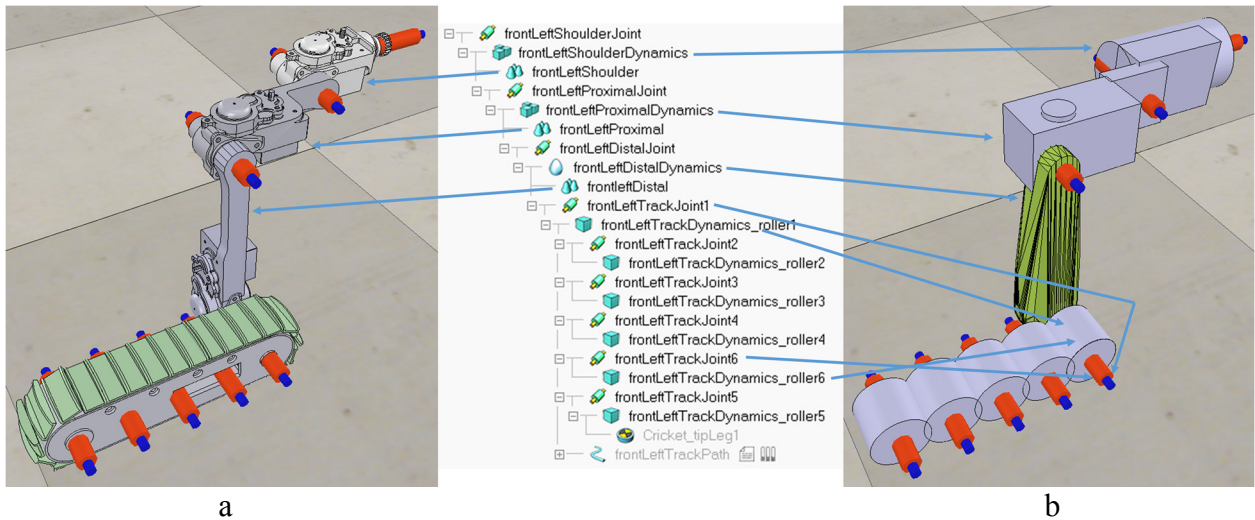


**Figure 7-3. One Leg Chain V-REP Model of Cricket.**

The other three leg models can be obtained by duplicating the leg model created shown in Figure 7-3 with adjusting relative positons to the body, then adding all their should joints as children of the body. A complete dynamic and respondable model of Cricket is created shown in Figure 7-4.

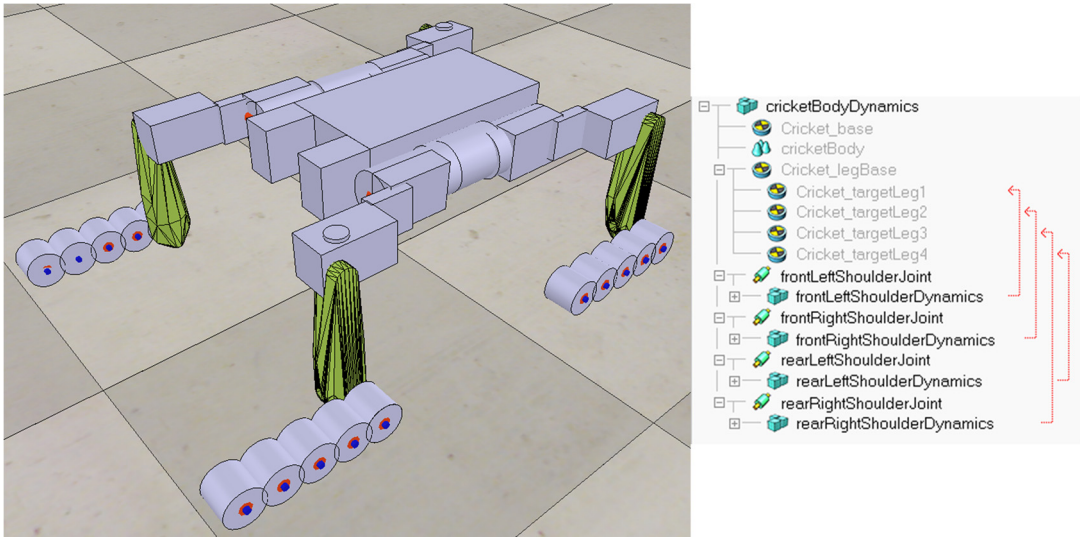


**Figure 7-4. Cricket Dynamic Respondable V-REP Model.**

## 7.2 Rolling Locomotion Configuration

Rolling is the default locomotion mode of Cricket. Rolling is both time and energy efficient on flat hard terrain without irregularities and discontinuities, and this is especially true for Cricket because the weight of its legs comprises over 60% of the vehicle weight.

As stated in the research constraints, the configuration of the rolling locomotion mode is non-changeable, thus the robot move as a traditional wheeled/tracked vehicle with its body and legs fixed to a given configuration. The fixed configuration is defined as the home rolling configuration where all joints are at their centers as shown in Figure 7-5.

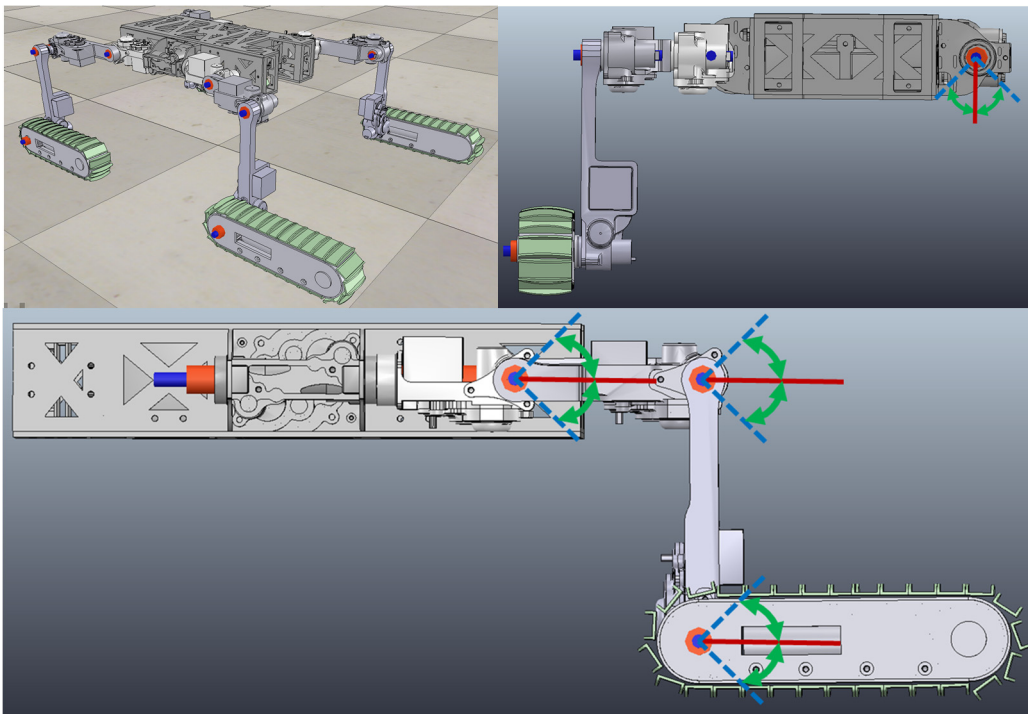


**Figure 7-5. Home Configuration of Rolling Locomotion Mode and Leg Joints' Position.**

### 7.3 Walking Locomotion Model Calculations

Rather than the rolling locomotion mode has continuous motions and fixed configurations, walking locomotion mode needs proper walking gaits to realize proper locomotion motions. In the walking gaits design, the kinematics of the system, especially the leg kinematics have to be solved. This section discusses the kinematics solutions of Cricket, focusing on the leg kinematics calculations.

#### 7.3.1 Leg Kinematics Calculation

The kinematics and dynamics problems of the models of the rolling and walking locomotion mode of wheel/track-legged robots were preliminary solved in Chapter Four and Five. In the calculations of external forces, a mass-spring-damper model was used to calculate the wheel-terrain interaction, however, the real vehicle-terrain interaction, which including wheel-terrain collision, is a very complex computation that is beyond the research topic of this

thesis. Thus, the robotics simulator V-REP is utilized to handle the wheel-terrain interaction computations. At the same time, V-REP also embedded with a well-developed kinematics calculation module that provides optimal calculations of inverse kinematics and trajectory generations of Cricket's highly articulated leg.

The kinematics calculations of Cricket's one leg is elaborated in this section. The kinematics can be divided into forward and inverse kinematics calculations. The kinematics is calculated by attaching coordinate frames to every link of the leg and the body. The attached frames of each link can be chosen arbitrarily [59], however, it is convenient to follows rules so the parameters of links and joints can be describe completely and uniformly.

A link is considered a rigid body that defines the spatial relationship between two neighbouring joint axes. A link can be specified by two parameters, its length  $a_j$  and its twist  $\alpha_j$ . Joints are also described by two parameters. The joint offsite  $b_j$  is the distance from one link coordinate frame to the next link coordinate frame along the axis of the joint. The joint angle  $\theta_j$  is the rotation of one link with respect to the next about the joint axis [68].

There are two well-known and commonly used methods in robotics area, one is the Denavit-Hartenberg (D-H) method [76], and another is the modified D-H method [67]. The essential difference between the standard and modified D-H method is where the coordinate frames are attached to each link. In the standard D-H method, the coordinate frames are attached to the far (distal) end of each link; while in the modified D-H method, the coordinate frame are attached to the near (proximal) end of each link. This causes the difference of kinematic conventions, and the transformation matrix between two successive frames. In order to clarify these differences, a detailed comparison of these two methods can be found in Appendix A.

The method used here is the standard D-H method with a modification of the coordinates frame subscript and the joint sequence (as same as the D-H method used in DeNOC). Instead of coordinate frame  $i$  is attached to the end of link  $i$ , the coordinate frame  $i + 1$  is attached to the end of link  $i$ . In the kinematic chain of Cricket leg shown in Figure 7-6, frame 1 is attached to link 0, which is the body, axis  $z_1$  is determined by the rotation axis of joint 1; frame 2 is attached to link 1, axis  $z_2$  is determined by the rotation axis of joint 2; frame 3, frame 4 and frame 5 is attached to link 2, link 3, and link 4 respectively.

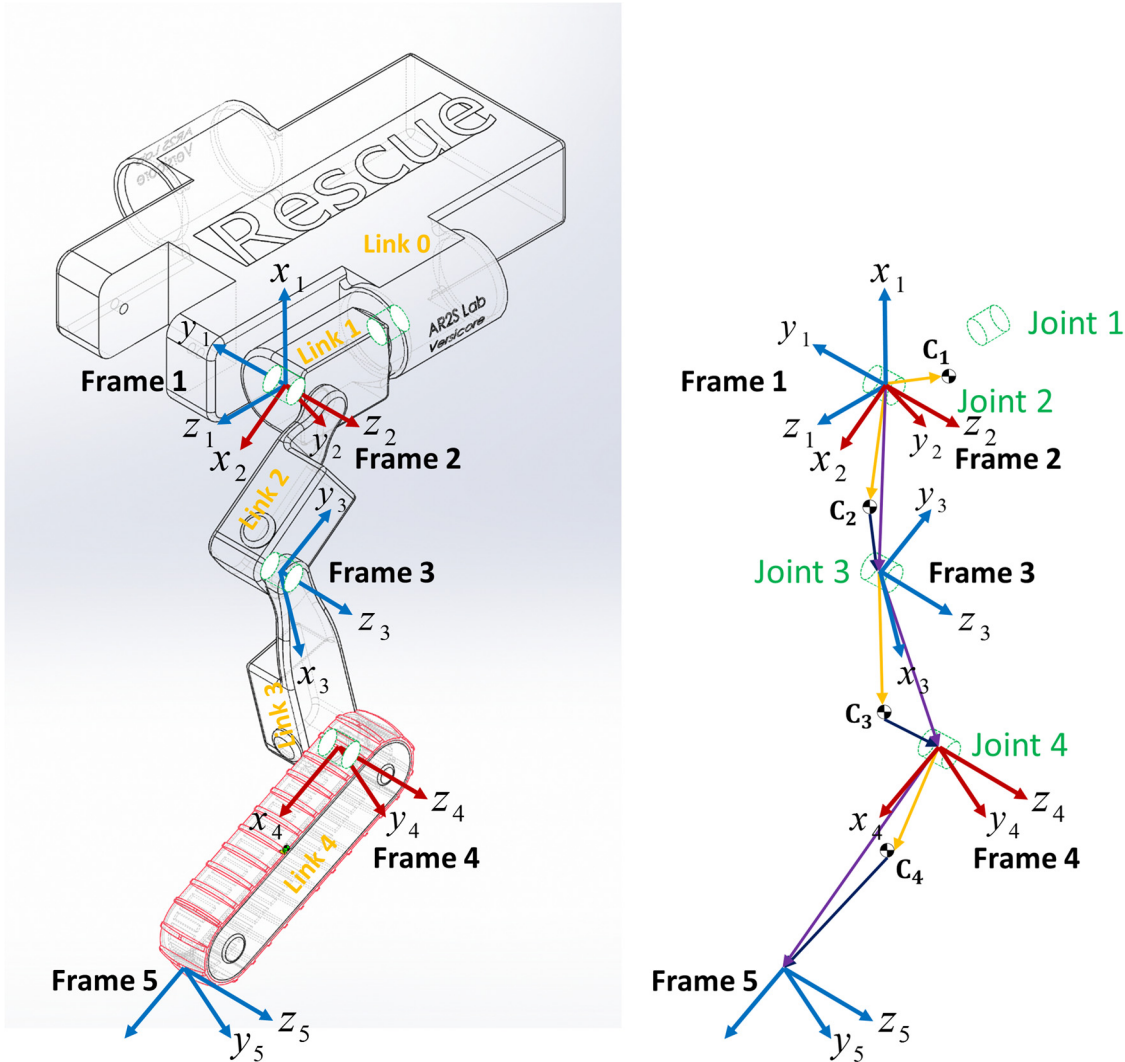


**Figure 7-6. Front Left Leg of Cricket Kinematics Calculations.**

The parameters definitions in Figure 7-6 can be referred to Chapter Five. And the D-H parameters of the front left leg are listed in Table 7-1 as:

**Table 7-1. D-H Parameters of the Front Leg of Cricket**

| Link | $b_i$                    | $\theta_i$ | $a_i$                    | $\alpha_i$ |
|------|--------------------------|------------|--------------------------|------------|
| 1    | $b_1 = 0 \text{ m}$      | $\theta_1$ | 0                        | $\pi/2$    |
| 2    | $b_2 = 0.102 \text{ m}$  | $\theta_2$ | $a_2 = 0.133 \text{ m}$  | 0          |
| 3    | $b_3 = 0.0185 \text{ m}$ | $\theta_3$ | $a_3 = 0.185 \text{ m}$  | 0          |
| 4    | $b_4 = 0.0285 \text{ m}$ | $\theta_4$ | $a_4 = 0.2196 \text{ m}$ | 0          |

The homogeneous transformation matrix describing the relative translation and rotation relationship from coordinate frame  $i + 1$  back to frame  $i$  is:

$$\begin{aligned} {}^i T_{i+1} &= \begin{bmatrix} t_{1,1} & t_{1,2} & t_{1,3} & t_{1,4} \\ t_{2,1} & t_{2,2} & t_{2,3} & t_{2,4} \\ t_{3,1} & t_{3,2} & t_{3,3} & t_{3,4} \\ t_{4,1} & t_{4,2} & t_{4,3} & t_{4,4} \end{bmatrix} \\ &= \begin{bmatrix} \cos\theta_i & -\sin\theta_i \cos\alpha_i & \sin\theta_i \sin\alpha_i & a_i \cos\theta_i \\ \sin\theta_i & \cos\theta_i \cos\alpha_i & -\cos\theta_i \sin\alpha_i & a_i \sin\theta_i \\ 0 & \sin\alpha_i & \cos\alpha_i & b_i \\ 0 & 0 & 0 & 1 \end{bmatrix} \end{aligned} \quad (7.2)$$

Then the matrices between neighboring links of the front leg of Cricket can be calculated based on the D-H parameters in Table 7-1 using Equation (7.2) as:

$${}^1 T_2 = \begin{bmatrix} \cos\theta_1 & 0 & \sin\theta_1 & 0 \\ \sin\theta_1 & 0 & -\cos\theta_1 & 0 \\ 0 & 1 & 0 & b_1 \\ 0 & 0 & 0 & 1 \end{bmatrix} \quad (7.3)$$

$${}^2 T_3 = \begin{bmatrix} \cos\theta_2 & -\sin\theta_2 & 0 & a_2 \cos\theta_2 \\ \sin\theta_2 & \cos\theta_2 & 0 & a_2 \sin\theta_2 \\ 0 & 0 & 1 & b_2 \\ 0 & 0 & 0 & 1 \end{bmatrix} \quad (7.4)$$

$${}^3T_4 = \begin{bmatrix} \cos\theta_3 & -\sin\theta_3 & 0 & a_3\cos\theta_3 \\ \sin\theta_3 & \cos\theta_3 & 0 & a_3\sin\theta_3 \\ 0 & 0 & 1 & b_3 \\ 0 & 0 & 0 & 1 \end{bmatrix} \quad (7.5)$$

$${}^4T_5 = \begin{bmatrix} \cos\theta_4 & -\sin\theta_4 & 0 & a_4\cos\theta_4 \\ \sin\theta_4 & \cos\theta_4 & 0 & a_4\sin\theta_4 \\ 0 & 0 & 1 & b_4 \\ 0 & 0 & 0 & 1 \end{bmatrix} \quad (7.6)$$

Thus, the frame 5 attached to the track link can be expressed with respect to the shoulder coordinate frame 1 as:

$$\begin{aligned} {}^1T_5 &= {}^1T_2 \ {}^2T_3 \ {}^3T_4 \ {}^4T_5 = \prod_1^5 {}^iT_{i+1} = \\ &\begin{bmatrix} \cos\theta_1\cos(\theta_2 + \theta_3 + \theta_4) & -\cos\theta_1\sin(\theta_2 + \theta_3 + \theta_4) & \sin\theta_1 & (b_2 + b_3 + b_4)\sin\theta_1 + \cos\theta_1(a_2\cos\theta_2 + a_3\cos(\theta_2 + \theta_3) + a_4\cos(\theta_2 + \theta_3 + \theta_4)) \\ \sin\theta_1\cos(\theta_2 + \theta_3 + \theta_4) & -\sin\theta_1\sin(\theta_2 + \theta_3 + \theta_4) & -\cos\theta_1 & -(b_2 + b_3 + b_4)\cos\theta_1 + \sin\theta_1(a_2\cos\theta_2 + a_3\cos(\theta_2 + \theta_3) + a_4\cos(\theta_2 + \theta_3 + \theta_4)) \\ \sin(\theta_1 + \theta_2 + \theta_3) & \cos(\theta_1 + \theta_2 + \theta_3) & 0 & a_2\sin\theta_2 + a_3\sin(\theta_2 + \theta_3) + a_4\sin(\theta_2 + \theta_3 + \theta_4) \\ 0 & 0 & 0 & 1 \end{bmatrix} \end{aligned} \quad (7.7)$$

Equation (7.7) can be re-written as:

$$\begin{aligned} {}^1T_5 &= {}^1T_2 \ {}^2T_3 \ {}^3T_4 \ {}^4T_5 = \prod_1^5 {}^iT_{i+1} \\ &= \begin{bmatrix} c_1c_{234} & -c_1s_{234} & s_1 & (b_2 + b_3 + b_4)s_1 + c_1(a_2c_2 + a_3c_{23} + a_4c_{234}) \\ s_1c_{234} & -s_1s_{234} & -c_1 & -(b_2 + b_3 + b_4)c_1 + s_1(a_2c_2 + a_3c_{23} + a_4c_{234}) \\ s_{123} & c_{123} & 0 & a_2s_2 + a_3s_{23} + a_4s_{234} \\ 0 & 0 & 0 & 1 \end{bmatrix} \end{aligned} \quad (7.8)$$

where  $s_i$  and  $c_i$  represents  $\sin \theta_i$  and  $\cos \theta_i$  respectively,  $s_{ij}$  and  $c_{ij}$  represents  $\sin(\theta_i + \theta_j)$  and  $\cos(\theta_i + \theta_j)$  respectively, and  $s_{ijk}$  and  $c_{ijk}$  represents  $\sin(\theta_i + \theta_j + \theta_k)$  and  $\cos(\theta_i + \theta_j + \theta_k)$  respectively.

In the walking gait design, when adjusting pose (positon and orientation) of the body, the robot performs like a parallel manipulator; when moving legs, the body is considered to be fixed, inverse kinematics are conducted to calculate angles of each joint based on the final pose of the

feet. For the legs with three or less degree of freedom, the inverse kinematics can be solved based on the relationship between the feet position vector  $d$  and the homogenous transformation matrix  $T$  in Equation (7.2) as:

$$\begin{bmatrix} t_{1,4} \\ t_{2,4} \\ t_{3,4} \end{bmatrix} = \begin{bmatrix} d_x \\ d_y \\ d_z \end{bmatrix} \quad (7.9)$$

Because each leg of Cricket has four revolute joints in the legged mode, the inverse kinematics of the leg can't be solved as:

$$\begin{bmatrix} (b_2 + b_3 + b_4)\sin\theta_1 + \cos\theta_1(a_2\cos\theta_2 + a_3\cos(\theta_2 + \theta_3) + a_4\cos(\theta_2 + \theta_3 + \theta_4)) \\ -(b_2 + b_3 + b_4)\cos\theta_1 + \sin\theta_1(a_2\cos\theta_2 + a_3\cos(\theta_2 + \theta_3) + a_4\cos(\theta_2 + \theta_3 + \theta_4)) \\ a_2\sin\theta_2 + a_3\sin(\theta_2 + \theta_3) + a_4\sin(\theta_2 + \theta_3 + \theta_4) \end{bmatrix} = \begin{bmatrix} d_x \\ d_y \\ d_z \end{bmatrix} \quad (7.10)$$

Since there are four unknown joints angles with three equation, additional equations between the rotation component part of the homogenous transformation matrix (i.e. left upper  $3 \times 3$  matrix) and the orientation vector of the feet are needed to be solved simultaneously. In the proposed walking gaits in the next chapter, the track belt face are always parallel to the ground, which means the shoulder joint angle  $\theta_1 = 0$ , thus Equation (7.10) can be solved.

For wheel/tracked-legged robots with similar mechanical design, such as Hylos [48] and MHT [77], the joint angles connecting the distal link and the wheel/track are known, for Cricket  $\theta_4 = -\pi/2$ , Equation (7.10) can also be solved analytically. The detailed inverse kinematics solutions of the Cricket leg in Figure 7-6 and a summarized generic inverse kinematics calculation process method can be found in Appendix C.

### **7.3.2 Kinematics and Dynamics Calculation Modules in V-REP**

In V-REP, there is a powerful built-in inverse kinematics calculation (IK) module that can be used to solve these complex problems involved in walking gaits designs. To utilize the IK

module, IK group is needed to be defined by elements including base (the start point of the kinematic chain), tip (the last object in the kinematic chain), target (the position and/or orientation the tip should follow) and tip-target link (a tip-target pair of inverse kinematics chain). The IK calculation group of Cricket was defined shown in Figure 7-7 a, in which IK elements are defined by attaching dummies (dummy is a point object with an attached reference frame) on them, i.e. Cricket\_base, Cricket\_tragetLeg and Cricket\_tipLeg in Figure 7-7 a represents the base, target and tip respectively, and bidirectional arrow dashed red lines are tip-target links. The kinematic relationship inside the leg (Equation (7.8)) has already automatically defined after adding joints constraints as discussed in Section 7.1.3, and IK groups can be registered using all defined IK elements as shown in Figure 7-7 b.

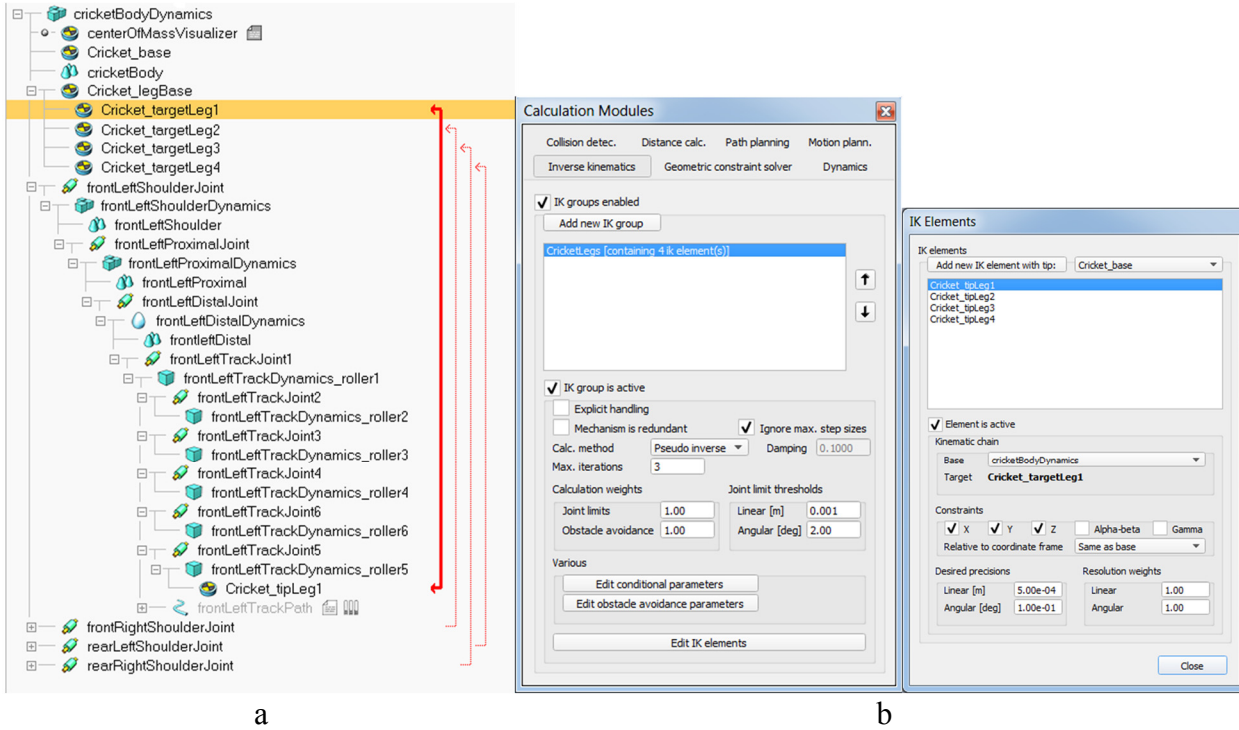


**Figure 7-7. Kinematics Calculation of Cricket in V-REP.**

The Reflexxes Motion Library [18, 78] that can be directly called inside the thread child scripts [79] in V-REP was used to generate smooth joint trajectories satisfying position, velocity, and acceleration constraints.

The dynamics for the robot's locomotion control and the vehicle-terrain interaction calculations were handled by a commercial, high fidelity, physical engine named Vortex [11] built in V-REP which provided stable simulation results. Verification of the Vortex physical engine was conducted by creating a one link model of Cricket's leg in V-REP and comparing the simulated torque outputs with the torque values calculated by the dynamic model using the method explained in Chapter Five. Moreover, Vortex provides a stable simulation process when communicating with other programming software, including MATLAB and Python.

#### 7.4 Environment Friction Parameters Tuning

The locomotion performances are highly affected by the terrain conditions, this is especially true to rolling locomotion mode because its efficiency is highly affected by the terrain qualities [2]. For the simulation environment used in this thesis, hard terrain is always assumed. Since the proposed locomotion mode transition method is based on energy performance criterion, vehicle-terrain interaction parameters such as frictional coefficient plays a dominant role.

In V-REP, frictional coefficients can be adjusted in the dynamics engines properties settings. The static frictional coefficients of tire and dry asphalt/concrete  $\mu_{tc}$  is between 0.8 and 1.0 [80], the ground friction was tuned by running simulations that could keep track static on a steep slope with angle equals to  $\arctan(\mu_{tc})$  as shown in Figure 7-8 a.

The track on slope was identified as static when the track state was identical to the track on the flat terrain (because of simulation noise) as shown in Figure 7-8 b. The track rollers were

set as the ‘wheelMaterial’ materials with the frictional coefficient  $\mu_w = 1$ , the frictional coefficient of terrain was tuned to be 0.87, and thus the combined frictional coefficient of the track-terrain was 0.87 during the simulation.

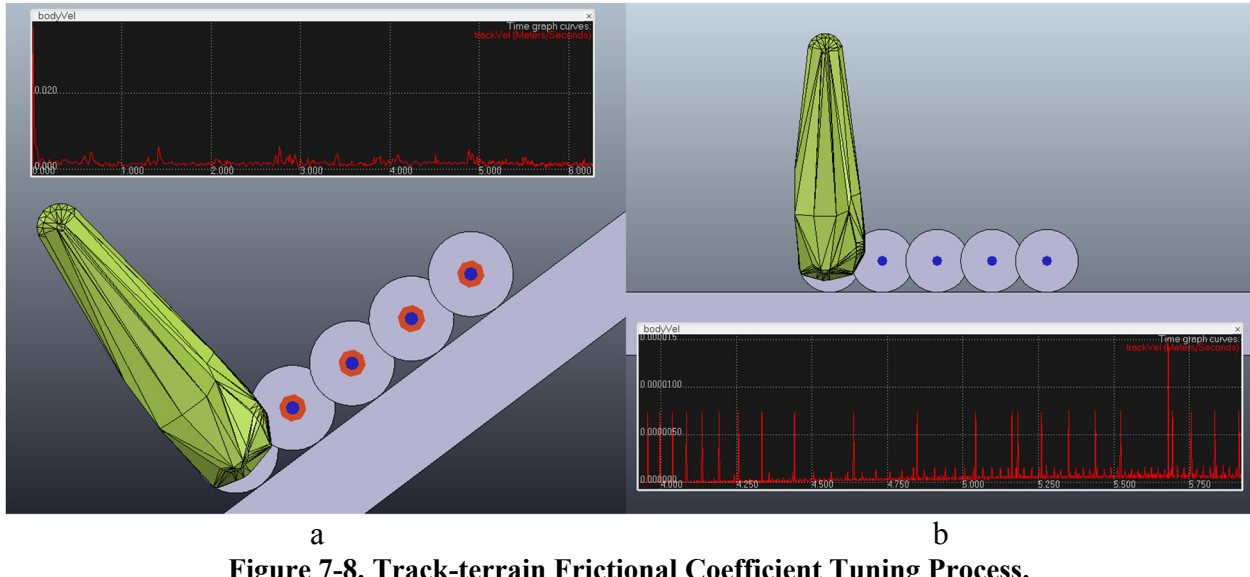


**Figure 7-8. Track-terrain Frictional Coefficient Tuning Process.**

## 7.5 Summary

This chapter explains the development process of the physical model for the Cricket robot in V-REP based on its mechanical design. And the kinematics calculations of one leg of the Cricket is also explained in this chapter, which is the groundwork of the walking gait design in Chapter Seven. The goal of this work is to make the rolling locomotion mode energy evaluation more reliable as well as to reduce the kinematics and dynamics complexity of the motion control for the walking locomotion of the Cricket.

## Chapter Eight: STEP CLIMBING GAITS

This chapter explains the development of the walking gaits to realize proper step negotiation performances of Cricket. The proposed walking gaits follow the static stable method to guarantee the stability of the system. Even though the proposed walking gaits are able to negotiate steps with different heights properly, no technique is applied to optimize the proposed walking gaits with respect to any criterion (e.g. minimum torque, leg displacement, and power etc.) yet.

Because the locomotion mode transition (rolling to walking) happens when robots negotiate rough terrains such as steps/stairs, so the steps negotiation of the walking locomotion is climbing. For the robots in rolling locomotion mode, the maximum height that the robot can transverse over is limited by the maximum height that the front and rear wheels/tracks can both achieve. Since the front wheels/tracks can transverse over much higher steps, it is the rear wheel/tracks limit the maximum achievable height [81, 82].

Due to the fact that the complexity of individual leg energy evaluation and the maximum step height the robot can transverse over limits by its rear wheel/tracks negotiation ability, two climbing gaits, i.e. the whole body climbing [83] and the rear body climbing gaits were proposed to negotiate steps with different heights properly.

### 8.1 Step-climbing Gaits of Wheel-legged Robot

Although legged locomotion, gaits (gait in robotics is defined as the sequence of legs and body motion to make the robot move properly) included, for robots has been studied for decades, the research of autonomous wheel-legged robotics is much more recent [77]. Within the wheel/track-legged robots area, the work on step-climbing gait of highly articulated robots is especially limited.

In the gait design, system stability needs to be guaranteed all the time. The concept of “stability” was first defined that a walking robot is statically stable if the horizontal projection of its center of gravity (COG) lies inside of the support polygon, formed by joining all of the feet in support [84]. As stability measurements, the shortest distance from the projection of the COG to the boundaries of the support polygon is calculated and defined as the Stability Margin ( $S_{SM}$ ).

In the reviewed literature of proposed step-climbing gaits, before stepping (lifting a wheel/track up to the negotiating step at a time), strategy either to change the support polygon by moving wheel [85, 86] or to shift away the robot weight from the lifting leg by moving body [82, 83] is used. Gaining more stability margin first to ensure static balance of the robot in the following stepping phase is the strategy goal.

The leg movement and body movement strategy can be explained by a front right (FR) leg stepping example. The legs movement strategy can be shown in Figure 8-1. In Figure 8-1, the deep blue rectangle, light blue rectangle, and black half-filled circle represent the foot positon, robot body, and center of gravity, respectively. And the back dotted triangular and red triangular represent supporting polygon of before leg movement and after leg movement, respectively. Before the front FR leg stepping, moving the rear right leg forward from positon a to positon b, thus the support polygon during the FR leg stepping is changed from triangular *acd* to *bcd*.

The body movement strategy is shown in Figure 8-2. In Figure 8-2, the deep blue rectangle, red triangular, and black half-filled circle represent the foot positons, supporting polygon, and center of gravity, respectively. And back dotted rectangles and light blue rectangles represent the robot body positon of before body movement and after body movement, respectively. The body is moved backward to push the COG (from positon a to positon b) lies inside of the support polygon during the FR leg stepping process. In general, the first strategy is

applied when legs' weight isn't dominant, even negligible of the whole system, thus the leg movement is instinctively more efficient; the second method is utilized when legs weight can't be neglected, or it is more stable to move body with all legs in the supporting phase.

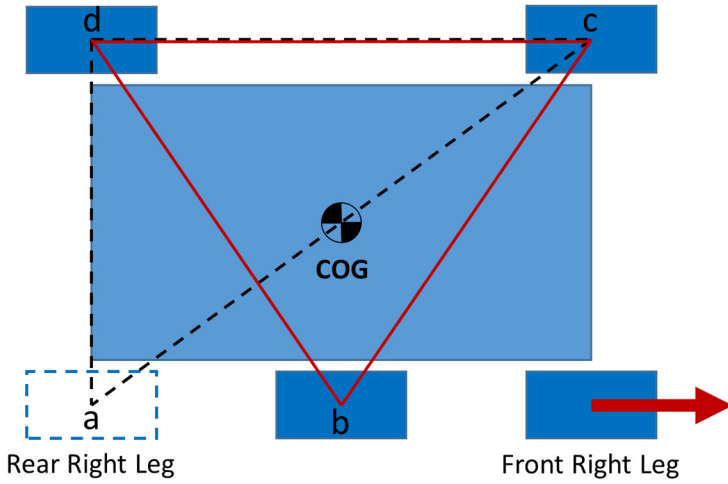


**Figure 8-1. Top-down View of the Step-climbing Gait Using Leg Movement Strategy.**

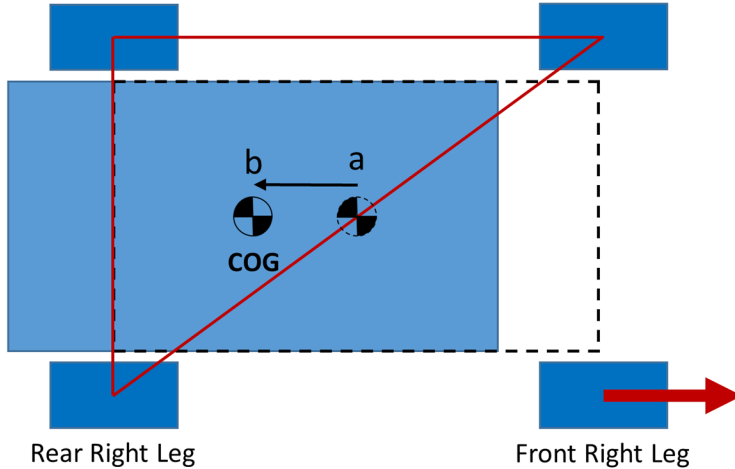


**Figure 8-2. Top-down View of the Step-climbing Gait Using Body Movement Strategy.**

## 8.2 The Whole Body Climbing Gait

For the Cricket robot, the weight of its legs comprises over 60% of the system weight. It is obvious that legs weight isn't negligible, and it is more stable to move body with all legs in the supporting phase before stepping legs. So the proposed step-climbing gait in this chapter is in the

second category, i.e. shifting away the robot weight from the stepping leg by moving the body.

The static stability margin  $S_{SM}$  is calculated to guarantee the system stability during the step negotiation.

The gait is generated by using the step height information as the input, stepping leg foot positon is under the position control by using a Proportional-Derivative (PD) controller on each leg joints. Here the top-down view of the COM and feet positons movement together with the gait snapshot are used to illustrate the proposed step-climbing gait in Figure 8-1 to Figure 8-13, in which the circle at each corner of the rectangle represents the corresponding foot-ground contact positons, the half bolded circle inside the rectangle represents the COM, red arrows indicate COM displacement vectors, green arrows represent front leg displacement vectors, and blue arrows are rear leg displacement vectors. The number  $i$  ( $i = 1, \dots, 11$ ) is used to indicates the movement sequence of the first move leg,  $i^*$  represents the movement sequence of the following move leg, and  $i^C$  represents the movement sequence of the COM.

The whole body climbing starts right in the front of the negotiating step, the robot is still in the home configuration of rolling locomotion mode with all tracks stationary at this moment shown in Figure 8-3.

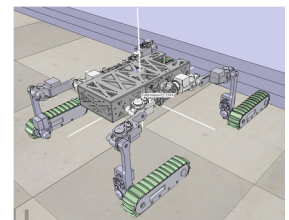
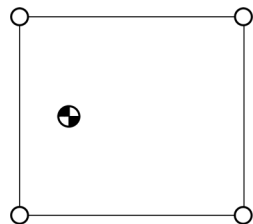


**Figure 8-3. Initial Position of the Whole Body Climbing Gait.**

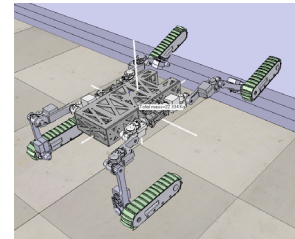
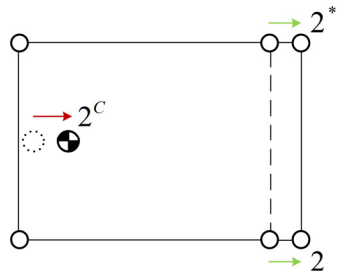
The whole body climbing can be divided into three phases: *i*) stepping front legs on the step, *ii*) moving forward on the step, and *iii*) stepping rear legs on the step. The first phase

contains three sub-phases shown in Figure 8-4 to Figure 8-6. The body starts to move backward to gain more stability margin, then the front right foot moves up to the step, the front left foot moves up to the step shown in Figure 8-4. It can be seen in Figure 8-3 that the COM is in the supporting polygon even without moving the body backward to conduct the first stepping movement of the front legs, it seems unnecessary to gain more stability margin before stepping front legs forwards. However, the reason to do so is that the foot-ground contact positons are always assumed to be the track tip positons which is not always true as can be seen in Figure 8-4. If the whole body climbing gait doesn't starts from the home configuration of rolling locomotion mode, the assumption isn't correct anymore. It is more generic to define the step-climbing gait in this manner since it doesn't rely on the rolling configuration as well as the track geometry. In fact, this step-climbing gait can be applied to various wheel/track-legged robots with similar leg designs shown in Figure 3-1. In this sub-phase 1 a, the front legs movement is defined as one front leg stride length and represents as one unit light green arrow as shown in Figure 8-4.



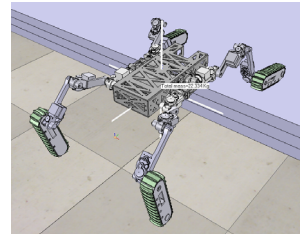
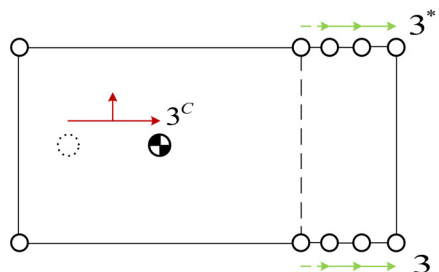
**Figure 8-4. Sub-phase 1 a: Move Body Backward, Move Front Legs Up.**

In Sub-phase 1 b, the body continues to move forward, then front legs moves forward for one front leg stride length shown in Figure 8-5. Besides the reason to gain move stability margin by moving the body forward first before moving legs forward, it's also because of the kinematic constraints, i.e. it is out of the front leg workspace without moving the body forward first.



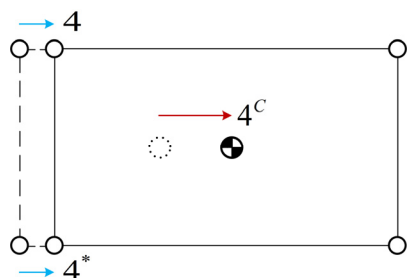
**Figure 8-5. Sub-phase 1 b: Move Body Forward, Move Front Legs Forward.**

Next, the body moves up and forward simultaneously, then front legs moves forward for two front leg stride length shown in Figure 8-6. In Figure 8-6, the green dashed lines indicate feet-ground contacts displacement because of the track forward rotation due to the body forward movement.



**Figure 8-6. Sub-phase 1 c: Move Body Up and Forward, Move Front Legs Forward.**

The Phase 2 starts with moving rear legs forward in sub-phase 2 a. The body move forward first, then the rear legs moves forward. In this sub-phase 2 a, the rear legs movement is defined as one rear leg stride length and represents as one unit blue arrow shown in Figure 8-7.



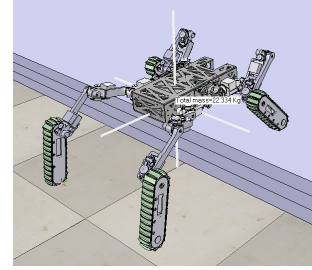
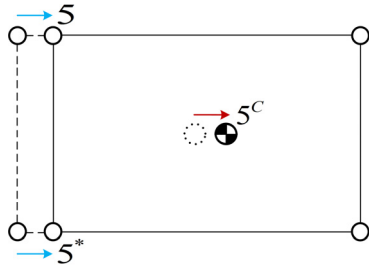


**Figure 8-7. Sub-phase 2 a: Move Body Forward, Moves Rear Legs Forward.**

The Phase 2 continues with moving front legs forward in sub-phase 2 b. The body moves backward to guarantee stability, then front legs moves forward for two front leg stride length shown in Figure 8-8.

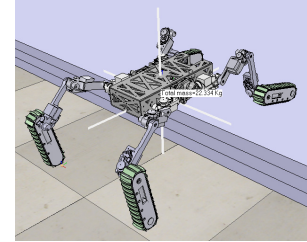
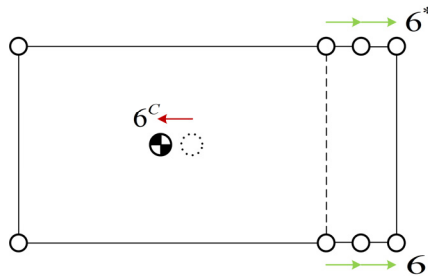


**Figure 8-8. Sub-phase 2 b: Move Body Backward, Moves Front Legs Forward.**

Next, Phase 2 continues to move rear legs forward in sub-phase 2 c. As same as sub-phase 2 a shown in Figure 8-7, the body move forward first, then the rear legs moves forward for one rear leg stride length each time shown in Figure 8-9.

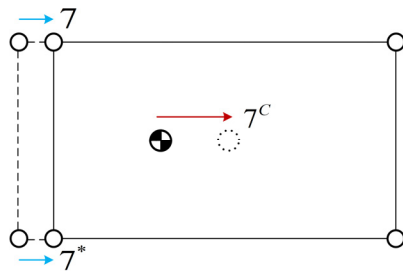




**Figure 8-9. Sub-phase 2 c: Move Body Forward, Moves Rear Legs Forward.**

Similar with sub-phase 2 b, the front legs moves forward for two front leg stride length after moving the body backwards first in Sub-phase 2 d shown in Figure 8-10.

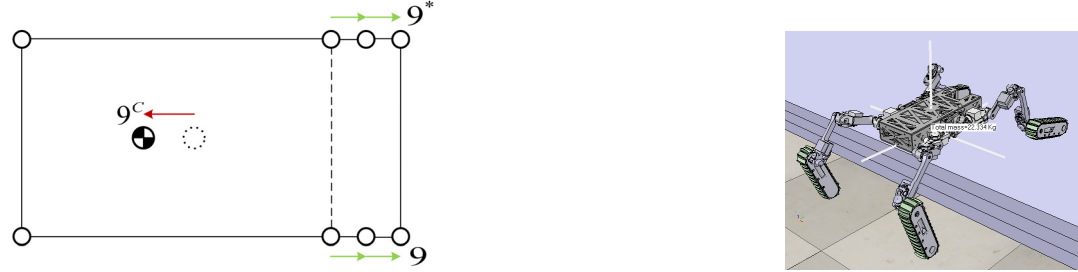


**Figure 8-10. Sub-phase 2 d: Move Body Backward, Moves Front Legs Forward.**

Then keep moving rear legs forward to prepare for stepping rear legs in Sub-phase 2 e. The body moves forward to gain more stability margin, then rear legs moves forward for one front leg stride length shown in Figure 8-11.

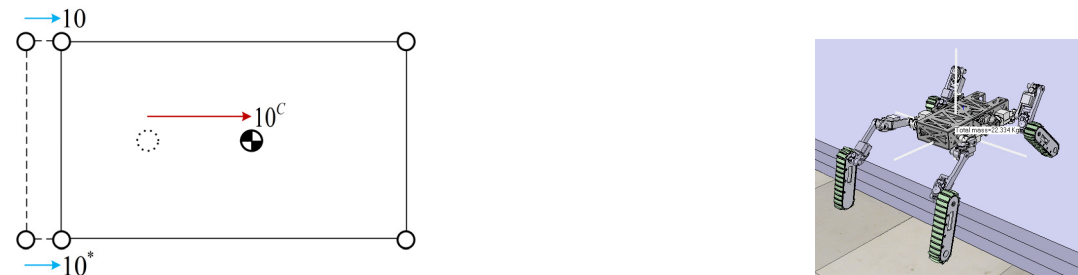


**Figure 8-11. Sub-phase 2 e: Move Body Forward, Moves Rear Legs Forward.**

Now it is stepping rear legs on the step phase. The body moves forward first to gain more stability margin, then rear legs lifts up and forward to the step shown in Figure 8-12. In Phase 3, the gained stability margin because of the forward movement of the body may not enough to step the rear legs because of the step height constraints, for example, the body can't move forward the same length when negotiating step height of  $2h_t$  and  $3h_t$  ( $h_t$  is the track height) because of track-step collision. So in this case, the body moves sideways after stepping the rear left leg to gain more stability margin, then stepping rear right leg shown in Figure 8-13.

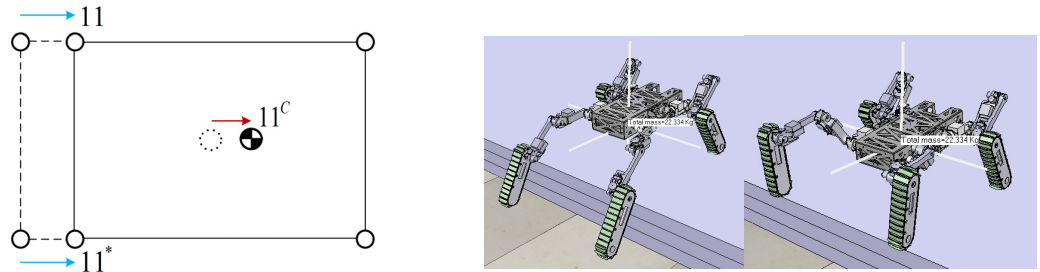


**Figure 8-12. Phase 3: Move Body Forward, Steps Rear Legs Forward.**

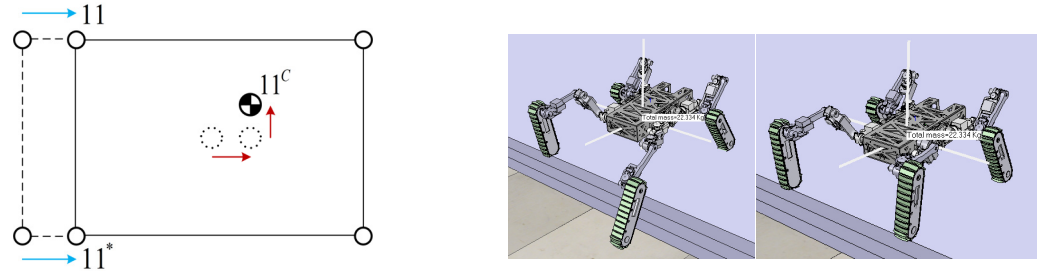


**Figure 8-13. Phase 3: Move Body Forward and Sideways, Steps Rear Legs Forward.**

The overall feet and body movement can be summarized as a top down view of the climbing gait shown in Figure 8-14, in which red dots indicate forward movement of the COM, and black dots represent backward movement of the COM; blue dots and green dots represent the feet-ground contact positons of the rear legs and the front legs respectively; red arrows, green arrows, and blue arrows are the displacement vector of the COM, the front legs, and the rear legs

respectively. It can be seen in Figure 8-14 that static stability is always guaranteed during the whole climbing gait.

The whole body climbing gait has the following characteristics:

1. The body is always moved first to shift the robot weight away from the lifting leg in order to gain more system stability margin, the reason to follow this strategy is because the legs stepping movement always loss partial stability margin of the system.
2. The body movements are forward and backward only in order to have bigger feet-ground contacts during the first two climbing phrases. In the third phase, when obstacle height was high (bigger than  $3h_t$ ), body moves sideways to gain more stability margin that can't be gained by just moving forward and backward because of the step height constraints as shown in Figure 8-13.

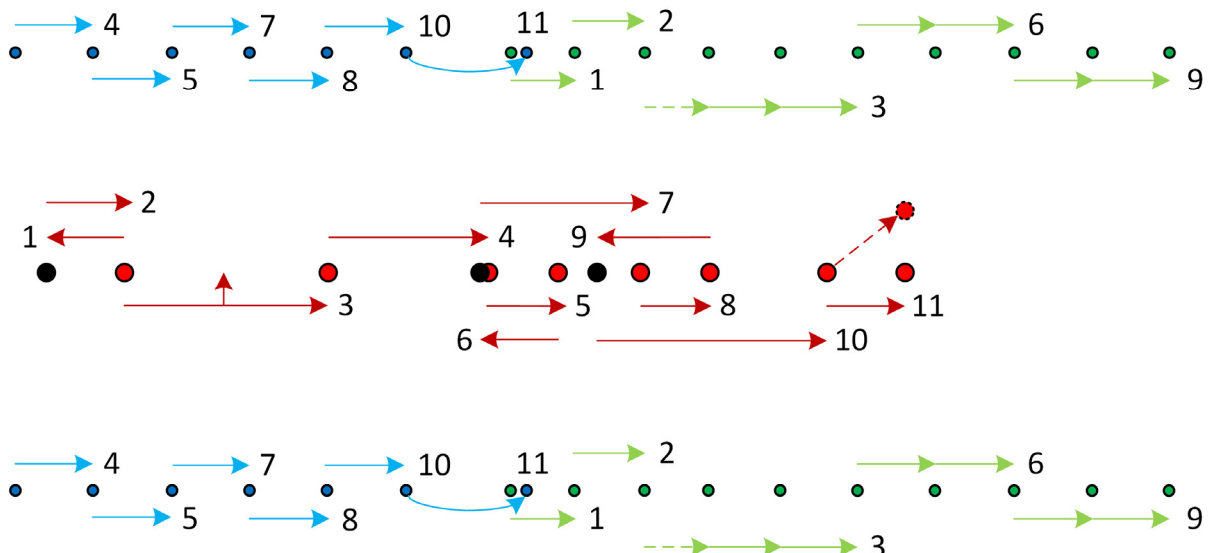


**Figure 8-14. The Foot and Body Displacement of the Whole Body Step Climbing Gait.**

### 8.3 The Rear Body Climbing Gait

Since it's the rear wheel/track step negotiation ability limits the maximum height that the hybrid robots can transverse in the rolling locomotion mode [81, 82], the locomotion mode transition is needed most likely at the rear wheel/track step negotiation phase. Moreover, the proposed autonomous locomotion mode transition method is based on the energy criterion, and the criterion threshold values are determined by the energy evaluations of the climbing locomotion mode, it is necessary to evaluate the rear leg step climbing only after finishing the front legs and body negotiation in rolling locomotion mode.

The rear body climbing gait can be considered as the rear legs climbing phase of the whole body climbing gait, which is to lift rears legs up to the negotiating steps when the front legs and body have already transverse up on steps in rolling locomotion. Thus, the rear body climbing gait consists of the font legs rolling and rear legs walking locomotion. The snapshots of the rear body climbing gait are shown in Figure 8-15.

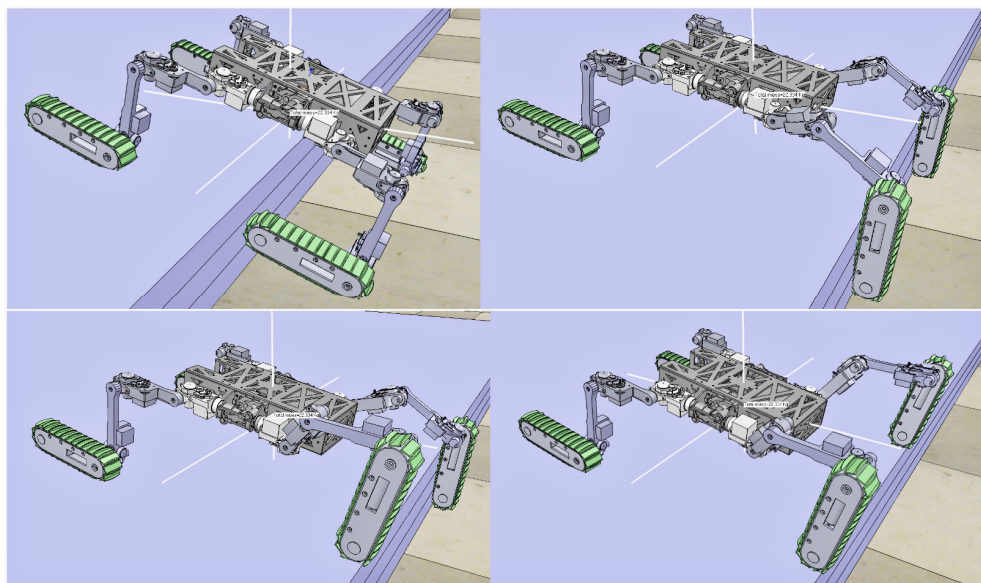


Figure 8-15. Rear Body Climbing Gait of Step Negotiation.

## **8.4 Summary**

In this chapter, two walking gaits, the whole body climbing and the rear body climbing gaits are proposed to negotiate steps with different heights. Due to the threshold values of the transition criterion are determined by the energy evaluations of the walking locomotion and the fact that it's always the rear legs limit the steps negotiation mobility of the rolling locomotion for the quadruped wheel/track-legged hybrid robots, thus the rear body climbing gait can be used to refine the first autonomous locomotion mode transition method proposed in Chapter Six. The details will be explained in Chapter Nine. Moreover, these two step climbing gaits are applicable to a wide range of quadruped wheel/track-legged robots with similar leg structure designs shown in Figure 3-1.

## Chapter Nine: RESULTS AND VERIFICATION

This chapter presents simulation results of Cricket's step negotiation energy performance using the proposed autonomous locomotion mode transition method. The energy performance of the step climbing gaits proposed in Chapter Eight are evaluated first in order to determine the criterion threshold values, then case study results of  $h_t$ ,  $2h_t$ , and  $3h_t$  step negotiation are shown as the verification of the proposed method.

### 9.1 Simulation Settings

The overall hierarchical scheme of the autonomous locomotion mode transition control is shown in Figure 9-1, in which the outside loop conducts the decision making process of the locomotion mode transition in MATLAB, and the inner loop controls each individual locomotion mode in V-REP. A link between the MATLAB environment and the robot's physical model (built in V-REP) is established using the remote API functionality of the V-REP simulation environment [3].

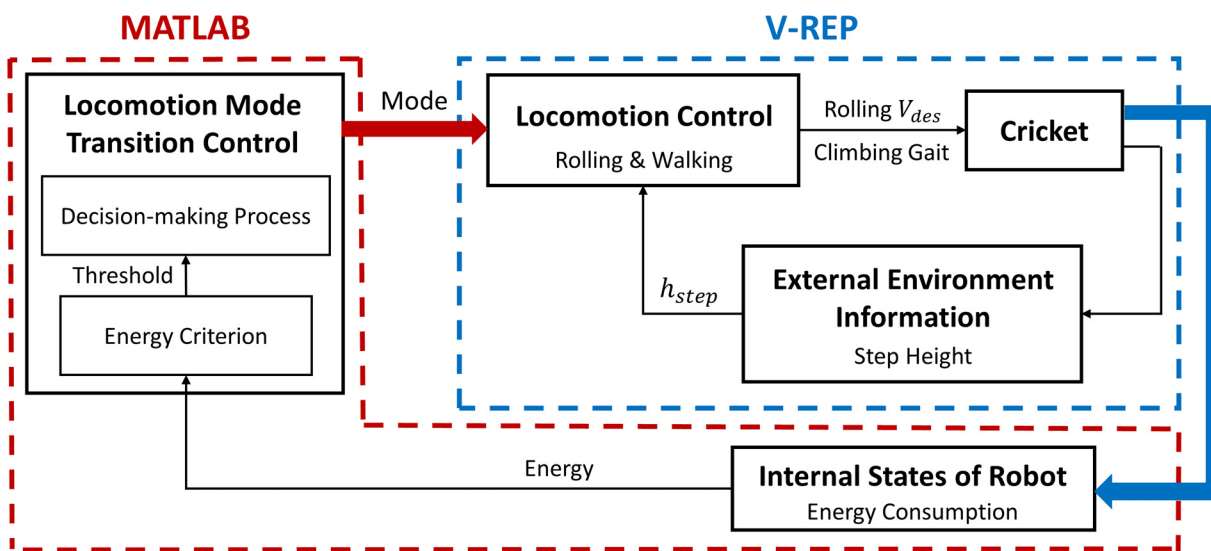


**Figure 9-1. Overall Hierarchical Scheme of the Autonomous Locomotion Mode Transition Control.**

In V-REP, the rolling locomotion is controlled to maintain the home configuration and a desired vehicle velocity. The walking locomotion control is realized by using the climbing gaits generated based on the step height information explained in Chapter Eight. The kinematics and dynamics calculations in the motion control of both the rolling locomotion and the walking locomotion modes are handled in V-REP. The simulation results includes the joint torque and the joint angular velocity are sent to MATLAB to conduct the data analysis and energy consumption calculations. In MATLAB, the energy evaluations includes the energy consumption of the whole step negotiation and the rear body negotiation. The whole step negotiation indicates the energy consumption from the front legs start to negotiate the step to the whole robot finishes the step negotiation, and the rear body negotiation means the energy consumption from the rear legs starts to negotiate the step to the whole robot finishes the step negotiation.

The threshold values of the criterion are determined by the case studies of the energy evaluations of the walking locomotion mode using the whole body and rear body climbing gaits. In current method, the threshold values are defined as same as the energy consumption of walking locomotion. Moreover, the decision-making process of the autonomous locomotion mode transition is implemented in MATLAB. The simulations are conducted with a 2 millisecond time step to approximate real-time dynamics of the step negotiation. For both rolling and walking locomotion, the energy consumption is evaluated from the position the vehicle starts to negotiate the step to the whole robot finishes the step negotiation.

## **9.2 Autonomous Locomotion Mode Transition Method**

Due to the fact the walking locomotion are evaluated by using both the whole body and rear body climbing gaits, the tentative decision making process of the autonomous locomotion mode transition method shown in Figure 6-9 are refined as shown in Figure 9-2.

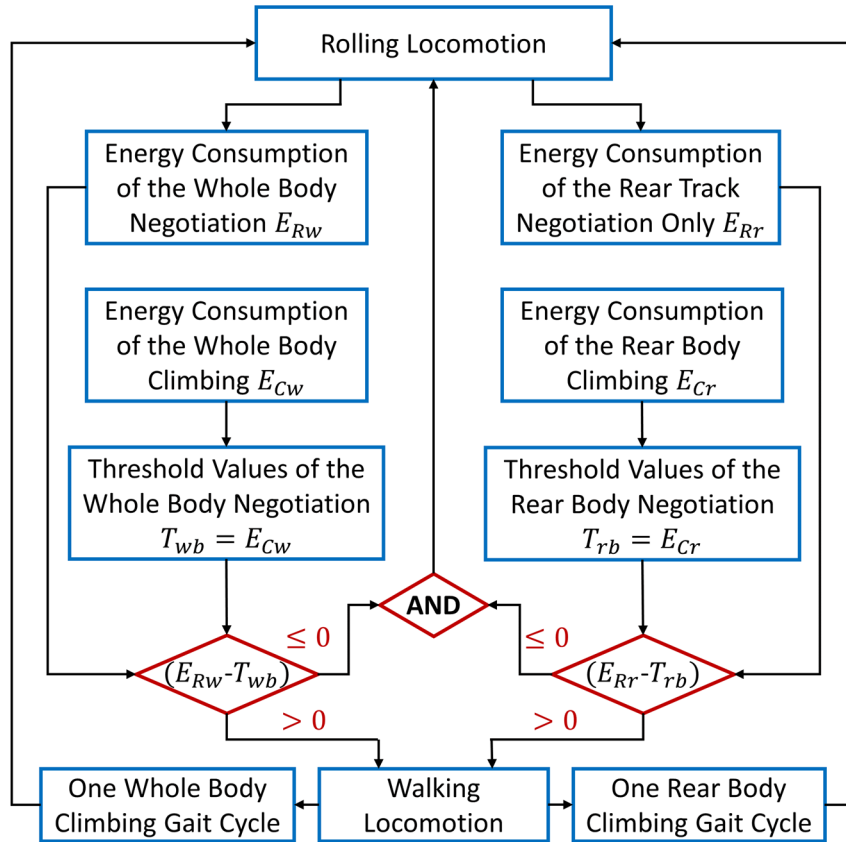


**Figure 9-2. The Refined Decision Making Process Flowchart.**

The decision making process operates in the following manner. The robot starts to negotiate the step in the rolling locomotion, measuring and recording the energy consumption since the negotiation start ( $E_R$ ); at the same time, checking and comparing the pre-studied energy consumption of the walking locomotion mode ( $E_C$ ); determining the threshold values ( $T_T$ ) by the energy consumption  $E_C$  ( $T_T$  is defined as same as  $E_C$ ); executing a decision-making process in a way that if  $E_R > E_C$ , the robot switches from rolling to walking locomotion until one climbing gait cycle finishes, then switches back to rolling locomotion; otherwise if  $E_R \leq E_C$ , the robot keeps rolling.

The on-line measuring and recording of the rolling energy evaluations include the energy consumption of the whole step negotiation ( $E_{Rw}$ ) and the rear body negotiation ( $E_{Rr}$ ). The pre-studied climbing energy consumption  $E_C$  also contains both the whole body climbing energy ( $E_{Cw}$ ) and rear body climbing energy ( $E_{Cr}$ ). Thus the locomotion transition can be invoked by either  $E_{Rw} > T_{wb}$  or  $E_{Rr} > T_{rb}$  in the decision making process as shown in Figure 9-2.

### 9.3 Walking Locomotion Energy Evaluation

As shown in Figure 9-2, the threshold values of the energy criterion ( $T_{wb}$  and  $T_{rb}$ ) are determined by the pre-studied energy evaluations of the walking locomotion to negotiate steps with different heights using the whole body climbing and the rear body climbing gates.

In the step negotiation simulations, it has been observed that the rolling locomotion can't transverse over steps with height more than  $3h_t$  due to the track traction forces limitation. It's obvious that the locomotion mode transition can only happen when the step negotiation can be achieved by both rolling and climbing locomotion modes. Thus, the energy evaluations of the step negotiation with heights of  $h$ ,  $2h$  and  $3h$  using the whole body climbing and the rear body climbing gaits are conducted.

The overall energy consumption performance of the two locomotion are evaluated first by conducting the power evaluations. Because the rear body climbing can be considered as the rear portion of the whole body climbing gait, only the power consumption of the whole body climbing gait is presented in Figure 9-3. By showing the overall energy consumption intensity, it's a straightforward approach to compare the two locomotion with different step negotiation time. Within the walking gait, the joint accelerations are held constant between tests leading to differences in the time required to overcome obstacles of differing heights – higher obstacles took longer to step over. As the time required to overcome a step also varied in the case of

rolling locomotion, the simulation time and power consumption in Figure 9-3 are presented in a normalized form with respect to the total negotiation time. The plots from top to bottom represent the power consumption for the robot overcomes steps with heights of  $h_t$ ,  $2h_t$  and  $3h_t$  respectively.

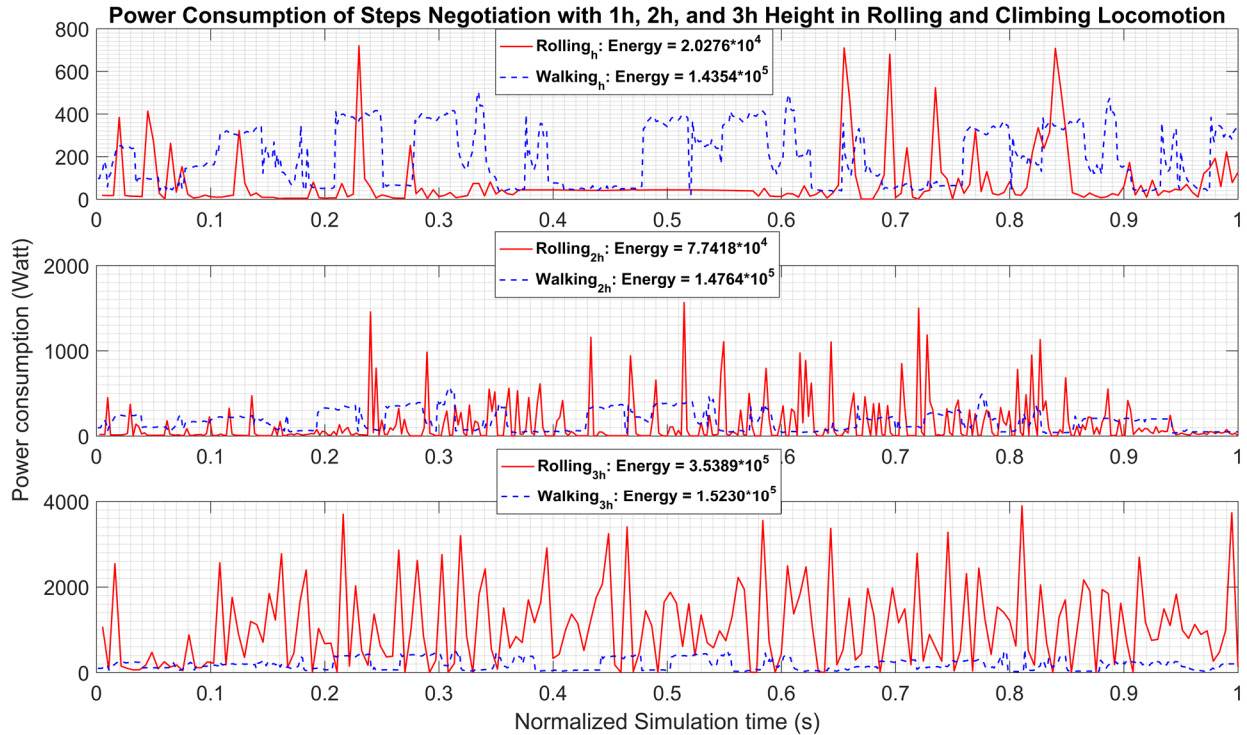


**Figure 9-3. Step Negotiation Power Comparison of the Rolling and Climbing Locomotion.**

The energy consumption of the whole body climbing with step heights of  $h_t$ ,  $2h_t$  and  $3h_t$  are evaluated and shown in Figure 9-4. It can be noticed that the differences of the energy consumption using the whole body climbing gait with different step heights are small in Figure 9-4. This is due to the fact that the climbing gaits are defined to have the same desired joint accelerations, the leg stride length, and the forward movement height. Thus the difference of the energy consumption of the different step negotiations come from the negotiation time and the body adjustment. The energy consumption of the rear body climbing with step heights of  $h_t$ ,  $2h_t$  and  $3h_t$  are also evaluated and shown in Figure 9-5.

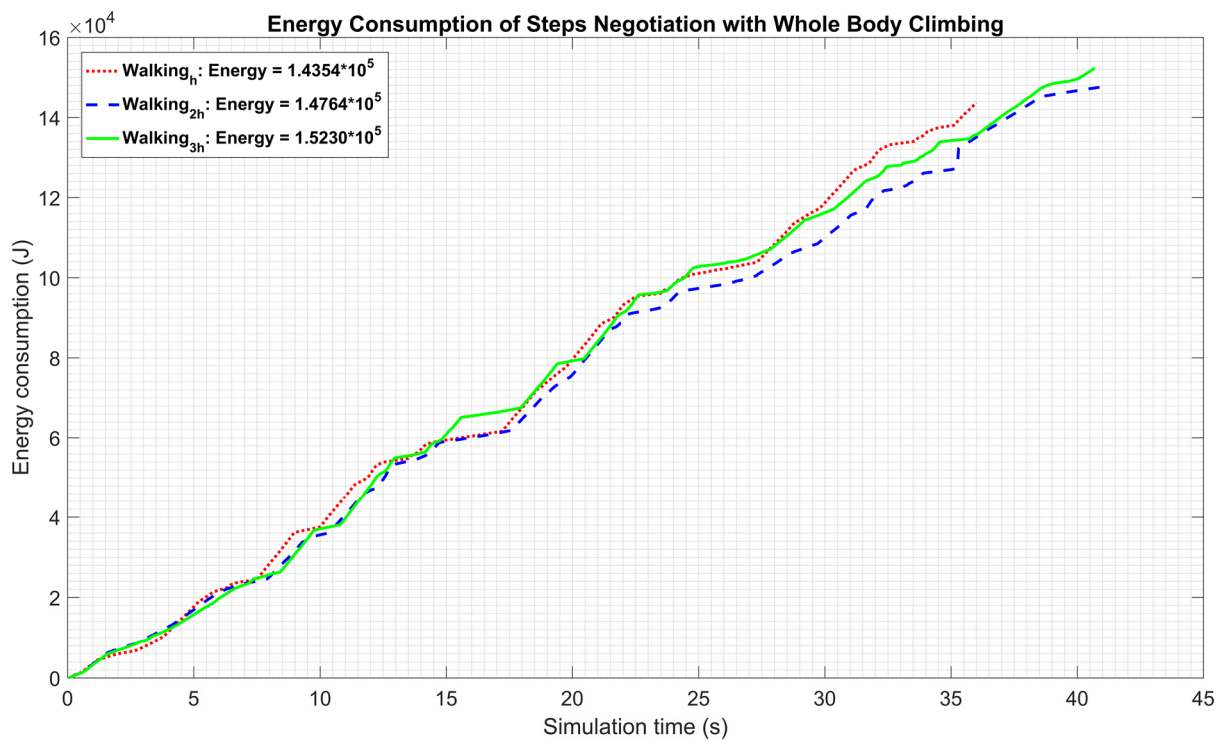


**Figure 9-4. Energy Evaluations of the Step Negotiations using the Whole Body Climbing Gait.**

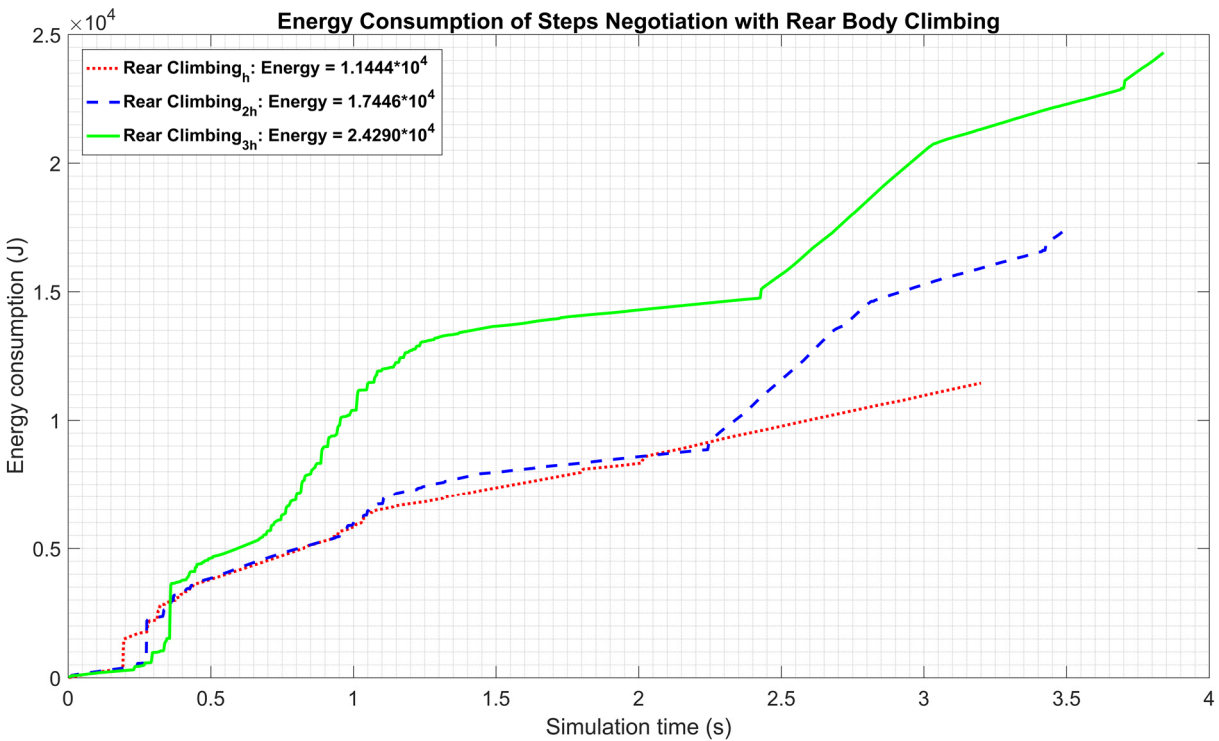


**Figure 9-5. Energy Evaluations of the Step Negotiations using the Rear Body Climbing Gait.**

Both the energy plots shown in Figure 9-4 and Figure 9-5 are the accumulated energy consumption during the step negotiation process. This is also true to the following energy plots of the transition verification simulations in section 9.5.

#### 9.4 Threshold Values

Before showing simulation results to verify the method proposed in section 9.2, features of the threshold values for the locomotion transition criterion are summarized in this section.

1. The threshold values for locomotion transition are determined by the energy consumption evaluation of the walking locomotion mode of hybrid robots. The threshold values are not based on empirical values like in other methods, instead a novel rule is used to determine the threshold values. In this research, the threshold values are defined to be equal to the energy consumption of the walking locomotion and is realized by the whole body climbing and the rear body climbing gaits, thus the threshold values are obtained by the energy evaluation results as shown in Figure 9-4 and Figure 9-5.
2. The threshold values aren't fixed, and they are determined by the robot's negotiation terrain profiles. As shown in Figure 9-4 and Figure 9-5, the energy evaluation case studies for the whole body climbing and the rear body climbing gaits to negotiate step heights of  $h_t$ ,  $2h_t$  and  $3h_t$  are evaluated respectively. Since the energy results vary with step height, the threshold values to invoke the locomotion mode transition of the robot differ with step height.
3. The proposed locomotion mode transition method is applicable to different hybrid robots. When applying the method to a hybrid robot, the threshold values should be determined first by conducting the energy evaluations for the walking locomotion of the robot.

4. Energy is used as a criterion to evaluate the locomotion performances of rolling and walking locomotion mode of hybrid robots, these performance results are then used to realize the locomotion mode transition between different locomotion modes. Thus, in the proposed method, the energy evaluations don't aim to realize other functions such as the walking gait selection for the walking locomotion mode.

## 9.5 Simulation Results

In this section, the step negotiations with heights of  $h_t$ ,  $2h_t$  and  $3h_t$  are conducted as case studies to verify the proposed autonomous locomotion mode transition method.

In the simulations, the energy consumption of the whole body negotiation ( $E_{Rw}$ ) and the rear track negotiation ( $E_{Rr}$ ) are recorded on-line to compare with the pre-studied the whole body climbing energy evaluation results ( $E_{Cw}$ ) shown in Figure 9-4 and the rear body climbing energy evaluation results ( $E_{Cr}$ ) shown in Figure 9-5, respectively. The energy consumption of the step negotiation in rolling locomotion mode only (without utilizing the proposed locomotion mode transition method) is plotted together with the on-line energy recordings. Thus, the energy advantage by using the proposed method can be seen in the Figure 9-6, Figure 9-7 and Figure 9-8.

In Figure 9-6, both  $E_{Rw} < E_{Cw}$  and  $E_{Rr} < E_{Cr}$  are satisfied for the whole step negotiation process, so the robot finishes negotiating the step with  $1h_t$  height using the rolling locomotion mode only without conducting the locomotion mode transition.

In Figure 9-7, it shows that when the robot negotiates a step with  $2h_t$  height, the locomotion mode transition is invoked. It enables the robot to change from rolling to walking locomotion mode when  $E_{Rr} > E_{Cr}$  is satisfied. Between rolling and walking locomotion mode,

there is a defined locomotion transition preparation phase, during which the robot move backward for a small distance to make rear tracks get apart from the step.

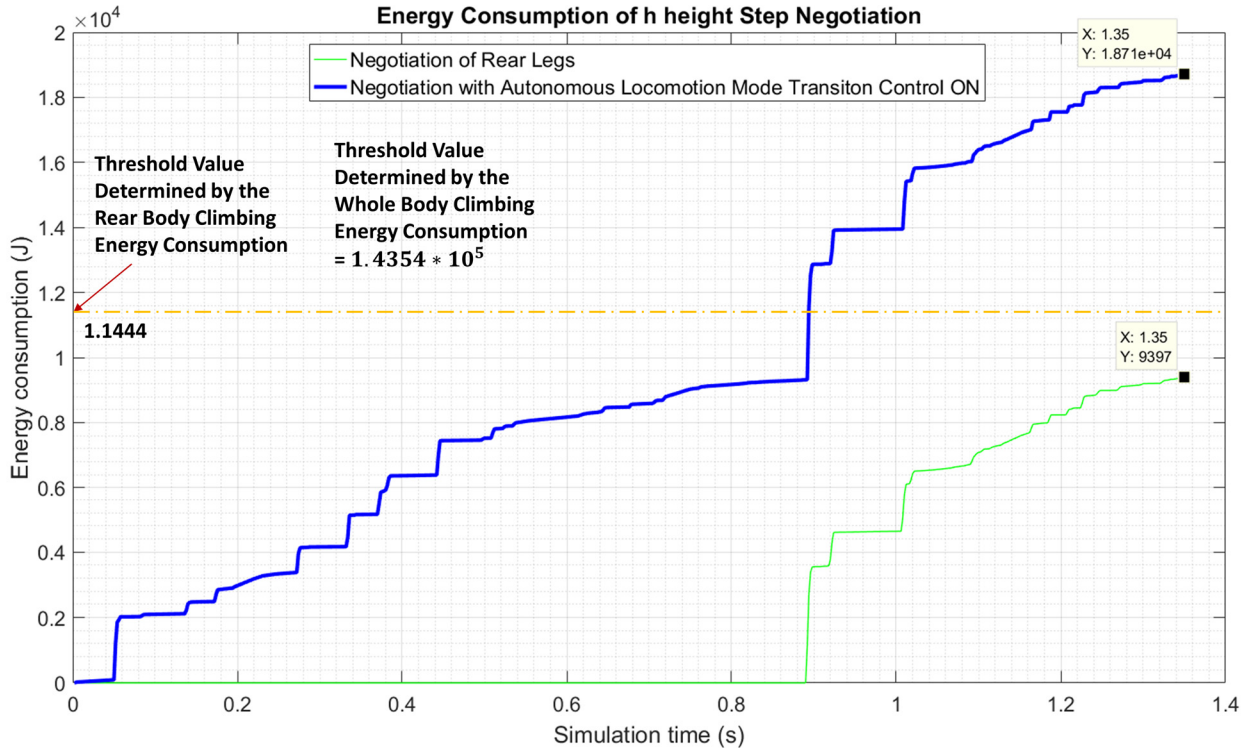


Figure 9-6. Energy Consumption of Step Negotiation with  $h_t$  height.

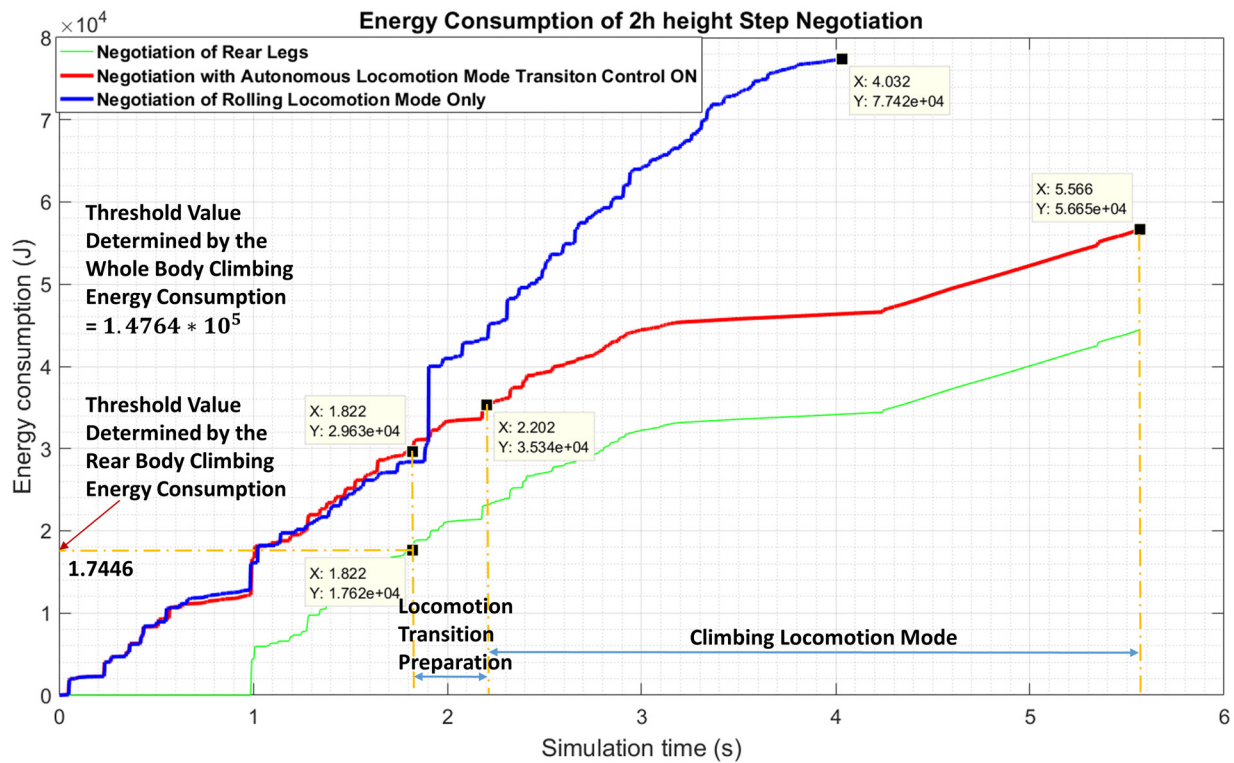
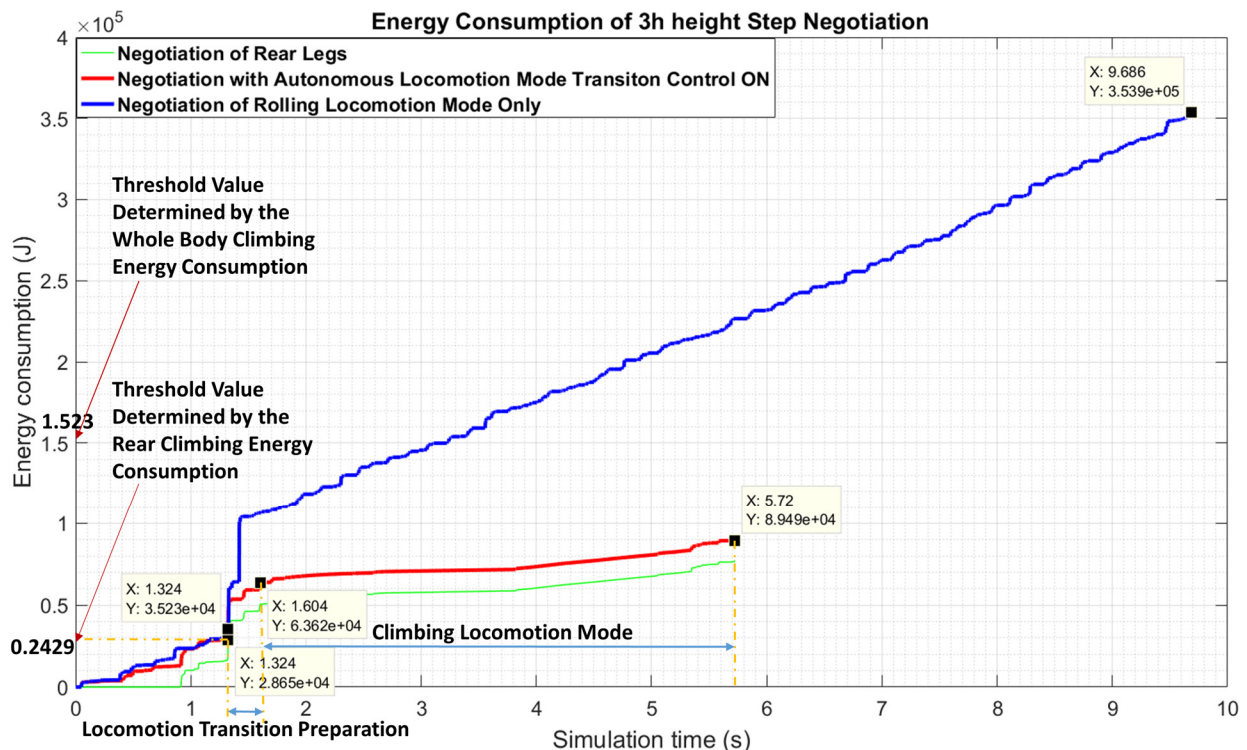


Figure 9-7. Energy Consumption of Step Negotiation with  $2h_t$  height.

When the robot negotiates step with  $3h$ , the locomotion mode transition is also conducted when the rear body energy consumption in rolling locomotion passes over the threshold value shown in Figure 9-8. It can be seen that it is much more energy efficient to conduct the step negotiation using the proposed locomotion mode transition method compared with step negotiations using the rolling locomotion mode only.



**Figure 9-8. Energy Consumption of Step Negotiation with  $3h_t$  height.**

## 9.6 Summary

In this chapter, the autonomous locomotion mode transition method is proposed by improving the first tentative method proposed in Chapter Six. The improvement is made mainly because there are two climbing gaits, the whole body climbing and rear body climbing gaits, are developed in Chapter Eight to negotiate the steps. By developing the rear body climbing gait to evaluate the walking locomotion, the threshold values are determined more resourceful, thus a more efficient locomotion mode transition strategy is added to the proposed method. This is due to the fact that it's always the rear wheels limit the steps negotiation mobility of the rolling locomotion for the quadruped wheel/track-legged hybrid robots.

The proposed method is verified by the step negotiation results of Cricket robot. It can be seen that the method can realize the locomotion mode transition automatically. However, the

threshold values are pre-determined by the case study of the walking locomotion mode, the alternative method to determine the threshold values by the predictive on-line calculation hasn't achieved.

The ultimate goal for the autonomous locomotion mode transition research of hybrid ground robots is that robots can transverse terrains in a completely hybrid locomotion style, i.e. each individual leg determines the most proper locomotion mode during their terrain negotiations for itself. If an adaptive walking gait is successfully proposed with respect to each individual leg, thus the energy performances can be evaluated to determine the threshold values for each leg of the hybrid robot, then the fully hybrid locomotion can be realized for the hybrid robot.

## Chapter Ten: CONCLUSION AND FUTURE WORK

This thesis solves the problem of the autonomous locomotion mode transition of wheel/track-legged hybrid robots. On the one hand, in the process to solve the problem following the sequence of steps outlined in Chapter Three, the proposed contributions (Chapter Three) are achieved. On the other hand, in order to keep this comprehensive problem bounded to a few manageable aspects by making several assumptions and constraints as well as simplifications, the future work need to be continued.

### 10.1 Conclusion

The work conducted in this thesis starts with proposing two dynamic modeling methods for the rolling and walking locomotion modes of the wheel/track-legged hybrid robots. Then, energy evaluations of the two locomotion modes are compared using the developed dynamic models, and a first tentative autonomous locomotion mode transition method of ground hybrid robots is proposed based on these results. Next, the work is continued on the Cricket system using a robotics simulation software, V-REP. This makes the energy evaluation of the rolling locomotion mode more reliable as well as reduced motion control (kinematics and dynamics) complexity of the walking locomotion mode. Two walking gaits to negotiate steps with different heights are also proposed in order to achieve a proper step negotiation locomotion and to be used to evaluate the energy consumption of the walking locomotion mode. Finally, the autonomous locomotion mode transition method is refined and verified by the step negotiation results of Cricket. Even though the method is refined based on work conducted on the Cricket robot, it doesn't lose its genericity to be applied to a wide range of quadruped wheel/track-legged robots.

The genericity of the proposed method is due to the fact that the solutions to the specified problem (Chapter Two) are not constrained to one particular robot structure as:

1. The energy criterion is used to evaluate the performance of the locomotion modes for the ground hybrid robots,
2. The energy evaluation of the rolling locomotion mode is obtained by measurement during the robots' on-going move,
3. The proposed walking locomotion mode modeling method is developed using a multibody dynamics algorithm that is applicable to various quadruped wheel/track-legged hybrid robots,
4. The proposed walking gait is applicable to all quadruped wheel/track-legged hybrid robots to negotiate steps with different height,
5. The locomotion mode transition criterion threshold values are determined by the alternative locomotion mode evaluation rather than empirical numbers.

Due to these facts, contributions are made to the autonomous locomotion mode transition area. Moreover, the proposed method doesn't depend on accurate models of the hybrid robots. This is especially true to the rolling locomotion mode.

It can be concluded that the proposed contribution listed in Chapter Two are all achieved. The proposed autonomous locomotion mode transition method in Chapter Nine is verified by the simulation results of the Cricket steps negotiation. However, future work of the autonomous locomotion mode transition of ground hybrid robots still need to be continued.

## **10.2 Future work**

Suggested future work can be categorized into short and long term activities. In the short term, future work includes: *i*) conducting more energy performance of the walking locomotion mode to negotiate step with different heights evaluations, then interpolating these cases study results as a look-up table that can be used as the threshold values for the locomotion mode

transition criterion; *ii*) establishing a complete dynamic model of the Cricket using the DeNOC algorithm to conduct the predictive energy evaluations and the walking gait optimizations; and *iii*) experimental testing and validation of the proposed method using a real robot platform.

The long term future research is envisioned to: *i*) test and validate the proposed autonomous locomotion mode transition method on different wheel/track-legged hybrid robotics platforms; *ii*) extend the proposed method to sub-locomotion transition (inside one main locomotion mode) control; and *iii*) extend the autonomous locomotion mode transition method to robots operating among multiple domains (e.g. terrestrial, scansorial, aerial, and aquatic).

## References

- [1] L. Bruzzone and G. Quaglia, "Review article: locomotion systems for ground mobile robots in unstructured environments," *Mechanical Sciences*, vol. 3, pp. 49-62, 2012.
- [2] R. Siegwart, I. R. Nourbakhsh, and D. Scaramuzza, *Introduction to autonomous mobile robots*: MIT press, 2011.
- [3] C. Taylor. (2016). *Robotics: Computational Motion Planning*. Available: <https://www.coursera.org/learn/robotics-motion-planning>
- [4] S. H. Lim and J. Teo, "Recent Advances on Locomotion Mechanisms of Hybrid Mobile Robots," *WSEAS Transactions on Systems*, vol. Volume 14, pp. 11-25, 2015.
- [5] C. Nie, X. P. Corcho, and M. Spenko, "Robots on the move: Versatility and complexity in mobile robot locomotion," *IEEE Robotics & Automation Magazine*, vol. 20, pp. 72-82, 2013.
- [6] *DARPA Robotics Challenge (DRC)*. Available: <http://www.darpa.mil/program/darpa-robotics-challenge>
- [7] *How South Korea's DRC-HUBO Robot Won the DARPA Robotics Challenge*. Available: <http://spectrum.ieee.org/automaton/robotics/humanoids/how-kaist-drc-hubo-won-darpa-robotics-challenge>
- [8] *Carnegie Mellon University - Tartan Rescue Multimedia*. Available: <http://www.nrec.ri.cmu.edu/projects/tartanrescue/multimedia/>
- [9] *Autonomous Intelligent Systems NimbRo Explorer*. Available: <http://www.nimbro.net/Explorer/>
- [10] *RoboSimian Drives, Walks and Drills in Robotics Finals*. Available: <http://www.jpl.nasa.gov/news/news.php?feature=4617>
- [11] L. Daler, S. Mintchev, C. Stefanini, and D. Floreano, "A bioinspired multi-modal flying and walking robot," *Bioinspiration & biomimetics*, vol. 10, p. 016005, 2015.
- [12] A. Kalantari and M. Spenko, "Modeling and performance assessment of the HyTAQ, a hybrid terrestrial/aerial quadrotor," *IEEE Transactions on Robotics*, vol. 30, pp. 1278-1285, 2014.
- [13] A. J. Ijspeert, A. Crespi, D. Ryczko, and J.-M. Cabelguen, "From swimming to walking with a salamander robot driven by a spinal cord model," *science*, vol. 315, pp. 1416-1420, 2007.
- [14] M. Takahaashi, K. Yoneda, and S. Hirose, "Rough terrain locomotion of a leg-wheel hybrid quadruped robot," in *Robotics and Automation (ICRA), 2006 IEEE International Conference on*, 2006, pp. 1090-1095.
- [15] T. Kobayashi, T. Aoyama, K. Sekiyama, Z. Lu, Y. Hasegawa, and T. Fukuda, "Locomotion selection of multi-locomotion robot based on falling risk and moving efficiency," in *Intelligent Robots and Systems (IROS), 2012 IEEE/RSJ International Conference on*, 2012, pp. 2869-2874.
- [16] T. Okada, W. T. Botelho, and T. Shimizu, "Motion analysis with experimental verification of the hybrid robot PEOPLER-II for reversible switch between walk and roll on demand," *The International Journal of Robotics Research*, 2009.
- [17] K. B. Lim and Y.-S. Yoon, "Reconfiguration planning for a robotic vehicle with actively articulated suspension in obstacle terrain during straight motion," *Advanced Robotics*, vol. 26, pp. 1471-1494, 2012.

- [18] Y. Luo, Q. Li, and Z. Liu, "Design and optimization of wheel-legged robot: Rolling-Wolf," *Chinese Journal of Mechanical Engineering*, vol. 27, pp. 1133-1142, 2014.
- [19] T. Fukuda, Y. Hasegawa, K. Sekiyama, and T. Aoyama, *Multi-locomotion robotic systems: new concepts of bio-inspired robotics* vol. 81: Springer, 2012.
- [20] T. Kobayashi, T. Aoyama, M. Sobajima, K. Sekiyama, and T. Fukuda, "Locomotion selection strategy for multi-locomotion robot based on stability and efficiency," in *Intelligent Robots and Systems (IROS), 2013 IEEE/RSJ International Conference on*, 2013, pp. 2616-2621.
- [21] I. Leppänen, "Automatic locomotion mode control of wheel-legged robots," Ph.D. Dissertation, Department of Automation and Systems Technology Helsinki University of Technology, 2007.
- [22] M. Yim, Z. Ying, and D. Duff, "Modular robots," *IEEE Spectrum*, vol. 39, pp. 30-34, 2002.
- [23] M. Yim, P. White, M. Park, and J. Sastra, "Modular self-reconfigurable robots," in *Encyclopedia of complexity and systems science*, ed: Springer, 2009, pp. 5618-5631.
- [24] A. Stentz, H. Herman, A. Kelly, E. Meyhofer, G. C. Haynes, D. Stager, *et al.*, "Chimp, the cmu highly intelligent mobile platform," *Journal of Field Robotics*, vol. 32, pp. 209-228, 2015.
- [25] R. R. Murphy, "Rescue robotics for homeland security," *Communications of the ACM*, vol. 47, pp. 66-68, 2004.
- [26] K. Davies, "A Novel Control Architecture for Mapping and Motion Planning of Reconfigurable Robots in Highly Confined 3D Environments," Master Thesis, Department of Mechanical and Manufacturing Engineering, University of Calgary, 2011.
- [27] Cricket UGV. Available: <http://www.versicore.com/past-projects/cricket>
- [28] K. Davies and A. Ramirez-Serrano, "A Reconfigurable USAR Robot Designed for Traversing Complex 3D Terrain," in *Canadian Congress of Applied Mechanics, 2009 Conference on*, Halifax, Nova Scotia, Canada, 2009, pp. 209-210.
- [29] R. Siegwart, P. Lamon, T. Estier, M. Lauria, and R. Piguet, "Innovative design for wheeled locomotion in rough terrain," *Robotics and Autonomous systems*, vol. 40, pp. 151-162, 2002.
- [30] R. A. Lindemann and C. J. Voorhees, "Mars Exploration Rover mobility assembly design, test and performance," in *Systems, Man and Cybernetics, 2005 IEEE International Conference on* 2005, pp. 450-455.
- [31] P. Lamon, "The solero rover," in *3D-Position Tracking and Control for All-Terrain Robots*, ed: Springer, 2008, pp. 7-19.
- [32] T. Thueer, A. Krebs, and R. Siegwart, "Comprehensive locomotion performance evaluation of all-terrain robots," in *Intelligent Robots and Systems (IROS), 2006 IEEE/RSJ International Conference on*, 2006, pp. 4260-4265.
- [33] W. Lee, S. Kang, M. Kim, and K. Shin, "Rough terrain negotiable mobile platform with passively adaptive double-tracks and its application to rescue missions," in *Robotics and Automation (ICRA), 2005 IEEE International Conference on*, 2005, pp. 1591-1596.
- [34] S. Hirose, T. Shirasu, and E. F. Fukushima, "Proposal for cooperative robot "Gunryu" composed of autonomous segments," *Robotics and Autonomous Systems*, vol. 17, pp. 107-118, 1996.

- [35] S.-C. Chen, K.-J. Huang, W.-H. Chen, S.-Y. Shen, C.-H. Li, and P.-C. Lin, "Quattroped: A Leg--Wheel Transformable Robot," *IEEE/ASME Transactions on Mechatronics*, vol. 19, pp. 730-742, 2014.
- [36] M. Schwarz, T. Rodehutskors, D. Droschel, M. Beul, M. Schreiber, N. Araslanov, *et al.*, "NimbRo Rescue: Solving Disaster - response Tasks with the Mobile Manipulation Robot Momaro," *Journal of Field Robotics*, 2016.
- [37] B. W. Satzinger, C. Lau, M. Byl, and K. Byl, "Tractable locomotion planning for RoboSimian," *The International Journal of Robotics Research*, 2015.
- [38] G. Quaglia, L. Bruzzone, G. Bozzini, R. Oderio, and R. P. Razzoli, "Epi. q-TG: mobile robot for surveillance," *Industrial Robot: An International Journal*, vol. 38, pp. 282-291, 2011.
- [39] P. G. De Santos, E. Garcia, and J. Estremera, *Quadrupedal locomotion: an introduction to the control of four-legged robots*: Springer Science & Business Media, 2007.
- [40] K. Inagaki and H. Kobayashi, "A gait transition for quadruped walking machine," in *Intelligent Robots and Systems (IROS), 1993 IEEE/RSJ International Conference on*, 1993, pp. 525-531.
- [41] L. Roussel, C. Canudas-de-Wit, and A. Goswami, "Generation of energy optimal complete gait cycles for biped robots," in *Robotics and Automation (ICRA), 1998 IEEE International Conference on*, 1998, pp. 2036-2041.
- [42] J. C. Grieco, M. Prieto, M. Armada, and P. G. de Santos, "A six-legged climbing robot for high payloads," in *Control Applications, 1998 IEEE International Conference on*, 1998, pp. 446-450.
- [43] H. Kimura, Y. Fukuoka, and A. H. Cohen, "Adaptive dynamic walking of a quadruped robot on natural ground based on biological concepts," *The International Journal of Robotics Research*, vol. 26, pp. 475-490, 2007.
- [44] M. Malenkov, V. Gromov, S. Matrosov, and S. Vladkyin, "Results of ESA/ESTEC and VNII Transmash & RCL Joint Activities Aimed at Planetary Rovers Development," in *ESA Workshop on Advanced Space Technologies for Robotics and Automation, 2004 Conference on*, Noordwijk, Netherlands, 2004.
- [45] M. G. Bekker, *Introduction to terrain-vehicle systems*: University of Michigan Press, 1969.
- [46] I. M. Leppanen, P. J. Virekoski, and A. J. Halme, "Sensing terrain parameters and the characteristics of vehicle-terrain interaction using the multimode locomotion system of a robot," in *Intelligent Robots and Systems (IROS), 2008 IEEE/RSJ International Conference on*, 2008, pp. 500-505.
- [47] J. Y. Wong, *Terramechanics and off-road vehicle engineering: terrain behaviour, off-road vehicle performance and design*: Butterworth-heinemann, 2009.
- [48] C. Grand, F. Benamar, F. Plumet, and P. Bidaud, "Stability and traction optimization of a reconfigurable wheel-legged robot," *The International Journal of Robotics Research*, vol. 23, pp. 1041-1058, 2004.
- [49] G. Besseron, C. Grand, F. B. Amar, F. Plumet, and P. Bidaud, "Locomotion Modes of an Hybrid Wheel-Legged Robot," in *Climbing and Walking Robots: Proceedings of the 7th International Conference CLAWAR 2004*, ed Berlin, Heidelberg: Springer Berlin Heidelberg, 2005, pp. 825-833.

- [50] F. B. Amar, C. Grand, G. Besseron, and F. Plumet, "Performance evaluation of locomotion modes of an hybrid wheel-legged robot for self-adaptation to ground conditions," in *ESA Workshop on Advanced Space Technologies for Robotics and Automation, 2004 Conference on*, Noordwijk, Netherlands, 2004, pp. 1-7.
- [51] A. Halme, I. Leppänen, J. Suomela, S. Ylönen, and I. Kettunen, "WorkPartner: interactive human-like service robot for outdoor applications," *The international journal of robotics Research*, vol. 22, pp. 627-640, 2003.
- [52] K. M. Krishna and P. K. Kalra, "Solving the local minima problem for a mobile robot by classification of spatio-temporal sensory sequences," *Journal of Robotic Systems*, vol. 17, pp. 549-564, 2000.
- [53] L. Bruzzone and G. Quaglia, "Review article: locomotion systems for ground mobile robots in unstructured environments," *Mech. Sci.*, vol. 3, pp. 49-62, 2012.
- [54] H. Gopal, "Modeling and Simulation of a Trailer with Band Track over Wheels," Master Thesis, Department of Mechanical Engineering, The University of Tennessee, Knoxville, 2005.
- [55] S. Taheri, "Finite Element Modeling Of Tire-Terrain Dynamic Interaction For Full Vehicle Simulation Applications," Master Thesis, Department of Mechanical Engineering, Virginia Polytechnic Institute and State University, 2014.
- [56] J. M. Badalamenti and J. G. R. Doyle, "Radial-Interradial Spring Tire Models," *Journal of Vibration, Acoustics, Stress, and Reliability in Design*, vol. 110, pp. 70-75, 1988.
- [57] F. Beer, E. R. Johnston, and E. Eisenberg, "Vector Mechanics for Engineers: Statics and Dynamics," 2009.
- [58] S. S. Roy and D. K. Pratihar, "Kinematics, dynamics and power consumption analyses for turning motion of a six-legged robot," *Journal of Intelligent & Robotic Systems*, vol. 74, pp. 663-688, 2014.
- [59] S. K. Saha, *Introduction to robotics*: Tata McGraw-Hill Education, 2014.
- [60] R. Featherstone and D. Orin, "Robot dynamics: equations and algorithms," in *Robotics and Automation (ICRA), 2000 IEEE International Conference on*, 2000, pp. 826-834.
- [61] S. Saha, S. Shah, and P. Nandihal, "Evolution of the DeNOC-based dynamic modelling for multibody systems," *Mech Sci*, vol. 4, pp. 1-20, 2013.
- [62] A. A. Shabana, *Dynamics of multibody systems*: Cambridge university press, 2013.
- [63] A. A. Shabana, *Computational dynamics*: John Wiley & Sons, 2009.
- [64] R. Huston and C. Passerello, "On constraint equations—A new approach," *Journal of Applied Mechanics*, vol. 41, pp. 1130-1131, 1974.
- [65] J. Angeles and O. Ma, "Dynamic simulation of n-axis serial robotic manipulators using a natural orthogonal complement," *The International Journal of Robotics Research*, vol. 7, pp. 32-47, 1988.
- [66] S. K. Saha, "Dynamics of serial multibody systems using the decoupled natural orthogonal complement matrices," *Journal of applied mechanics*, vol. 66, pp. 986-996, 1999.
- [67] J. J. Craig, *Introduction to robotics: mechanics and control* vol. 3: Pearson Prentice Hall Upper Saddle River, 2005.
- [68] P. Corke, *Robotics, vision and control: fundamental algorithms in MATLAB* vol. 73: Springer, 2011.
- [69] G. W. Stewart, *Introduction to matrix computations*: Elsevier, 1973.

- [70] R. Featherstone and D. Orin, "Robot dynamics: equations and algorithms," in *ICRA*, 2000, pp. 826-834.
- [71] R. Featherstone, *Rigid body dynamics algorithms*: Springer, 2014.
- [72] E. Rohmer, S. P. Singh, and M. Freese, "V-REP: A versatile and scalable robot simulation framework," in *2013 IEEE/RSJ International Conference on Intelligent Robots and Systems*, 2013, pp. 1321-1326.
- [73] M. Freese, S. Singh, F. Ozaki, and N. Matsuhira, "Virtual robot experimentation platform v-rep: a versatile 3d robot simulator," in *International Conference on Simulation, Modeling, and Programming for Autonomous Robots*, 2010, pp. 51-62.
- [74] *Bullet physics library*. Available: <http://bulletphysics.org/wordpress/>
- [75] F. Beer, E. R. Johnston, and E. Eisenberg, *Vector Mechanics for Engineers: Statics and Dynamics*, 2009.
- [76] J. Angeles and J. Angeles, *Fundamentals of robotic mechanical systems* vol. 2: Springer, 2002.
- [77] T. Thomson, I. Sharf, and B. Beckman, "Kinematic control and posture optimization of a redundantly actuated quadruped robot," in *Robotics and Automation (ICRA), 2012 IEEE International Conference on*, 2012, pp. 1895-1900.
- [78] T. Kröger, "Opening the door to new sensor-based robot applications—The Reflexxes Motion Libraries," in *Robotics and Automation (ICRA), 2011 IEEE International Conference on*, 2011, pp. 1-4.
- [79] *Child scripts*. Available: <http://www.coppeliarobotics.com/helpFiles/en/childScripts.htm>
- [80] K. Popp and W. Schiehlen, *Ground vehicle dynamics*: Springer Science & Business Media, 2010.
- [81] K. Turker, I. Sharf, and M. Trentini, "Step negotiation with wheel traction: a strategy for a wheel-legged robot," in *Robotics and Automation (ICRA), 2012 IEEE International Conference on*, 2012, pp. 1168-1174.
- [82] C. Wong, "Posture reconfiguration and step climbing maneuvers for a wheel-legged robot," Master Thesis, 2014.
- [83] J. Wang and A. Ramirez-Serrano, "Stair-climbing and energy consumption evaluation of a leg-tracked quadruped robot," in *Advanced Intelligent Mechatronics (AIM), 2016 IEEE International Conference on*, Banff, Alberta, Canada, 2016, pp. 1448-1453.
- [84] R. B. McGhee and A. A. Frank, "On the stability properties of quadruped creeping gaits," *Mathematical Biosciences*, vol. 3, pp. 331-351, 1968.
- [85] M. Schwarz, T. Rodehutskors, M. Schreiber, and S. Behnke, "Hybrid Driving-Stepping Locomotion with the Wheeled-legged Robot Momaro," in *Robotics and Automation (ICRA), 2016 IEEE International Conference on*, Stockholm, Sweden, 2016, pp. 5589-5595.
- [86] S. Singh and K. M. Krishna, "Gait sequence generation of a hybrid wheeled-legged robot for negotiating discontinuous terrain," in *Control Applications (CCA), 2013 IEEE International Conference on*, 2013, pp. 766-771.

## **APPENDIX A: THE STANDARD AND MODIFIED D-H METHOD**

In order to calculate the kinematics relation between the end-effector and the base, coordinate frames are attached to each link between the end-effector and the base. In general, the frames can be arbitrarily attached as long as they represent links properly. However, it is convenient to follow rules so the parameters of links and joints can be described completely and uniformly.

A link can be specified by two parameters, its length  $a_i$  and its twist  $\alpha_i$ . Joints are also described by two parameters. The joint offset  $b_i$  is the distance from one link coordinate frame to the next link coordinate frame along the axis of the joint. The joint angle  $\theta_i$  is the rotation of one link with respect to the next about the joint axis.

The first commonly used and well known method in robotics area is the Denavit-Hartenberg (D-H) method. Besides the originally standard D-H method, a modified D-H method is also commonly used. The modified D-H method notions are clearer and tidier, however, its introduction has increased the scope for confusion, particular to those who would like to use developed kinematics function library without a clarification of which D-H method the library was developed to solve their own problems. So this section is summarized to make a comprehensive comparison of the standard and modified D-H method for clarification.

### **A.1. Standard D-H method**

The D-H method is first proposed in 1955. In order to distinguish the following modified D-H method, the standard D-H method is used to name it. In standard D-H method, the coordinate frame  $i$  is attached to the far (distal) end of link  $i$  as shown in Figure I.

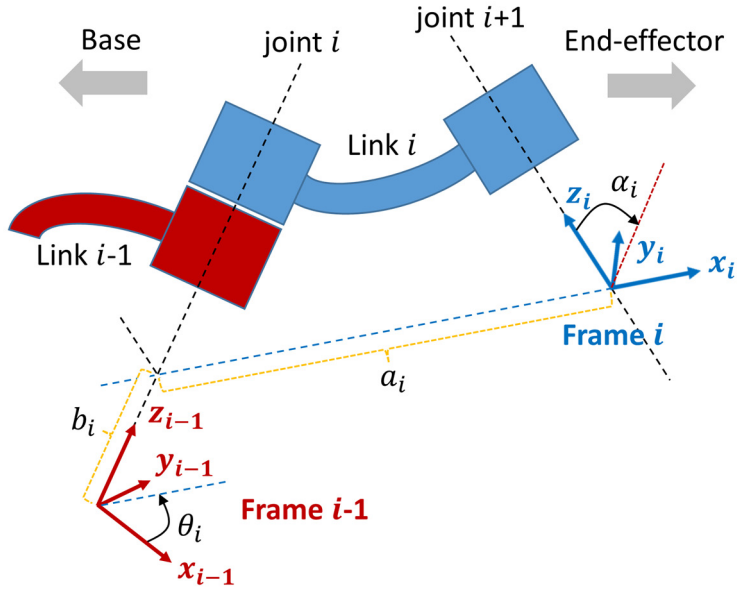


**Figure I. Standard D-H Method**

The link and joint parameters are defined as D-H parameters and are summarized in Table B. These parameters definitions remain the same for all kinds of D-H methods.

**Table B. Parameters of Standard D-H Method**

|              |            |  |                |
|--------------|------------|--|----------------|
| Joint angle  | $\theta_i$ | The angle between $x_{i-1}$ and $x_i$ axis about $z_{i-1}$ axis    | Joint variable |
| Joint offset | $b_i$      | The distance between $x_{i-1}$ and $x_i$ axis along $z_{i-1}$ axis | Constant       |
| Link length  | $a_i$      | The distance between $z_{i-1}$ and $z_i$ axis along $x_i$ axis     | Constant       |
| Link twist   | $\alpha_i$ | The angle between $z_{i-1}$ and $z_i$ axis about $x_i$ axis        | Constant       |

The transformation from coordinate frame  $i$  to frame  $i - 1$  is defined in terms of elementary rotations and the translations as:

$${}^{i-1}T_i(\theta_i, b_i, a_i, \alpha_i) = R_z(\theta_i)T_z(b_i)T_x(a_i)R_x(\alpha_i) \quad (\mathbf{K})$$

Which can be calculated as:

$${}^{i-1}T_i = \begin{bmatrix} \cos\theta_i & -\sin\theta_i \cos\alpha_i & \sin\theta_i \sin\alpha_i & a_i \cos\theta_i \\ \sin\theta_i & \cos\theta_i \cos\alpha_i & -\cos\theta_i \sin\alpha_i & a_i \sin\theta_i \\ 0 & \sin\theta_i & \cos\alpha_i & b_i \\ 0 & 0 & 0 & 1 \end{bmatrix} \quad (\text{L})$$

## A.2. Standard D-H method

Later, Craig first introduced the modified D-H parameters in 1986 in which the link coordinate frames are attached to the near (proximal), rather than the far end of each link as shown in Figure J.

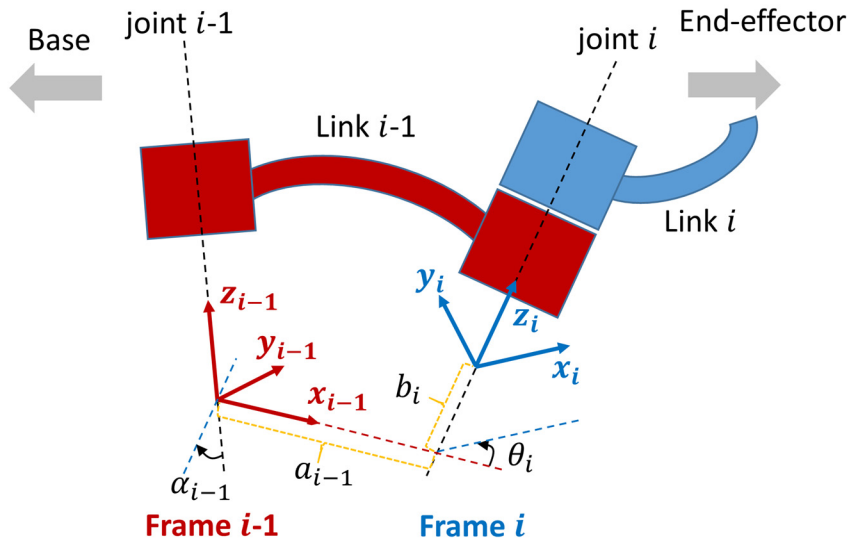


**Figure J. Modified D-H Method**

The link transformation from frame  $i$  to frame  $i - 1$  can be written as:

$${}^{i-1}T_i = R_x(\alpha_{i-1})T_x(a_{i-1})R_z(\theta_i)T_z(b_i) \quad (\text{M})$$

Which can be derived as:

$${}^{i-1}T_i = \begin{bmatrix} \cos\theta_i & -\sin\theta_i & 0 & a_{i-1} \\ \sin\theta_i \cos\alpha_{i-1} & \cos\theta_i \cos\alpha_{i-1} & -\sin\alpha_{i-1} & -\sin\alpha_{i-1} b_i \\ \sin\theta_i \sin\alpha_{i-1} & \cos\theta_i \sin\alpha_{i-1} & \cos\alpha_{i-1} & \cos\alpha_{i-1} b_i \\ 0 & 0 & 0 & 1 \end{bmatrix} \quad (\text{N})$$

Because rotations are not commutative, which is the nub of this problem, more attention should be taken. The homogeneous transformation matrix differences of the standard and

modified D-H method (Equation **(L)** and Equation **(N)**) is because of the rotation sequence difference expressed in Equation **(K)** and Equation **(M)**. The first three columns and rows in the transformation matrix is the rotation matrix, which is only determined by the multiplication sequence of the joint angle  $\theta_i$  and link twist  $\alpha_i$ . And as long as the two joint parameters  $\theta_i$  and  $d_i$  and two link parameters  $\alpha_i$  and  $a_i$  are neighboured with each other in the multiplication transformation equation (Equation **(L)** and Equation **(N)**), both the rotation matrix and translation matrix inside transformation matrix are the same.

When building the kinematic parameters using D-H method, it is equally fine to use either the standard or the modified one. The rule is all parameters should follow exactly the same method chose from the beginning. Too often this important statement isn't mentioned at all in textbooks and papers.

### A.3. D-H Method of DeNOC Algorithm

The D-H method used in the DeNOC algorithm is different with both standard and modified D-H method discussed above. This D-H method can be categorized into the standard one because of the coordinate frames are attached to the far (distal) end of links, and its rotation sequence of the homogeneous transformation matrix derivation is equivalent to Equation **(K)** as:

$${}^i T_{i+1}(\theta_i, b_i, a_i, \alpha_i) = T_z(b_i) R_z(\theta_i) T_x(a_i) R_x(\alpha_i) \quad (\text{O})$$

Instead of the coordinate frame  $i$  is defined to be attached to the end of link  $i$ , the coordinate frame  $i + 1$  is attached to the end of link  $i$ . By changing the frame subscript, the coordinates frame subscript is as same as the joint sequence shown in Figure K. The homogeneous transformation matrix is in the same form as Equation **(L)** as:

$${}^i T_{i+1} = \begin{bmatrix} \cos\theta_i & -\sin\theta_i \cos\alpha_i & \sin\theta_i \sin\alpha_i & a_i \cos\theta_i \\ \sin\theta_i & \cos\theta_i \cos\alpha_i & -\cos\theta_i \sin\alpha_i & a_i \sin\theta_i \\ 0 & \sin\theta_i & \cos\alpha_i & b_i \\ 0 & 0 & 0 & 1 \end{bmatrix} \quad (\textbf{P})$$

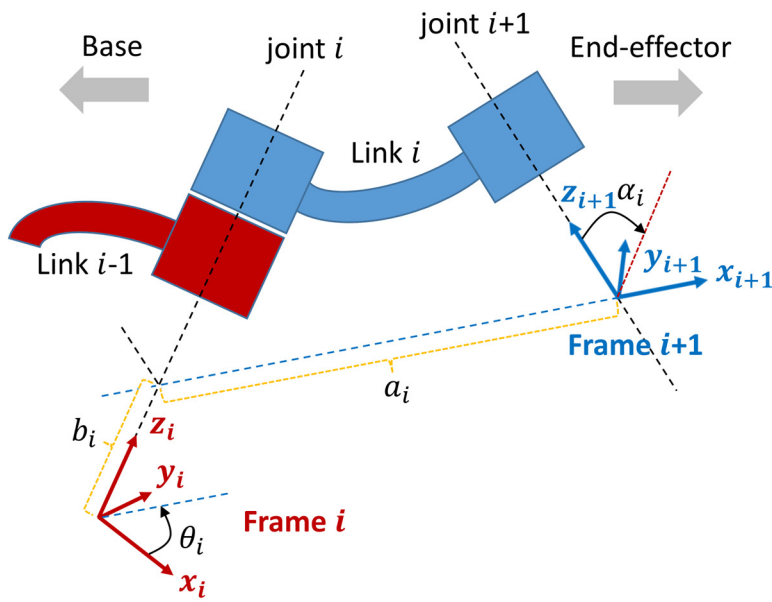


**Figure K. D-H Method in DeNOC Algorithm**

## APPENDIX B: ANALYTICAL EXPRESSIONS OF THE DENOC DYNAMIC EQUATIONS OF MOTION VARIABLES

The variables of the dynamic equations of motion in Equation (5.23) derived by DeNOC method, i.e. the GIM, MCI, VCI, and the generalized forces defined by Equation (5.24), (5.25), (5.26), and (5.27) respectively can be expressed analytically in this section.

### B.1. Generalized Inertia Matrix (GIM)

The  $n \times n$  matrix GIM  $\mathbf{I}$  defined in Equation (5.24) is reproduced here,

$$\mathbf{I} = N^T MN = N_d^T N_l^T MN_l N_d = N_d^T \tilde{M} N_d \quad (\mathbf{Q})$$

where  $\tilde{M} = N_l^T MN_l$  is the  $6n \times 6n$  symmetric composite mass matrix, which can be obtained as:

$$\tilde{M} = \begin{bmatrix} \tilde{M}_1 & B_{21}^T \tilde{M}_2 & B_{31}^T \tilde{M}_3 & \cdots & B_{n1}^T \tilde{M}_n \\ \tilde{M}_2 B_{21} & \tilde{M}_2 & B_{32}^T \tilde{M}_3 & \cdots & B_{n2}^T \tilde{M}_n \\ \tilde{M}_3 B_{31} & \tilde{M}_3 B_{32} & \tilde{M}_3 & \cdots & B_{n3}^T \tilde{M}_n \\ \vdots & \vdots & \vdots & \ddots & \vdots \\ \tilde{M}_n B_{n1} & \tilde{M}_n B_{n2} & \tilde{M}_n B_{n3} & \cdots & \tilde{M}_n \end{bmatrix} \quad (\mathbf{R})$$

in which the  $6 \times 6$  matrix  $\tilde{M}_i$ , for  $i = 1, \dots, n$  is defined as:

$$\tilde{M}_i = M_i + \sum_{i+1}^n B_{i+1,i}^T M_{i+1} B_{i+1,i} \quad (\mathbf{S})$$

An algorithm computing  $\tilde{M}_i$ , for  $i = 1, \dots, n$  from Equation (S) requires computations of order  $n^2$ . While, a close look to this equation considering the two properties of  $B_{ij}$ , Equation (S) can be evaluated recursively  $\sum_{i+1}^n B_{i+1,i}^T M_{i+1} B_{i+1,i} = B_{i+1,i}^T \tilde{M}_{i+1} B_{i+1,i}$ , for  $i = n, \dots, 1$  with  $\tilde{M}_{n+1} = O$ , because there is no  $(n+1)^{th}$  link in the system. Hence, the above equation has the following recursive relation as:

$$\tilde{M}_i = M_i + B_{i+1,i}^T \tilde{M}_{i+1} B_{i+1,i}, \text{ for } i = n, \dots, 1, \text{ and } \tilde{M}_n = M_n \quad (\mathbf{T})$$

Here,  $\tilde{M}_i$  is the mass matrix of a body composing of  $(n - i + 1)$  rigidly connected bodies, i.e. link  $\#n, \dots, \#i$ . Rigidly connection means the joint between each links are assumed to be not exist, links are welded at each joint point, so they cannot move respect to each other.  $\tilde{M}_i$  means the total mass and inertia tensor calculated about the mass center of link  $\#i$ . So that is defined as composite body, as indicated in Figure 5-1, meaning link  $\#n, \dots, \#i$  are treated as one body.

Next the symmetric GIM  $\mathbf{I}$  using the Equation (T) is derived as:

$$\mathbf{I} = \begin{bmatrix} p_1^T \tilde{M}_1 p_1 & p_1^T B_{21}^T \tilde{M}_2 p_2 & p_1^T B_{31}^T \tilde{M}_3 p_3 & \cdots & p_1^T B_{n1}^T \tilde{M}_n p_n \\ p_2^T \tilde{M}_2 B_{21} p_1 & p_2^T \tilde{M}_2 p_2 & p_2^T B_{32}^T \tilde{M}_3 p_3 & \cdots & p_2^T B_{n2}^T \tilde{M}_n p_n \\ p_3^T \tilde{M}_3 B_{31} p_1 & p_3^T \tilde{M}_3 B_{32} p_2 & p_3^T \tilde{M}_3 p_3 & \cdots & p_3^T B_{n3}^T \tilde{M}_n p_n \\ \vdots & \vdots & \vdots & \ddots & \vdots \\ p_n^T \tilde{M}_n B_{n1} p_1 & p_n^T \tilde{M}_n B_{n2} p_2 & p_n^T \tilde{M}_n B_{n3} p_3 & \cdots & p_n^T \tilde{M}_n p_n \end{bmatrix} \quad (\mathbf{U})$$

The  $(i,j)$  scalar element of the GIM, denoted as  $i_{ij}$  can be derived analytically,

$$i_{ij} = p_i^T \tilde{M}_i B_{ij} p_j, \text{ for } i = n, \dots, 1; j = i, \dots, 1 \quad (\mathbf{V})$$

## B.2. Matrix of Convective Inertia (MCI)

The analytical expressions of the MCI terms are developed from the MCI Equation (5.25),

$$\mathbf{C} = N^T (M \dot{N} + W M N) = N_d^T (\tilde{M}_l + \tilde{M}_\omega + \tilde{M}_e) N_d \quad (\mathbf{W})$$

Matrix  $\tilde{M}_l$  can be obtained as:

$$\tilde{M}_l = N_l^T M N_l$$

$$= \begin{bmatrix} 1 & B_{21}^T & B_{31}^T & \cdots & B_{n1}^T \\ 0 & 1 & B_{32}^T & \cdots & B_{n2}^T \\ 0 & 0 & 1 & \cdots & B_{n3}^T \\ \vdots & \vdots & \vdots & \ddots & \vdots \\ 0 & 0 & 0 & 0 & 1 \end{bmatrix} \begin{bmatrix} M_1 & 0 & 0 & \cdots & 0 \\ 0 & M_2 & 0 & \cdots & 0 \\ 0 & 0 & M_3 & \cdots & \vdots \\ \vdots & \vdots & \vdots & \ddots & 0 \\ 0 & 0 & 0 & 0 & M_n \end{bmatrix} \begin{bmatrix} 0 & 0 & 0 & \cdots & 0 \\ \dot{B}_{21} & 0 & 0 & \cdots & 0 \\ \dot{B}_{31} & \dot{B}_{32} & 0 & \cdots & 0 \\ \vdots & \vdots & \vdots & \ddots & \vdots \\ \dot{B}_{n1} & \dot{B}_{n2} & \dot{B}_{n3} & \cdots & 0 \end{bmatrix} \quad (\mathbf{X})$$

in which the  $6 \times 6$  matrix is given as:

$$\dot{B}_{i+1,i} = \begin{bmatrix} 0 & 0 \\ \dot{c}_{i+1,i} \times 1 & 1 \end{bmatrix} = \begin{bmatrix} 0 & 0 \\ -(\dot{R}_i + \dot{d}_{i+1}) \times 1 & 0 \end{bmatrix} \quad (\mathbf{Y})$$

Here,

$$\dot{r}_i = \omega_i \times r_i \text{ and } \dot{d}_{i+1} = \omega_{i+1} \times d_{i+1} \quad (\mathbf{Z})$$

The expression of  $\tilde{M}_l$  is then can be rewritten as:

$$\tilde{M}_l = \begin{bmatrix} B_{21}^T \tilde{H}_{21} & B_{31}^T \tilde{H}_{32} & \cdots & B_{n1}^T \tilde{H}_{n,n-1} & 0 \\ \tilde{H}_{21} & B_{32}^T \tilde{H}_{32} & \cdots & B_{n2}^T \tilde{H}_{n,n-1} & 0 \\ \tilde{H}_{31} & \tilde{H}_{32} & \ddots & \vdots & \vdots \\ \vdots & \vdots & \vdots & B_{n,n-1}^T \tilde{H}_{n,n-1} & \vdots \\ \tilde{H}_{n1} & \tilde{H}_{n2} & \cdots & \tilde{H}_{n,n-1} & 0 \end{bmatrix} \quad (\mathbf{AA})$$

in which  $\tilde{H}_{ij}$  can be derived as:

$$\tilde{H}_{ij} = \tilde{M}_i \dot{B}_{ij} + B_{i+1,i}^T \tilde{H}_{i+1,i}, \text{ and for } i = n, \tilde{H}_{n+1,n} = 0 \quad (\mathbf{BB})$$

Then, the  $6n \times 6n$  matrix  $\tilde{M}_\omega$  is formed as:

$$\begin{aligned} \tilde{M}_\omega &= \tilde{M}_\Omega \\ &= \begin{bmatrix} \tilde{M}_1 & B_{21}^T \tilde{M}_2 & B_{31}^T \tilde{M}_3 & \cdots & B_{n1}^T \tilde{M}_n \\ \tilde{M}_2 B_{21} & \tilde{M}_2 & B_{32}^T \tilde{M}_3 & \cdots & B_{n2}^T \tilde{M}_n \\ \tilde{M}_3 B_{31} & \tilde{M}_3 B_{32} & \tilde{M}_3 & \cdots & B_{n3}^T \tilde{M}_n \\ \vdots & \vdots & \vdots & \ddots & \vdots \\ \tilde{M}_n B_{n1} & \tilde{M}_n B_{n2} & \tilde{M}_n B_{n3} & \cdots & \tilde{M}_n \end{bmatrix} \begin{bmatrix} \Omega_1 & 0 & 0 & \cdots & 0 \\ 0 & \Omega_2 & 0 & \cdots & 0 \\ 0 & 0 & \Omega_3 & \cdots & 0 \\ \vdots & \vdots & \vdots & \ddots & \vdots \\ 0 & 0 & 0 & \cdots & \Omega_n \end{bmatrix} \quad (\mathbf{CC}) \\ &= \begin{bmatrix} \tilde{M}_1 \Omega_1 & B_{21}^T \tilde{M}_2 \Omega_2 & B_{31}^T \tilde{M}_3 \Omega_3 & \cdots & B_{n1}^T \tilde{M}_n \Omega_n \\ \tilde{M}_2 B_{21} \Omega_1 & \tilde{M}_2 \Omega_2 & B_{32}^T \tilde{M}_3 \Omega_3 & \cdots & B_{n2}^T \tilde{M}_n \Omega_n \\ \tilde{M}_3 B_{31} \Omega_1 & \tilde{M}_3 B_{32} \Omega_2 & \tilde{M}_3 \Omega_3 & \cdots & B_{n3}^T \tilde{M}_n \Omega_n \\ \vdots & \vdots & \vdots & \ddots & \vdots \\ \tilde{M}_n B_{n1} \Omega_1 & \tilde{M}_n B_{n2} \Omega_2 & \tilde{M}_n B_{n3} \Omega_3 & \cdots & \tilde{M}_n \Omega_n \end{bmatrix} \end{aligned}$$

Next, the  $6n \times 6n$  matrix  $\tilde{M}_e$  is calculated by:

$$\begin{aligned} \tilde{M}_e &= N_l^T W M N_l \\ &= \begin{bmatrix} 1 & B_{21}^T & B_{31}^T & \cdots & B_{n1}^T \\ 0 & 1 & B_{32}^T & \cdots & B_{n2}^T \\ 0 & 0 & 1 & \cdots & B_{n3}^T \\ \vdots & \vdots & \vdots & \ddots & \vdots \\ 0 & 0 & 0 & 0 & 1 \end{bmatrix} \begin{bmatrix} W_1 M_1 & 0 & 0 & \cdots & 0 \\ 0 & W_2 M_2 & 0 & \cdots & 0 \\ 0 & 0 & W_3 M_3 & \cdots & \vdots \\ \vdots & \vdots & \vdots & \ddots & 0 \\ 0 & 0 & 0 & 0 & W_n M_n \end{bmatrix} \end{aligned} \quad (\text{DD})$$

$$\begin{bmatrix} 1 & 0 & 0 & \cdots & 0 \\ B_{21} & 1 & 0 & \cdots & 0 \\ B_{31} & B_{32} & 1 & \cdots & 0 \\ \vdots & \vdots & \vdots & \ddots & \vdots \\ B_{n1} & B_{n2} & B_{n3} & \cdots & 1 \end{bmatrix} = \begin{bmatrix} \tilde{M}'_1 & B_{21}^T \tilde{M}'_2 & B_{31}^T \tilde{M}'_3 & \cdots & B_{n1}^T \tilde{M}'_n \\ \tilde{M}'_2 B_{21} & \tilde{M}'_2 & B_{32}^T \tilde{M}'_3 & \cdots & B_{n2}^T \tilde{M}'_n \\ \tilde{M}'_3 B_{31} & \tilde{M}'_3 B_{32} & \tilde{M}'_3 & \cdots & B_{n3}^T \tilde{M}'_n \\ \vdots & \vdots & \vdots & \ddots & \vdots \\ \tilde{M}'_n B_{n1} & \tilde{M}'_n B_{n2} & \tilde{M}'_n B_{n3} & \cdots & \tilde{M}'_n \end{bmatrix}$$

where  $\tilde{M}'_i$  for  $i = n, \dots, 1$  is calculated by:

$$\tilde{M}'_i = M'_i + B_{i+1,i}^T \tilde{M}'_{i+1} B_{i+1,i} \quad (\text{EE})$$

in which  $M'_i = W_i M_i$ , for  $i = n, \dots, 1$ , and  $\tilde{M}'_n = M'_n$ . Combine equations, the MCI matrix  $\mathbf{C}$  can then be calculated as,

$$\mathbf{C} = N_d^T (\tilde{M}_l + \tilde{M}_\omega + \tilde{M}_e) N_d$$

$$\begin{aligned}
&= \begin{bmatrix} p_1 & 0 & 0 & \cdots & 0 \\ 0 & p_2 & 0 & \cdots & 0 \\ 0 & 0 & p_3 & \cdots & 0 \\ \vdots & \vdots & \vdots & \ddots & \vdots \\ 0 & 0 & 0 & \cdots & p_n \end{bmatrix} \begin{bmatrix} B_{21}^T \tilde{H}_{21} & B_{31}^T \tilde{H}_{32} & \cdots & B_{n1}^T \tilde{H}_{n,n-1} & 0 \\ \tilde{H}_{21} & B_{32}^T \tilde{H}_{32} & \cdots & B_{n2}^T \tilde{H}_{n,n-1} & 0 \\ \tilde{H}_{31} & \tilde{H}_{32} & \ddots & \vdots & \vdots \\ \vdots & \vdots & \vdots & B_{n,n-1}^T \tilde{H}_{n,n-1} & \vdots \\ \tilde{H}_{n1} & \tilde{H}_{n2} & \cdots & \tilde{H}_{n,n-1} & 0 \end{bmatrix} \\
&+ \begin{bmatrix} \tilde{M}_1 \Omega_1 & B_{21}^T \tilde{M}_2 \Omega_2 & B_{31}^T \tilde{M}_3 \Omega_3 & \cdots & B_{n1}^T \tilde{M}_n \Omega_n \\ \tilde{M}_2 B_{21} \Omega_1 & \tilde{M}_2 \Omega_2 & B_{32}^T \tilde{M}_3 \Omega_3 & \cdots & B_{n2}^T \tilde{M}_n \Omega_n \\ \tilde{M}_3 B_{31} \Omega_1 & \tilde{M}_3 B_{32} \Omega_2 & \tilde{M}_3 \Omega_3 & \cdots & B_{n3}^T \tilde{M}_n \Omega_n \\ \vdots & \vdots & \vdots & \ddots & \vdots \\ \tilde{M}_n B_{n1} \Omega_1 & \tilde{M}_n B_{n2} \Omega_2 & \tilde{M}_n B_{n3} \Omega_3 & \cdots & \tilde{M}_n \Omega_n \end{bmatrix} \\
&+ \begin{bmatrix} \tilde{M}'_1 & B_{21}^T \tilde{M}'_2 & B_{31}^T \tilde{M}'_3 & \cdots & B_{n1}^T \tilde{M}'_n \\ \tilde{M}'_2 B_{21} & \tilde{M}'_2 & B_{32}^T \tilde{M}'_3 & \cdots & B_{n2}^T \tilde{M}'_n \\ \tilde{M}'_3 B_{31} & \tilde{M}'_3 B_{32} & \tilde{M}'_3 & \cdots & B_{n3}^T \tilde{M}'_n \\ \vdots & \vdots & \vdots & \ddots & \vdots \\ \tilde{M}'_n B_{n1} & \tilde{M}'_n B_{n2} & \tilde{M}'_n B_{n3} & \cdots & \tilde{M}'_n \end{bmatrix} \begin{bmatrix} p_1^T & 0 & 0 & \cdots & 0 \\ 0 & p_2^T & 0 & \cdots & 0 \\ 0 & 0 & p_3^T & \cdots & 0 \\ \vdots & \vdots & \vdots & \ddots & \vdots \\ 0 & 0 & 0 & \cdots & p_n^T \end{bmatrix} \tag{FF}
\end{aligned}$$

For  $i, j = n, \dots, 1$ ,  $c_{ij}$  can be obtained explicitly as:

$$\text{For } i \leq j: \quad c_{ij} = p_i^T [B_{j+1,i}^T \tilde{H}_{j+1,i} + B_{ji}^T (\tilde{M}_j \Omega_j + \tilde{M}'_j)] p_j \tag{GG}$$

$$\text{For } i > j: \quad c_{ij} = p_i^T (\tilde{H}_{ij} + \tilde{M}_i B_{ij} \Omega_j + \tilde{M}'_i B_{ij}) p_j \tag{HH}$$

Above is the explicit analytical expression of each element of MCI, which is more suitable for physical interpretations and debugging rather than calculating of vector  $\mathbf{h}$  ( $= \mathbf{C}\dot{\theta}$ ).

The explicit calculation of MCI requires order ( $n^2$ ) calculations, a more computational efficient recursively calculation requires order ( $n$ ) of  $\mathbf{h}$  is explained in the following section.

### B.3. Vector of Convective Inertia (VCI)

The vector of convective inertia (VCI) terms  $\mathbf{h}$  is given as:

$$\mathbf{h} = \mathbf{C}\dot{\theta} = N_d^T \tilde{w}', \text{ where } \tilde{w}' = N_l^T (Mt' + WMt), t' = (\dot{N}_l + N_l \Omega) N_d \dot{\theta}, \dot{N}_d = \Omega N_d \tag{II}$$

Note that  $t'$  is the generalized twist rate vector  $\dot{t}$  when  $\ddot{\theta} = 0$ , this relationship can be shown as:

$$\dot{t} = (N\dot{\theta})' = \dot{N}_l N_d \dot{\theta} + N_l \dot{N}_d \dot{\theta} + N_l N_d \ddot{\theta} = (\dot{N}_l + N_l \Omega) N_d \dot{\theta} = t' \quad (\text{JJ})$$

Matrix  $t'$  contains the centrifugal and coriolis acceleration terms. Introducing the following notations as:

$$M' = WM, \text{ and } w' = Mt' + M't \quad (\text{KK})$$

Substituting the equation of  $N_l$  into above two equations yields

$$\tilde{w}' = \begin{bmatrix} 1 & B_{21}^T & B_{31}^T & \cdots & B_{n1}^T \\ 0 & 1 & B_{32}^T & \cdots & B_{n2}^T \\ 0 & 0 & 1 & \cdots & B_{n3}^T \\ \vdots & \vdots & \vdots & \ddots & \vdots \\ 0 & 0 & 0 & 0 & 1 \end{bmatrix} \begin{bmatrix} w'_1 \\ w'_2 \\ w'_3 \\ \vdots \\ w'_n \end{bmatrix} = \begin{bmatrix} \tilde{w}'_1 \\ \tilde{w}'_2 \\ \tilde{w}'_3 \\ \vdots \\ \tilde{w}'_n \end{bmatrix} \quad (\text{LL})$$

where  $w'_i = M_i t'_i + M'_i t_i$ , for  $i = n, \dots, 1$ . Note that the  $6n$ -dimensional vector  $w'$  can be interpreted as the generalized wrench due to the convective inertia term. Moreover, the elements of the vector  $\tilde{w}'$ , can be obtained recursively as:

$$\tilde{w}'_i = w'_i + B_{i+1,i}^T \tilde{w}'_{i+1}, \text{ and } \tilde{w}'_n = w'_n \quad (\text{MM})$$

Furthermore, using the equation of  $N_d$ , the VCI  $\mathbf{h}$  can be calculated by:

$$\mathbf{h} = \begin{bmatrix} p_1^T \tilde{w}'_1 \\ p_2^T \tilde{w}'_2 \\ p_3^T \tilde{w}'_3 \\ \vdots \\ p_n^T \tilde{w}'_n \end{bmatrix} \quad (\text{NN})$$

In which each element of  $\mathbf{h}$ , denoted as  $h_i$ , is written as:

$$h_i = p_i^T \tilde{w}'_i, \text{ for } i = n, \dots, 1 \quad (\text{OO})$$

#### B.4. Generalized Forces

The element expressions of the generalized force  $\tau$  is given as follows,

$$\boldsymbol{\tau} = N_d^T \tilde{w}^E, \text{ where } \tilde{w}^E = N_l^T w^E \quad (\text{PP})$$

Substituting the expression of  $N_l$  into above equation, then the  $6n$ -dimensional vector  $\tilde{w}^E$  can be written as:

$$\tilde{w}^E = \begin{bmatrix} 1 & B_{21}^T & B_{31}^T & \cdots & B_{n1}^T \\ 0 & 1 & B_{32}^T & \cdots & B_{n2}^T \\ 0 & 0 & 1 & \cdots & B_{n3}^T \\ \vdots & \vdots & \vdots & \ddots & \vdots \\ 0 & 0 & 0 & 0 & 1 \end{bmatrix} \begin{bmatrix} w_1^E \\ w_2^E \\ w_3^E \\ \vdots \\ w_n^E \end{bmatrix} = \begin{bmatrix} \tilde{w}_1^E \\ \tilde{w}_2^E \\ \tilde{w}_3^E \\ \vdots \\ \tilde{w}_n^E \end{bmatrix} \quad (\textbf{QQ})$$

The elements of the vector  $\tilde{w}^E$  can be obtained recursively as:

$$\boldsymbol{\tau} = \begin{bmatrix} p_1^T \tilde{w}_1^E \\ p_2^T \tilde{w}_2^E \\ p_3^T \tilde{w}_3^E \\ \vdots \\ p_n^T \tilde{w}_n^E \end{bmatrix} \quad (\textbf{RR})$$

Then, each element of the  $n$ -dimensional vector  $\boldsymbol{\tau}$  is obtained by:

$$\tau_i = p_i^T \tilde{w}_i^E, \text{ for } i = n, \dots, 1 \quad (\textbf{SS})$$

## APPENDIX C: INVERSE KINEMATICS CALCULATION METHOD SUMMARY

In this section, the inverse kinematics calculation of the front left leg of Cricket when  $\theta_4 = -\pi/2$  is explained. Then a generic method process to solve the inverse kinematics problem with three degree of freedom is summarized.

### C.1. The Leg Inverse Kinematics Calculation

For a generic wheel/tracked-legged robot, the joint angle connecting the distal link and the wheel/track is known, for Cricket  $\theta_4 = -\pi/2$ , the inverse kinematics calculation equation can be reproduced as:

$$d = \begin{bmatrix} (b_2 + b_3 + b_4)\sin\theta_1 + \cos\theta_1(a_2\cos\theta_2 + a_3\cos(\theta_2 + \theta_3) + a_4\cos(\theta_2 + \theta_3 + \theta_4)) \\ -(b_2 + b_3 + b_4)\cos\theta_1 + \sin\theta_1(a_2\cos\theta_2 + a_3\cos(\theta_2 + \theta_3) + a_4\cos(\theta_2 + \theta_3 + \theta_4)) \\ a_2\sin\theta_2 + a_3\sin(\theta_2 + \theta_3) + a_4\sin(\theta_2 + \theta_3 + \theta_4) \end{bmatrix} \quad (\text{TT})$$

$$= \begin{bmatrix} p_x \\ p_y \\ p_z \end{bmatrix}$$

Rearrange Equation (TT) by  $d(1) * \sin\theta_1 - d(2) * \cos\theta_1$ , then

$$p_x\sin\theta_1 - p_y\cos\theta_1 = b_2 + b_3 + b_4 \quad (\text{UU})$$

$$\text{So } \theta_1 = 2 \tan^{-1} \frac{p_x \pm \sqrt{p_x^2 + p_y^2 - (b_2 + b_3 + b_4)^2}}{b_2 + b_3 + b_4 - p_y}.$$

Substituting  $\theta_4 = -\pi/2$  into Equation (TT), then vector  $d$  becomes:

$$d$$

$$= \begin{bmatrix} (b_2 + b_3 + b_4)\sin\theta_1 + \cos\theta_1(a_2\cos\theta_2 + a_3\cos(\theta_2 + \theta_3) + a_4\sin(\theta_2 + \theta_3)) \\ -(b_2 + b_3 + b_4)\cos\theta_1 + \sin\theta_1(a_2\cos\theta_2 + a_3\cos(\theta_2 + \theta_3) + a_4\sin(\theta_2 + \theta_3)) \\ a_2\sin\theta_2 + a_3\sin(\theta_2 + \theta_3) - a_4\cos(\theta_2 + \theta_3) \end{bmatrix} \quad (\text{VV})$$

$$= \begin{bmatrix} p_x \\ p_y \\ p_z \end{bmatrix}$$

Rearrange Equation (VV) by  $d(1)^2 + d(2)^2$ , then

$$\begin{aligned}
& a_3 \cos(\theta_2 + \theta_3) + a_4 \sin(\theta_2 + \theta_3) \\
&= \pm \sqrt{p_x^2 + p_y^2 - (b_2 + b_3 + b_4)^2 - a_2 \cos \theta_2}
\end{aligned} \tag{WW}$$

Plus Equation (WW) with  $d(3)^2$ , then rearrange equation as:

$$m \cos \theta_2 + n \sin \theta_2 = k \tag{XX}$$

Here  $m = \pm 2\sqrt{p_x^2 + p_y^2 - (b_2 + b_3 + b_4)^2}$ ;  $n = 2p_z a_2$ ;  $k = p_x^2 + p_y^2 + p_z^2 + a_2^2 - a_3^2 - a_4^2 - (b_2 + b_3 + b_4)^2$ . The solutions of Equation (XX) are

$$\theta_2 = \tan^{-1} \frac{k}{\pm \sqrt{m^2 + n^2 - k^2}} - \tan^{-1} \frac{m}{n} \tag{YY}$$

The last step is to solve  $\theta_3$ . Rearrange Equation (VV) by  $d(1) * \cos \theta_1 + d(2) * \sin \theta_1$ , then

$$a_2 \cos \theta_2 + a_3 \cos(\theta_2 + \theta_3) + a_4 \sin(\theta_2 + \theta_3) = p_x \cos \theta_1 + p_y \sin \theta_1 \tag{ZZ}$$

Rearrange Equation (VV) by  $d(3) * \sin \theta_2$ , then

$$a_2 \sin^2 \theta_2 + a_3 \sin \theta_2 \sin(\theta_2 + \theta_3) - a_4 \sin \theta_2 \cos(\theta_2 + \theta_3) = p_z \sin \theta_2 \tag{AAA}$$

Multiply Equation (ZZ) with  $\cos \theta_2$ , then add both sides with Equation (AAA) as

$$a_2 + a_3 \cos \theta_3 - a_4 \sin \theta_3 = p_x \cos \theta_1 \cos \theta_2 + p_y \sin \theta_1 \cos \theta_2 + p_z \sin \theta_2 \tag{BBB}$$

Equation (BBB) can be rearranged into the form of Equation (UU) as

$$a_3 \cos \theta_3 + (-a_4) \sin \theta_3 = p_x \cos \theta_1 \cos \theta_2 + p_y \sin \theta_1 \cos \theta_2 + p_z \sin \theta_2 - a_2 \tag{CCC}$$

Since  $\theta_3$  is the only unknown variable,  $\theta_3$  can be solved by Equation (CCC).

## C.2. Inverse Kinematics Calculation Steps Summary

The generic steps to solve three dimension inverse kinematics equations can be summarized into 4 steps as follows.

1. Calculate one of the three angels,  $\theta_i, \theta_j, \theta_k$  based on comprehensive observations of three equations, for example  $\theta_i$ .

2. Rearrange two equations into the following format:

$$\alpha_1 + \beta_1 \cos\theta_j + \gamma_1 \sin(\theta_j + \theta_k) = M$$

$$\alpha_2 + \beta_2 \cos\theta_j + \gamma_2 \sin(\theta_j + \theta_k) = N$$

3. Rearrange equations in step 2 as

$$a \cos\theta_j + b \sin\theta_j = c$$

The solution of above equation is

$$\theta_j = \tan^{-1} \frac{c}{\pm\sqrt{a^2 + b^2 - c^2}} - \tan^{-1} \frac{a}{b}$$

4. Repeat step 2 and step 3 to solve  $\theta_k$ .